MINISTERE DE L'ENSEIGNEMENT SUPERIEUR ET DE LA RECHERCHE SCIENTIFIQUE
UNIVERSITE MOULOUD MAMMERI DE TIZI-OUZOU
FACULTE DU GENIE DE LA CONSTRUCTION
DEPARTEMENT DE GENIE MECANIQUE

THESE

EN VUE DE L'OBTENTION DU DIPLOME DE

DOCTORAT LMD

SPECIALITE : *GENIE MECANIQUE*

OPTION : *CONSTRUCTION MECANIQUE*

PAR

Hocine BELGAID

THEME

CALCUL PRÉVISIONNEL DU COMPORTEMENT DYNAMIQUE DES STRUCTURES MÉCANIQUES

PREDICTIVE CALCULATION OF THE DYNAMICAL BEHAVIOUR OF MECHANICAL STRUCTURES

Soutenue le: 02 décembre 2018.
Devant le comité examinateur compose de:

AOUCHICHE Hocine	Professeur	UMMTO	Président
BOUAZZOUNI Amar	Professeur	UMMTO	Rapporteur
NECIB Brahim	Professeur	UFMC1, Constantine	Examinateur
TAAZOUNT Mustapha	Dr-HDR	UCA,Clermont-Ferrand, France	Examinateur
ASMA Farid	Professeur	UMMTO	Examinateur

Dedication

"God brought you out of your mothers' wombs, not knowing anything; and He gave you the hearing, and the eyesight, and the brains; that you may give thanks."
(Quran 16:78)

Thank you, ALLAH.

Acknowledgements

Firstly, I would like to express my sincere gratitude to my advisor Prof. BOUAZZOUNI Amar for the continuous support of my doctorate study and related research, for his patience, motivation, and immense knowledge. His guidance helped me in all the time of research and writing of this thesis. I could not have imagined having a better advisor and mentor for my Ph.D study.

I would like to thank Professor AOUCHICHE Hocine for the interest he has shown for my work by accepting to chair the defense jury.

I thank Professor NECIB Brahim from UFM Constantine 1 and Dr-HDR TAAZOUNT Mustapha from UCA, Clermont-Ferrand, France, for taking their time to review the work and for taking the time to be at the defense.

I would like to thank Professor ASMA Farid from UMMTO for honouring me by being part of the jury.

I would like to express my gratitude to Professor SINI Mourad from the Austrian Academy of Sciences and Professor Antonio MORASSI from the University of Udine (Italy) for kindly agreeing to read the contents of the article and to make valuable remarks.

I would like to express my deepest sympathies and gratitude to my friends, colleagues and professors at the Faculty of Construction Engineering and LMSE Laboratory at UMMTO.

Last but not the least, I would like to thank my family for their comprehension, their patience, their understanding and for the time I could not devote to them during the writing of this thesis.

Contents

List of captions

List of tables

Introduction

In his quest to understand and master nature, man has long established theories and principles on its functioning. These principles were later translated into mathematical formulas that are sometimes abusively called "laws ". Abusively, because the physical principles are established from more or less true and accurate suppositions as well as more or less precise and partial observations. For example, it is admitted today that, as a“law”, Newtonian mechanics presents a major flaw in the principle because it does not take into account all the properties of space and time. In addition, this defect goes unnoticed to the classical experimental observation, because the latter is limited in precision. Anyway, from this theory arise among others, the law of conservation of movement and the fundamental law of dynamics which are very good approximations on the scale of engineering. This is to say that the approximation begins at a very early stage of the development of the scientific theory. In fact, it starts from the transition from the stage of principle to that of mathematical formalism “modelling” (read: A Einstein, the world as I see it, chapter: On scientific truth and chapter: What is the theory of relativity).

John von Neumann said: “If people do not believe that mathematics is simple, it is only because they do not realise how complicated life is.” In mechanical engineering, and more precisely in the field of mechanical structures modelling, the nature of the problems dealt with initially imposes the following challenges: that of mathematically reproducing a particular aspect of the behaviour of an element (relationship between stress and deformation, behaviour of damaged zones, thermal deformation ...), that of assembling all the aspects of its behaviour in a same mathematical system, that of modelling the influence of external elements on the element in question (boundary condition, initial conditions, contact, friction ...) and finally, that of assembling this element with others when modelling an entire structure. The challenges mentioned above place us in front of two kinds of difficulties: the complication of the elementary physical phenomena to be modelled and the complexity of the obtained systems. Analytical models of mechanical structures are concretely presented as systems of partial differential equations PDEs. The nature and the complexity of these depend of course on the nature of the problems treated.

In a second time, comes the challenge of resolving the derived system of equations. On this subject, Professor J. P. Boyd said: "A computation is a temptation that should be resisted as long as possible [1]." It is obvious that an exact analytical solution would be ideal; however, the state of the art proves that up to now, this kind of solution exists only for very limited cases of relatively simple geometry structures. More than that, ironically, the ambition to find an exact analytical solution sometimes pushes researchers to sacrifice the quality of the model; for example, the hypothesis of the Euler-Bernoulli theory concerning the bending of beams stipulates that the straight sections remain orthogonal to the average line of the beam in flexion, this makes it possible to simplify the equation of motion in order to solve it analytically. However this simplification also induces the negligence of transverse shear phenomenon and rotational inertia; which affects the quality the results, especially, when the thickness of the beam with respect to its length and / or the effect of the rotational inertia become considerable.

Since the advent of computers and the exponential development of calculator's power, numerical methods have occupied the first place in the field of scientific computing. In fact, numerical methods and computer technology are two almost inseparable domains; one only has to remember that the 1947 paper by John von Neumann and Herman Goldstine, "Numerical Inverting of Matrices of High Order" (Bulletin of the AMS, Nov. 1947) [2,3], is considered as the birth certificate of numerical analysis. Since its publication, the evolution of this domain has been enormous. Two years before thisVon Newmann, presented his famous incomplete report "Draft of a Report on the EDVAC" [4] where he described design architecture for an electronic digital computer for the first time.Most modern calculators are built according to Von Neumann'sarchitecture. In the field of applied mechanics, numerical computation has made its beginnings in the 1960s and more intensively in the 1970s by the developments of J. H. Argyris& al in the field of finite element analysis. In the late 1960's NASA sponsored the original version of NASTRAN, and the University of California Berkeley made the finite element program SAP IV. In Norway, the ship classification society "Det Norske Veritas" developed SESAM in 1969 for use in analysis of ships. Since then, researchers have constantly made improvements on existing methods and developed new methods not only to increase accuracy or save the cost of the calculation but also to solve the anomalies and weaknesses of current methods.

Various methods were successively proposed for the resolution of such PDE problems, each one trying to remedy to the failures of the preceding ones. In the chronological order, we may cite the finite differences method, the finite element method (FEM), the collocation methods (pseudo-spectral methods) [1], the isogeometric method (IGA) [5] and finally the isogeometric collocation method (IGA-C) [6]. In what follows, we summarise the advantages and the disadvantages of those methods that brought us to investigate and develop further the isogeometric collocation method.

Nowadays, most of the software developed for the structures analysis uses the FEM. This method had a very broad diffusion and proved to be reliable in many applications. However, it remains limited and not very effective for approximating a certain number of fields of solutions. For example, the polynomial functions like Lagrange or Hermit ones that traditional FEM uses as shape functions do not accurately represent the fields of solutions of circular or elliptical shape [5], i.e. there is no polynomial parametric description capable of accurately representing circular and elliptical solutions shapes. In addition, the polynomials basis, quickly become unstable with the increasing degree of approximation (p-refinement). As a consequence, these properties limit the precision.

In 2005, T.J.R Hughs et al. introduced the concept of isogeometric analysis. Following their work, other authors published many results whose main concern was primarily to validate and improve it. Initially, the main concern in the isogeometric analysis was to remedy to the difficulties of integration between finite elements computers codes and geometrical modellers (CAD software) [5].Indeed, nowadays, it is estimated that about 60% of the relative time of analysis is devoted to the conversion of the geometric model of the part to geometry adequate for analysis Fig.1.Roughly, the proposed solution is to use the basis functions of the geometric modeller (CAD software) as shape functions in the finite element method. This method resumes the isoparametric concept and the method of Galerkin used in the FEM. Its originality lies primarily in the type of shape functions it uses. Indeed, the basis functions initially used only for the geometrical modellers of the CAD software (Bézier, B-spline, NURBS, T-Spline) are here also used as shape functions in the analysis. This of course leads to major differences compared with the traditional FEM. The main advantage of this method is that it considerably reduces the error on the shape approximation. In this case, convergence of the solution is ensured. Moreover, the nature of the NURBS functions (which are rational functions) allows exact representation of the fields of solutions (field of displacements for example) in elliptic or circular form. In addition, compared to the polynomials, these functions have a great stability at high degree of resolution, which allows a very high p-refinement. However, with all advantages it presently presents, the Isogeometric analysis (IGA) is still not at perfect. Indeed, although it proved its success to remedy to the errors in form approximation, there still remain errors due to numerical quadratures [7].

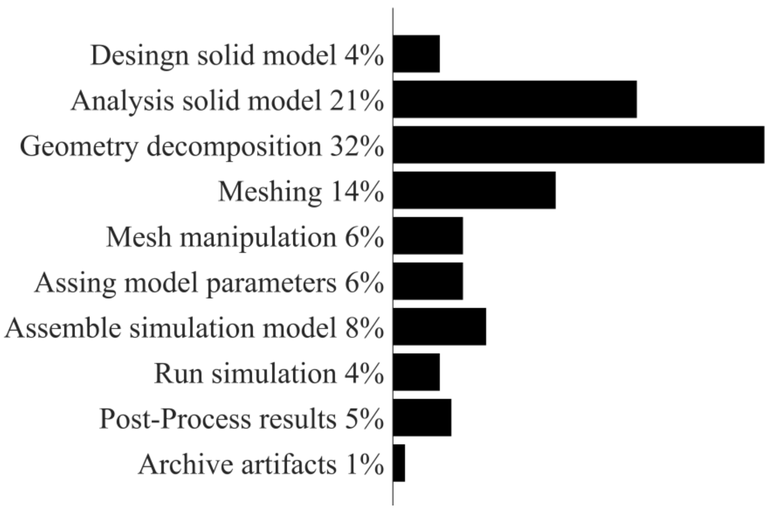

Fig 1: Dedicated relative time for each operation entering the process of numerical analysis of a mechanical structure by the classical finite element method [5].

To our opinion, the so-called semi-analytic methods may be possible alternatives to handle these numerical quadratures. One approach that is of particular interest to us is the collocation methods. Although these methods were developed in the 1970's, they remained little known because of their limits to analyze structures of complex forms and the considerable development of the FEM. However, the collocation methods have the advantage of not having recourse to numerical quadraturesthus reducing calculation costs.

The limits of the collocation methods come out to be those of the shape functions used for approximating the solutions. In 2010, progress on this matter has been achieved giving rise to the isogeometric collocation method [6]; the latter is presented as a collocation method using NURBS as shape functions. Hugh's article was followed and complemented by other works [8, 9, 10, 11,12 and 13].

In the light of this state of art, the four main objectives we aimed to achieve in this work are:

a. To provide an automatic method for imposing common and special (damaged) boundary conditions. The proposed method is simple to use without making resort to too much intuition, solves a lot of posed problems, and is very worthwhile for implementation of the isogeometric collocation method in CAD software.
b. To study the applicability of IGA-C, determine the optimal parameters for its use, construct isogeometric models for mechanical structures and evaluate the method over existing methods.
c. To develop comprehensive and detailed algorithms for the practical implementation of the IGA-C. Indeed, until today, the said method has been presented only in a very abstract mathematical formalism. Moreover, it is in this objective that all the applications have been fully detailed. We hope this will certainly help its implementation in CAD software.
d. To construct new models of structures under study and the enrichment of the scientific database.
e. To develop methods for damage modelling in structures.

The manuscript is subdivided into ten chapters including the introduction and the conclusion. The first three chapters provide a thorough theoretical understanding of all mathematical tools and principles used for the application of the IGA-C method in structural dynamics, namely analytical modelling of beams and plates, geometric modelling with B-Splines and NURBS functions and the Isogeometric collocation method.

Chapter 4 to 9 relate to the particular numerical applications of the proposed improved IGA-C method that were considered.To highlight the efficiency of the method;for each application we have included all the mathematical developments necessary for the particular implementation of the IGA-C. Consequently, any reader wishing to apply this IGA-C method to solve some PDE without going into the details of the theory can simply refer to these applications.

To highlight our contributions, six numerical test cases to which the IGA-C was applied are proposed and respective obtained results are discussed. First, in chapter 4 and 5, Isogeometric collocation models of Timoshenko straight and curved beams are constructed and solved in cases of ideal as well as non ideal (damaged) boundary conditions. The results are compared with recently published works in order to evaluate the accuracy of the presented models. Secondly, in chapter 6, to compare the results with the experimental ones, in-plane vibrations of concrete-steel composite beam model are studied using IGA-C. Then, in chapter 7, an application is dedicated to the study of the dynamical behaviour of out-of-plane helical springs where convergence curves are plotted and discussed. After that, we present in chapter 8 a new formulation of damage modelling in beams. Finally, chapter 9 is dedicated to the dynamical analysis of Reisner-Mindlin plate.

All numerical computations have been programmed and executed in Matlab. NURBS basis functions and structure's geometries have been programmed and no geometrical modeller has been used. Eigenvalue problems have been solved using Matlab "eig" function.

Ch1

1. Analytical modelling of mechanical structures

1.1. Timoshenko beam theory

Compared to the classical Euler-Bernoulli model, the Timoshenko one has the advantage of taking into account the transversal shear deformation and rotatary inertia effects that result from beam's bending. These advantages provide more accurate results and more realistic behaviour in the cases of thick beams and sandwich composite ones, as in the case of high frequency vibration analysis of beams when the inertia effects become considerable.

Timoshenko beam model was developed at the beginning of the 20th century by Stephen Timoshenko [14] & [15], and is still until now one of the most accurate.

Unfortunately, some difficulties arise when Timoshenko beam modelis used for thin beams situations due to the excessive influenceof the transverse shear deformation terms. The "shear locking" phenomenon is not directly related to Timosheko theory but to the numerical method used for solving equations. Elimination of shear locking is possible via choosing an adequate numerical method; this will be treated later in this work.

Derivation of the Timoshenko beam equation:

The Timoshenko beam theory assumes the deformed cross-section planes remain plane but not normal to the middle axis (Fig.2). The displacement field for this beam theory is defined as in (1.1).

$$U(x,z,t) = -z\Theta(x,t)\ ,\ \ V(x,z,t) = V(x,t) \tag{1.1}$$

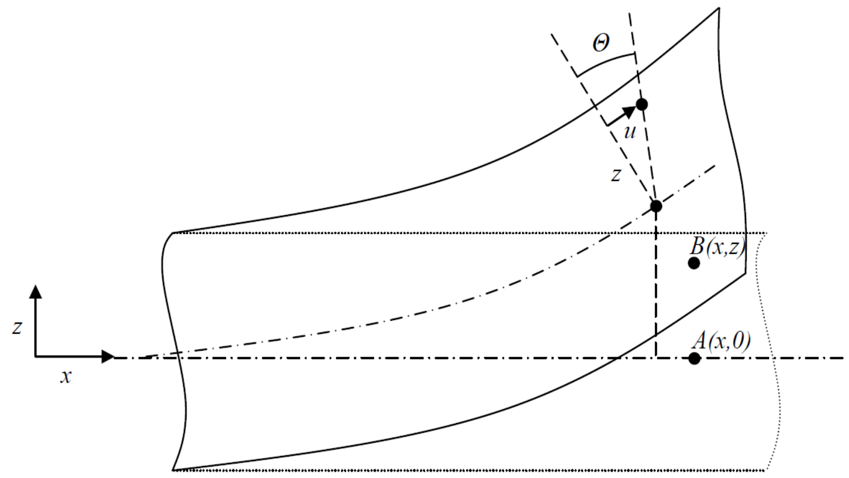

Fig 2.Deformation of a Timoshenko beam. The normal rotates by an amount *Θ* independent from *V*.

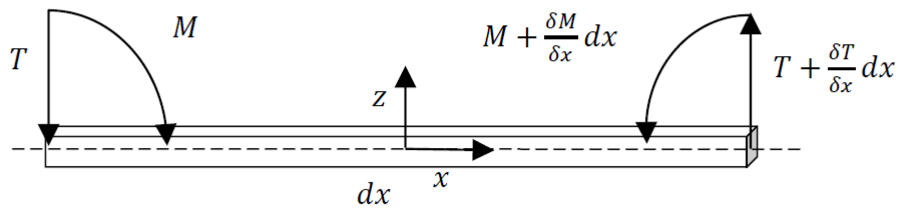

Fig 3.Static equilibrium of a beam of length *dx*.

Dynamical equilibrium of a beam element of length *dx* is given in (1.2).

$$\begin{cases} \dfrac{\partial M}{\partial x} + T = \rho I \dfrac{\partial^2 \Theta}{\partial t^2} \\ \dfrac{\partial T}{\partial x} = \rho h \dfrac{\partial^2 \mathrm{V}}{\partial t^2} \end{cases} \tag{1.2}$$

where *V=V (x, t)* is the transverse deflection, *Θ=Θ (x, t)* the rotation of the transverse line about the y axis, ρ the mass density of the beam material, *h* the thickness of the beam, *I* the second moment of inertia. *M=M (x, t)* the bending moment and *T=T (x, t)* the shearing force.

M and *T* are given by (1.3).

$$\begin{cases} M = EI \dfrac{\partial \Theta}{\partial x} \\ T = \alpha G h (\dfrac{\partial \mathrm{V}}{\partial x} - \Theta) \end{cases} \tag{1.3}$$

where *E* is the Young modulus, *G* the shear modulus and α the shear correction factor.

The Fourier method of variables separation is used to find functions satisfying system (1.2). It is assumed that each function *V (x, t)* and *Θ (x, t)* can be represented in the form of product of a function dependent on spatial coordinate *x* and function dependent on time coordinate variable *t* (1.4).

$$\begin{cases} \Theta(x,t) = \theta(x)\cos(\omega t) \\ \mathrm{V}(x,t) = v(x)\cos(\omega t) \end{cases} \tag{1.4}$$

Substituting (1.3) and (1.4) into (1.2) yields (1.5).

$$\begin{cases} EI\dfrac{d^2\theta}{dx^2} + \alpha hG\left(\dfrac{\partial v}{\partial x} - \theta\right) = -\omega^2\rho I\theta \\ -\alpha hG\dfrac{d\theta}{dx} + \alpha hG\dfrac{d^2 v}{dx^2} = -\omega^2\rho h v \end{cases} \tag{1.5}$$

Equation (1.5) is an eigenvalue problem. Its resolution amounts to finding the eigenvalues ω_j and their associated eigenmodes.

Boundary conditions

The classical boundary conditions usually applied to beams are shown in Table 1; they make it possible to model the cases of support that the most frequent structures undergo.

Table 1: Classical boundary conditions of beams elements.

BC	affects of the BC
Clamped **(C)**	*w=0*
	θ=0
Free **(F)**	*M=0*
	T=0
Sliding **(S)**	*θ=0*
	T=0
Pinned **(P)**	*w=0*
	M=0

1.2. Reisner-Mindlin plate

The Reisner-Mindlin plate theory could be described as a generalisation of Timoshenko theory for beams in two dimensional space. It assumes that the normal's section to the plate do not remain orthogonal to the mid-plane after deformation. So, it has the advantage of taking into account the transversal shear deformation and the rotary inertia resulted from plate's bending [16] and [17].

As a consequence, as when Timoshenko beam theory is applied to slender beam, shear locking defect is encountered.

Reissner-Mindlin plate theory can be readily extended to shell analysis. The simplicity of this model and their versatility for analysis of thick and thin plates with homogeneous and composite material has contributed to their popularity for practical applications.

Assuming the displacement field described in (1.6), one could derive the force/displacement relations (1.7). Then, equations (1.7) are substituted in the dynamical equilibrium equations (1.8) of a plate element represented in Fig.4 to yield the Reisner-Mindlin plate equations (1.9).

$$U_x(x,y,z,t) = -z\Theta_{\mathrm{y}}(x,y,t),\ U_y(x,y,z,t) = -z\Theta_{\mathrm{x}}(x,y,t)\ ,\ V_z(x,y,z,t) = V_z(x,y,t) \quad (1.6)$$

$$M_{xx} = -D\left(\frac{\delta\Theta_x}{\delta x} + \nu\frac{\delta\Theta_y}{\delta y}\right) \quad (1.7.a)$$

$$M_{yy} = -D\left(\frac{\delta\Theta_y}{\delta y} + \nu\frac{\delta\Theta_x}{\delta x}\right) \quad (1.7.b)$$

$$M_{xy} = -\frac{D}{2}(1-\nu)\left(\frac{\delta\Theta_x}{\delta y} + \frac{\delta\Theta_y}{\delta x}\right) \quad (1.7.c)$$

$$T_x = -\alpha^2 Gh\left(\Theta_x - \frac{\delta \mathrm{V}_z}{\delta x}\right) \quad (1.7.d)$$

$$T_y = -\alpha^2 Gh\left(\Theta_y - \frac{\delta \mathrm{V}_z}{\delta y}\right) \quad (1.7.e)$$

where:

$V_z=V_z(x,y,\ t)$ is the transverse deflection in the *z* direction.

$\Theta_x=\Theta_x\ (x,y,\ t)$ and $\Theta_y=\Theta_y\ (x,y,\ t)$are the rotation of the transverse line about the*x* and *y* axis respectively.

$M_{xy}=M_{\ xy}(x,y,\ t)$ the bending moment about y axis (so it's acting on the normal section at *x*).

$M_{yx}=M_{\ yx}(x,y,\ t)$ the bending moment about *x* axis (so it's acting on the normal section at *y*).

$T_x=T_{\ x}(x,y,\ t)$ and $T_y=\ _y(x,y,\ t)$ the shearing forces on the normal section to *x* and *y* respectively.

ρ the mass density of the beam material, *h* the thickness of the plate,*E* is the Young modulus, $G=E/(2(1+\nu))$ the shear modulus and α the shear correction factor and $D=Eh^3/(12(1-\nu^2))$.

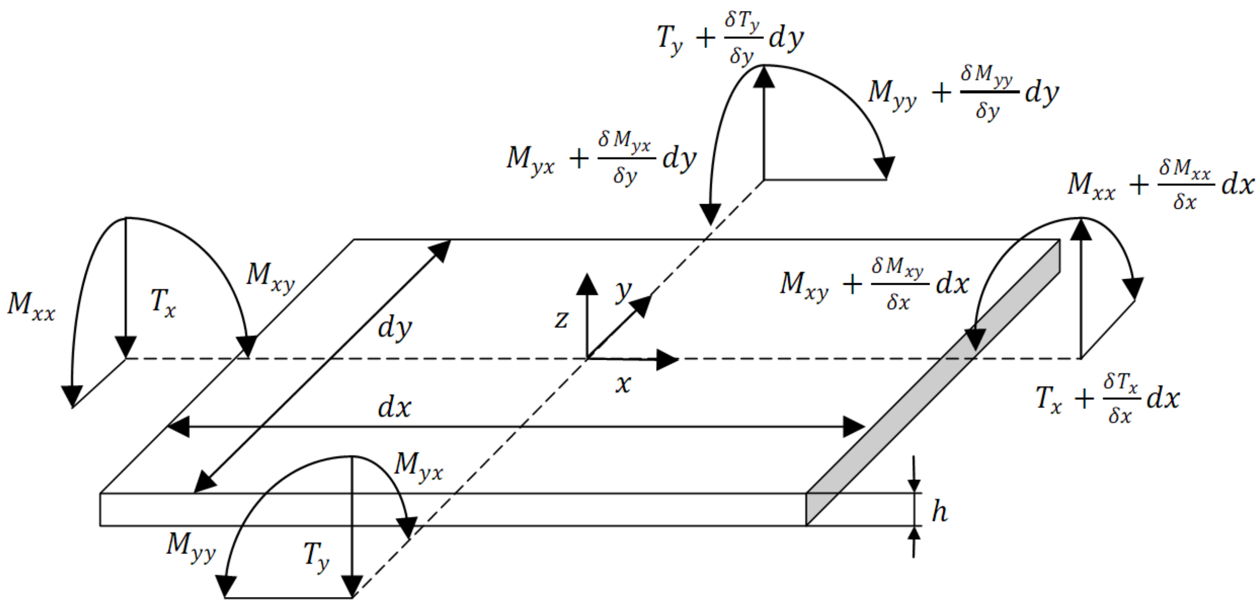

Fig 4. Static equilibrium of a plate of lengths*dx* and*dy*.

$$\frac{\delta M_{xx}}{\delta x} + \frac{\delta M_{xy}}{\delta y} - T_x = \frac{1}{12}\rho h^3 \omega^2 \Theta_x \tag{1.8.a}$$

$$\frac{\delta M_{xy}}{\delta x} + \frac{\delta M_{yy}}{\delta y} - T_y = \frac{1}{12}\rho h^3 \omega^2 \Theta_y \tag{1.8.b}$$

$$\frac{\delta T_x}{\delta x} + \frac{\delta T_y}{\delta y} = -\rho h \omega^2 V_z \tag{1.8.c}$$

Substituting (1.7) into (1.8) yields (1.9).

$$k^2 G h \Theta_x - D\frac{\delta^2 \Theta_x}{\delta x^2} - \frac{D}{2}(1-\nu)\frac{\delta^2 \Theta_x}{\delta y^2} - D\left(\frac{\nu+1}{2}\right)\frac{\delta^2 \Theta_y}{\delta y \delta x} - k^2 G h \frac{\delta V_z}{\delta x} = \frac{1}{12}\rho h^3 \omega^2 \Theta_x \tag{1.9.a}$$

$$-D\left(\frac{\nu+1}{2}\right)\frac{\delta^2 \Theta_x}{\delta x \delta y} + k^2 G h \Theta_y - \frac{D}{2}(1-\nu)\frac{\delta^2 \Theta_y}{\delta^2 x} - D\frac{\delta^2 \Theta_y}{\delta y^2} - k^2 G h \frac{\delta V_z}{\delta y} = \frac{1}{12}\rho h^3 \omega^2 \Theta_y \tag{1.9.b}$$

$$-k^2 G h \frac{\delta \Theta_x}{\delta x} - k^2 G h \frac{\delta \Theta_y}{\delta y} + k^2 G h \frac{\delta^2 V_z}{\delta x^2} + k^2 G h \frac{\delta^2 V_z}{\delta y^2} = -\rho h \omega^2 V_z \tag{1.9.c}$$

Boundary Conditions

As for Timoshenko beam case, the classical boundary conditions usually applied for an edge parallel to the *y* axis are shown in Table 2; they make it possible to model the cases of support that most common structures undergo.

Table 2: Classical boundary conditions for an edge parallel to the *y* axis.

BC	affects of the BC
Clamped (**C**)	$\Theta_x=0$
	$\Theta_y=0$
	$V=0$
Free (**F**)	$M_{xy}=0$
	$M_{xx}=0$
	$T_y=0$
Sliding (**S**)	$\Theta_y=0$
	$M_{xy}=0$
	$M_{xx}=0$
Pinned (**P**)	$\Theta_x=0$
	$V=0$
	$M_{xy}=0$

In this first chapter, we presented two analytical models for the vibrations of beams and plates; respectively, the Timoshenko equation and the Reisner-Mindlin equation. Although the use of the aforementioned models is widely used in the field of structural analysis and exact analytical solutions exist for cases of elementary structures under rather basic conditions. Nevertheless, The use of numerical solutions to solve cases of complex structures remains a necessity.

In the rest of this work, we will use the Timoshenko beam and Reisner-Mindlin plate equations as basis for the construction of richer analytical models of practical interest, in particular; multilayer composite beams, damaged structures, curved beams and structures subjected to non-ideal boundary conditions.

The next step is to present the necessary mathematical tools as well as the fundamental principles of the isogeometric collocation method developed to solve the equations presented above. To do this, Chapter 2 will be devoted to the study of Non-Uniform B-Splines functions (NURBS), which will later serve as shape functions for the isogeometric collocation method, which as for it, will be presented in chapter 3. Finally, Chapter 4 will be devoted to the development of the first application and at the same time to the presentation of the developed boundary conditions impositionmethod.

Ch2

2. Geometrical modelling

2.1. B-splines and NURBS

In order to master all aspects of B-Splines and NURBS technology for using them in numerical analysis, this chapter will be devoted to study NURBS curves and surfaces in their original framework which is Computer Aided Design.

The origin of nomination “B-Splines” comes from the thin wood or metal strips used in building ship construction (Fig.5). The main objective of developing mathematical Splines was definition of a curve as a set of piecewise simple polynomial functions connected together

Fig.5. Hooked weights, called “ducks,” accurately secure a spline. Here, no more than a thin strips of balsa for tracing the hull of a sailing vessel. Source: Edson International.

The first studies of point-controlled curves and surfaces were made in the late 1950's in Auto industry. De Casteljau, in 1959, and Bézier in 1962, introduced the polynomial curves controlled by a polygon of points. These curves will later be known as Bézier curves. These first works will be completed in 1972 by those of A.Forrest. The Polynomial Spline Curves were introduced by Ferguson in 1964. Their use became widespread starting in 1972 with the development of the Cox & De Boor algorithm. The polynomial surfaces are treated by De Casteljau in 1963, and in Bezier form at the end of the 1960s. The polynomial spline surfaces are described by Furguson, in 1964. The use of CAD rational curves appears in 1967.In 1974, Ball introduced rational surfaces constructed from certain rational cubics [5].

the development of the works mentioned above is due to the interactions between the progress of computers, mathematical research, industrial demand (bodywork, fuselage and aircraft wings, boat hulls, turbine blades, mechanical parts, clothing, video games, etc.). But also the demand of the applied sciences: geology (reconstitution of a geological structure starting from measurements), medicine (reconstitution of an organ), graphic art....

Such curves and surfaces are determined using a set of parameters such as: Knot vectors, mass vectors, B-Spline basis functions, control points and control polygon ... etc; each of these parameters will be detailed at the appropriate time in this section.

2.1.1. Knot vector

A knot vector is a sequence of non-decreasing values representing coordinates in parametric space; this is noted $\Xi = \left\{\underline{\xi}_1, \underline{\xi}_2, \dots, \underline{\xi}_{n+p+1}\right\}$ such that $\underline{\xi}_i \in \mathbb{R}$ represents the i^{th} knot, $i=1, 2, \dots, n+p+1$, p being the polynomial order and n the number of functions used for the construction of the B-spline curve. It is important to note that in practice a so called “non uniform open knot vector” is usually used; this one is defined as a knot vector in which the first and the last knot is repeated $p+1$ times each one (see Fig.6). As will be seen in the next section, this kind of knot vector produces an interpolated curve at the ends.

2.1.2. B-spline basis functions

Having defined the knot vector, we then recursively define B-Splines basis functions starting with the order ($p=0$) with relation (2.1).

$$N_{i,0}(\xi) = \begin{cases} 1 & if\, \underline{\xi}_i \leq \xi \leq \xi_{i+1} \\ 0 & otherwise \end{cases} \tag{2.1}$$

then for $p=1,2,\dots$ with relation(2.2).

$$N_{i,p}(\xi) = \frac{\xi - \underline{\xi}_i}{\underline{\xi}_{i+p} - \underline{\xi}_i} N_{i,p-1}(\xi) + \frac{\underline{\xi}_{i+p+1} - \xi}{\underline{\xi}_{i+p+1} - \underline{\xi}_i} N_{i+1,p-1}(\xi) \tag{2.2}$$

For the case of repeated knots, as the denominator of these functions is zero, one adopts the convention $x/0=0$. This offers an important propriety of B-Splines, which is the possibility of controlling the continuity of curves by knot repetition.

Fig.6 illustrates three B-spline basis (a), (b) and (c) of order p=1,2 and 3 respectively. The three bases are respectively built with open knot vectors $\Xi_1 = \{0,0,1/8,2/8,3/8,4/8,5/8,6/8,7/8,1,1\}$, $\Xi_2 = \{0,0,0,1/7,2/7,3/7,4/7,5/7,6/7,1,1,1\}$ and $\Xi_3 = \{0,0,0,0,1/6,2/6,3/6,4/6,5/6,1,1,1,1\}$.

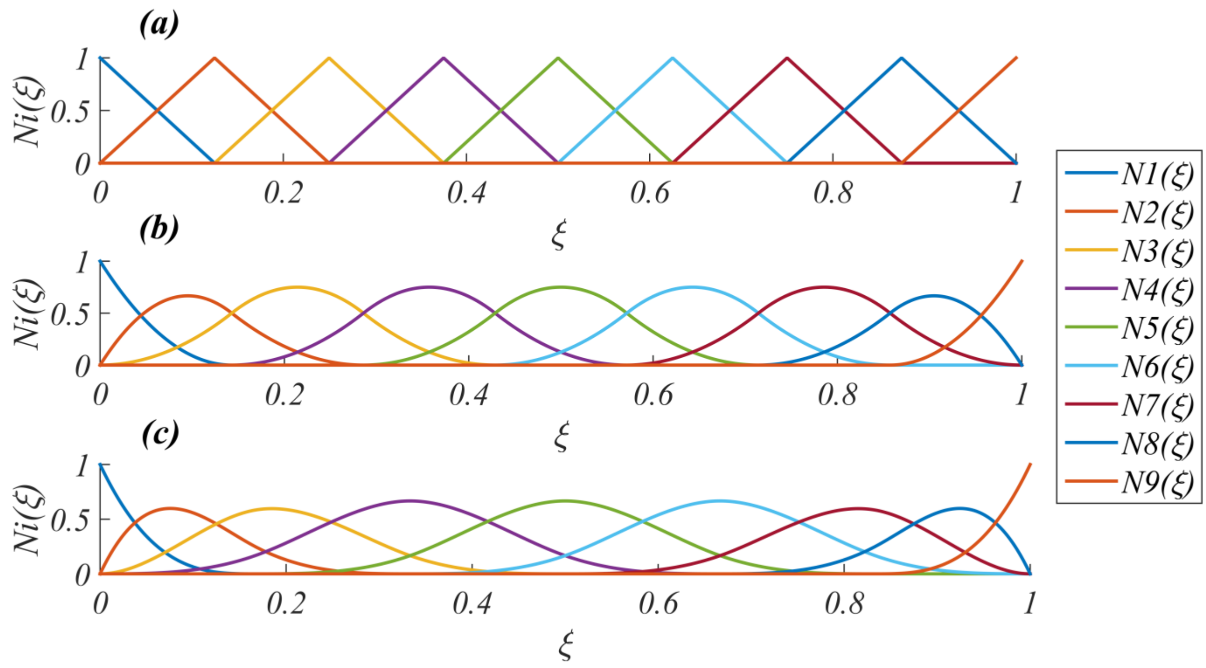

Fig. 6.Three B-Spline basis (*a*), (*b*) and (*c*) of order *p*=1,2 and 3 respectively. The three bases are respectively built with open knot vectors: Ξ_1={0,0,1/8,2/8,3/8,4/8,5/8,6/8,7/8,1,1}, Ξ_2={0,0,0,1/7,2/7,3/7,4/7,5/7,6/7,1,1,1} and $\boldsymbol{\Xi_3 = \{0,0,0,0,1/6,2/6,3/6,4/6,5/6,1,1,1,1}$.

2.1.3. Derivatives of B-spline basis functions

The derivatives of the B-splines basis functions can be analytically defined in terms of B-splines of a lower order. That results from the recursive definition of the basis B-splines functions given by (2.2). For a given polynomial of order p and knot vector Ξ, the first derivative of the i^{th} basis function is given by (2.3).

$$\frac{d}{d\xi}(N_{i,p}(\xi)) = \frac{p}{\underline{\xi}_{i+p} - \underline{\xi}_i} N_{i,p-1}(\xi) - \frac{p}{\underline{\xi}_{i+p+1} - \underline{\xi}_{i+1}} N_{i+1,p-1}(\xi). \tag{2.3}$$

This relation can be generalized to find derivatives of higher orders as in (2.4).

$$\frac{d^k}{d^k\xi}(N_{i,p}(\xi)) = \frac{p}{\underline{\xi}_{i+p} - \underline{\xi}_i}\left(\frac{d^{k-1}}{d^{k-1}\xi}(N_{i,p-1}(\xi))\right) - \frac{p}{\underline{\xi}_{i+p+1} - \underline{\xi}_{i+1}}\left(\frac{d^{k-1}}{d^{k-1}\xi}(N_{i+1,p-1}(\xi))\right) \tag{2.4}$$

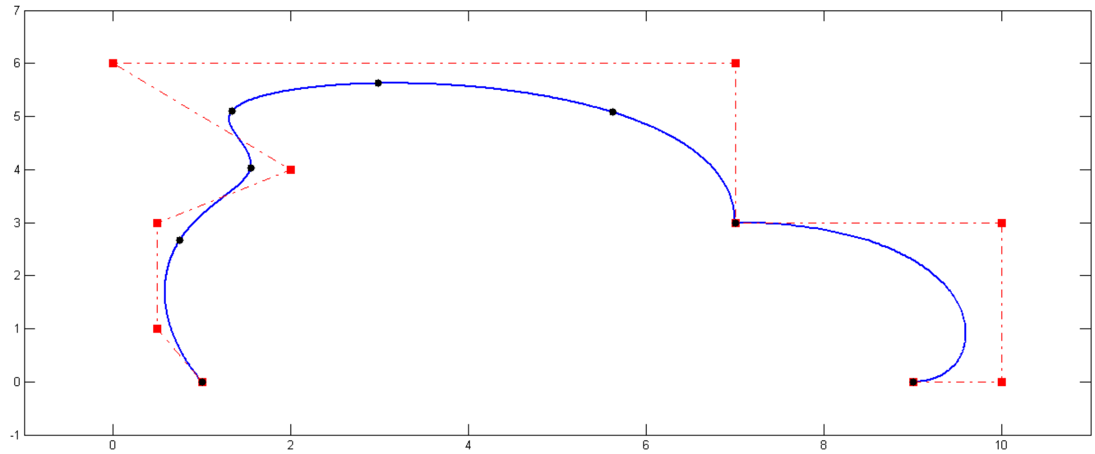

Fig.7. B-Spline curve of order $p = 3$ in R^2. The control points are symbolized by: ■. Knots define a mesh by dividing the curve into elements, they are denoted by: ●. The basis functions and the knot vector are shown in Fig.8.

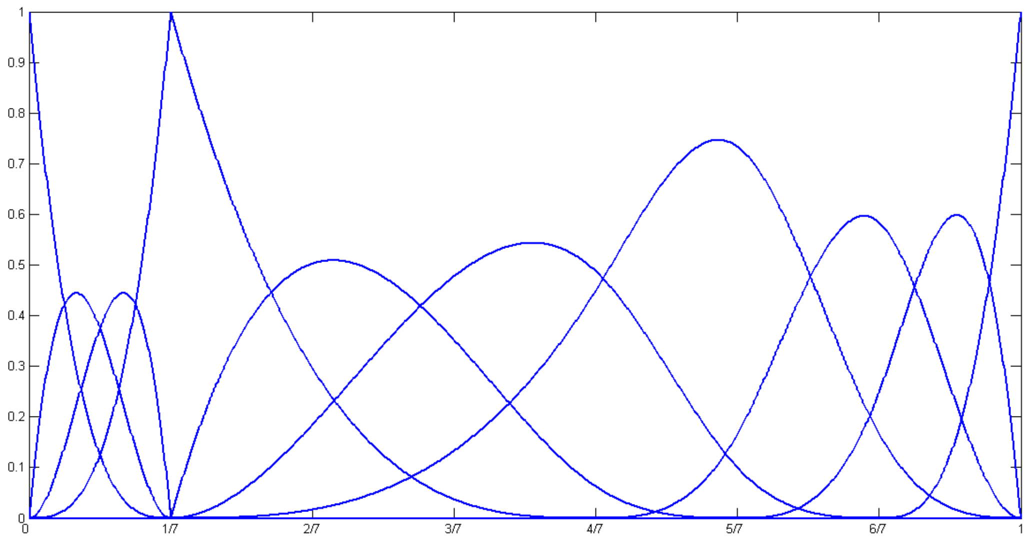

Fig.8. B-Spline basis functions of order $p = 3$ and knot vector

$$\Xi = \left\{0, 0, 0, 0, {}^{1}/_{7}, {}^{1}/_{7}, {}^{1}/_{7}, {}^{4}/_{7}, {}^{5}/_{7}, {}^{6}/_{7}, 1, 1, 1, 1\right\}.$$

The example shown in Fig.7 is constructed by the cubic (p=3) NURBS basis functions shown in Fig.8. The curve is interpolated at the first and last control points, the main feature of the curves being constructed by an open knot vector. To note that the curve is also interpolated at the fourth control point; this is due to the fact that the multiplicity of the knot ξ = 1/7 is equal to the order of the basis $p = 3$. Also, to note that the curve is tangent to the control polygon at the first, last and fourth control points.

The curve has a continuity of $C^{p-1} = C^2$ everywhere, except at the position of the repeated knots, $\xi = 1/7$, where the continuity of the curve is $C^{p-3} = C^0$. Finally, it could be noted that the knots divides the curve into elements (see Fig 7).

Some other properties of B-Spline curves:

Several properties of B-Spline curves derive directly from the properties of their basis functions:

B-Spline curve of degree p has $p-1$ continuous derivatives in the absence of repeated knots or control points.

Due to the local support of the B-Spline basic functions, the displacement of a control point can affect the geometry in only p + 1 curve elements (see Fig.7 and Fig.8).

The non-negativity and unit partition properties of the basis functions, combined with the local support property, imply that the B-Spline curve is completely contained in the convex hull defined by its control points (see Fig.7 and Fig.8).

Property of the decreasing variance: no plane has more intersections with the curve than with its control polygon.

2.2. Non Uniform Rational B-Splines (NURBS)

Non-uniform rational B-Splines NURBS have the definite advantage of being able to accurately represent cones sections (circles and ellipses). In addition, the NURBS basis offers an additional parameter called weight allowing a more flexible handling on the shape of the curve as will be seen further in this section.

From a geometrical point of view, NURBS curve defined in R^d is obtained by projective transformation of a B-Spline curve defined in R^{d+1}on the hyperplane (z = 1). To understand this concept, we consider the example illustrated in Fig.9, in which a circle defined in R^2 is constructed from a quadratic B-Spline curve defined in R^3. The transformation is performed by applying a projection of each point of the curve onto the plane (z = 1). We obtain the control points of the NURBS curve by performing the same transformation for the control points of the "original" B-Spline curve. In this context, the B-Spline curve $C^w(\xi)$ is called the "projective curve" associated with the "projective control points", B_i^w. The terms "curve" and "control point" are reserved for the curve NURBS $C(\xi)$ and B_i respectively.

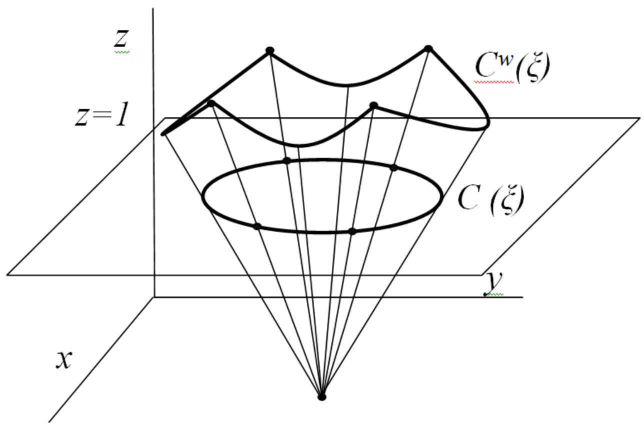

Fig. 9. A circle in R^2 constructed by the projective transformation of a piecewise quadratic B-spline in R^3

Weights w_i are the z component of B_i^w. The projective transformation of the B-Spline curve $C^w(\xi)$ produces the curve NURBS $C\ (\xi)$.

Control points of the curve are obtained by (2.5) and (2.6).

$$(B_i)_j = \frac{(B_i^w)_j}{w_i}, \quad j = 1, \dots, d \tag{2.5}$$

$$w_i = ((B_i^w)_{d+1} \tag{2.6}$$

where$(B_i)_j$ is the j^{th}component of B_i and w_i is the i^{th}*weight*.

In Fig.9 the weights are nothing more than the z components of the projective control points, these values are positive in most engineering applications. The division of the projective control points by their respective weights amounts to applying a projective transformation to them. In order to obtain the NURBS curve, the same transformation is applied to the projective B-Spline curve, this is done by dividing each basis function by its respective weight, this is done by defining the weight function (2.7).

$$W(\xi) = \sum_{i=1}^{n} N_{i,p}(\xi) w_i, \tag{2.7}$$

where$N_{i,p}(\xi)$ is a standard B-Spline basis function in R^3, $W(\xi)=z(\xi)$ is the weight of the curve according to parameter ξ. We can now define the NURBS curve by the relation (2.8).

$$(C(\xi))_j = \frac{(C^w(\xi))_j}{W(\xi)}, \quad j = 1, \dots., d. \tag{2.8}$$

Since $C^w\ (\xi)$ and $W\ (\xi)$ are both piecewise polynomial functions. The function $C^w\ (\xi)$ is a piecewise rational function, where each element is a "polynomial divided by another polynomial". In the previous relation (2.8), the two polynomials are of the same order; thus, "The order of the NURBS curve", is none other than the order of its basic functions.

Now we can approach the construction of NURBS curves in a more direct way. The main advantage of B-Spline curves is the ability to change their shape intuitively by adjusting the control points. The goal is to be able to manipulate the NURBS in the same intuitive way. To this end, we need to build NURBS basis functions from knot vector, then build the NURBS curves from a linear combination of the basis functions and control points. In this way, all that has been presented about B-Spline curves is also valid for NURBS. In this way NURBS basis functions are given by (2.9).

$$R_i^p = \frac{N_{i,p} w_i}{W(\xi)} = \frac{N_{i,p} w_i}{\sum_{i=1}^{n} N_{i,p}(\xi) w_i} \tag{2.9}$$

This is clearly, a piecewise rational function. Using (2.9) at the junction with the control points presented in (2.5), we arrive at the NURBS curve equation (2.10).

$$C(\xi) = \sum_{i=1}^{n} R_i^p(\xi) w_i \tag{2.10}$$

NURBS basis functions inherit the properties of their polynomial predecessors; in particular, the continuity and local support that derive directly from the knot vector. The base is always a partition of unity and is positive in every point.

It should be noted that weights play an important role in the definition of the base, but they are not associated with any explicit geometric interpretation in this setting. So, we are free to choose the control points regardless of their associated weights. Also, it should be noted that if all the weights are equal, we have$R_i^p(\xi) = N_{i,p}(\xi)$ and the curve is a polynomial again, so the B-Splines are just one particular case of NURBS.

The weights offer an additional degree of freedom for manipulating the curve without manipulating the control points, the effect of the variation of the weights on the curve is illustrated in Fig.10.

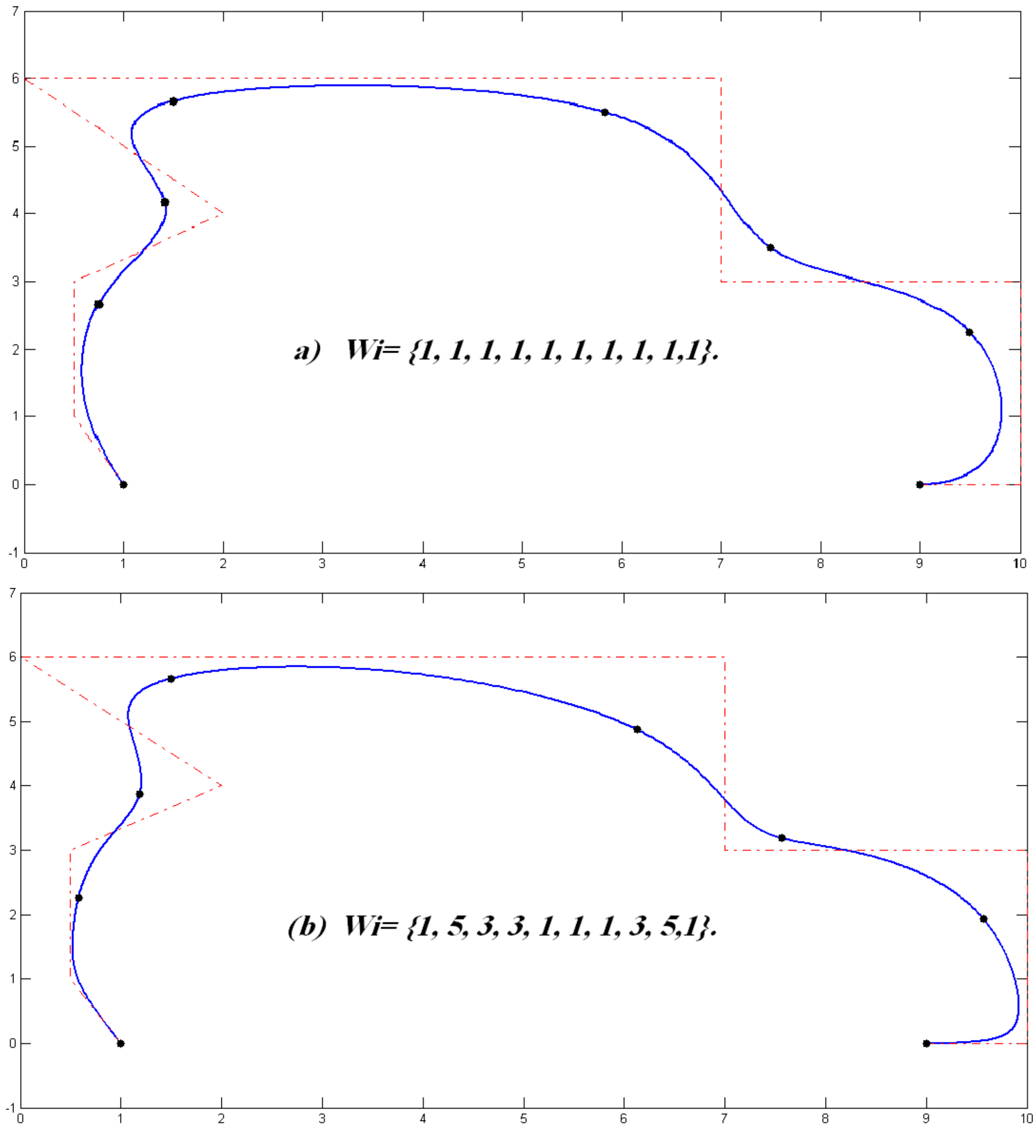

Fig.10.Manipulating the shape of a NURBS curve by adjusting the weightsw_i.

2.2.1. Derivatives of NURBS basis functions

As NURBS basis functions are built in terms of B-spline basis functions, the derivatives of the rational basis functions will certainly depend on their non rational counterparts; this may be proved by simply differentiating equation (2.8). The first derivative of NURBS basis function is given by relations (2.11) and (2.12).

$$\frac{d}{d\xi}(R_i^p(\xi)) = w_i \frac{W(\xi)\frac{d}{d\xi}(N_{i,p}(\xi)) - \frac{d}{d\xi}(W(\xi))(\xi)N_{i,p}(\xi)}{(W(\xi))^2} \tag{2.11}$$

where:
$$\frac{d}{d\xi}(W(\xi)) = \sum_{i=1}^{n} \frac{d}{d\xi}(N_{i,p}(\xi))w_i. \tag{2.12}$$

The differentiation of expression (2.11) gives the second derivative of the i^{th} rational basis function $\frac{d^2}{d\xi}R_i^p(\xi)$.

For the derivative of a higher order, an effective algorithm is proposed in reference [5].

2.3. Surface modeling

2.3.1. B-Spline surface

Given the network of control points $B_{i,j}$, $i=1, 2, \ldots, n$, $j=1, 2, \ldots, m$ and two B-Spline bases denoted $N_{i,p}(\xi)$ and $M_{j,q}(\eta)$ respectively of order p and q and knot vectors $\Xi=\{\xi_1, \xi_1, \ldots, \xi_{n+p+1}\}$ and $H=\{\eta_1, \eta_2, \ldots, \eta_{m+q+1}\}$. A B-Spline surface is given by (2.13).

$$S(\xi,\eta)=\sum_{i=1}^{n}\sum_{j=1}^{m}N_{i,p}(\xi)M_{j,q}(\eta)B_{i,j} \tag{2.13}$$

<u>Proprieties of B-Spline surfaces:</u>

Several properties of B-Spline surfaces result from the fact that they are obtained with a tensor product.Hereafterare enumerated some of these:

- The base is non-negative and forms a partition of the unit, since: $\forall(\xi,\eta)\in[\xi_1,\xi_{n+p+1}]\times[\eta_1,\eta_{m+q+1}]$,
$$\sum_{i=1}^{n}\sum_{j=1}^{m}N_{i,p}(\xi)M_{j,q}(\eta)=\left(\sum_{i=1}^{p}N_{i,p}(\xi)\right)\left(\sum_{j=1}^{q}M_{j,q}(\eta)\right) \tag{2.14}$$
- The number of continuous partial derivatives in a given parametric direction can be determined from the nodal vector and the polynomial order associated with this direction.
- Control point networks exert affine covariance and convex hull properties on the surface (see Fig.11).
- Local support for basic functions derives directly from the one-dimensional basic functions that form them. The support of a given function $\widetilde{N}_{i,j;p,q}(\xi,\eta)=N_{i,p}(\xi)M_{j,q}(\eta)$ is exactly: $[\xi_i,\xi_{i+p+1}]\times[\eta_j,\eta_{j+q+1}]$.

Now, consider the example of a biquadratic B-Spline surface (p = q = 2), represented in Fig.11 formed by the knot vectors Ξ = {0, 0, 0, 0.5 1, 1 , 1} and H = {0, 0, 0, 1, 1, 1}, with the control points network given in Table 3.

Table 3: Control points coordinates of B-Spline surface represented in Fig.11.

i	j	$B_{i,j}$
1	1	(0, 0, 0)
1	2	(-1, 0, 0)
1	3	(-2, 0, 0)
2	1	(0, 1, 0)
2	2	(-1, 2, 0)
2	3	(-2, 2, 0)
3	1	(1, 0.5, 1)
3	2	(1, 4, 1)
3	3	(1, 5, 1)
4	1	(3, 1.5, 1)
4	2	(3, 4, 1)
4	3	(3, 5, 1)

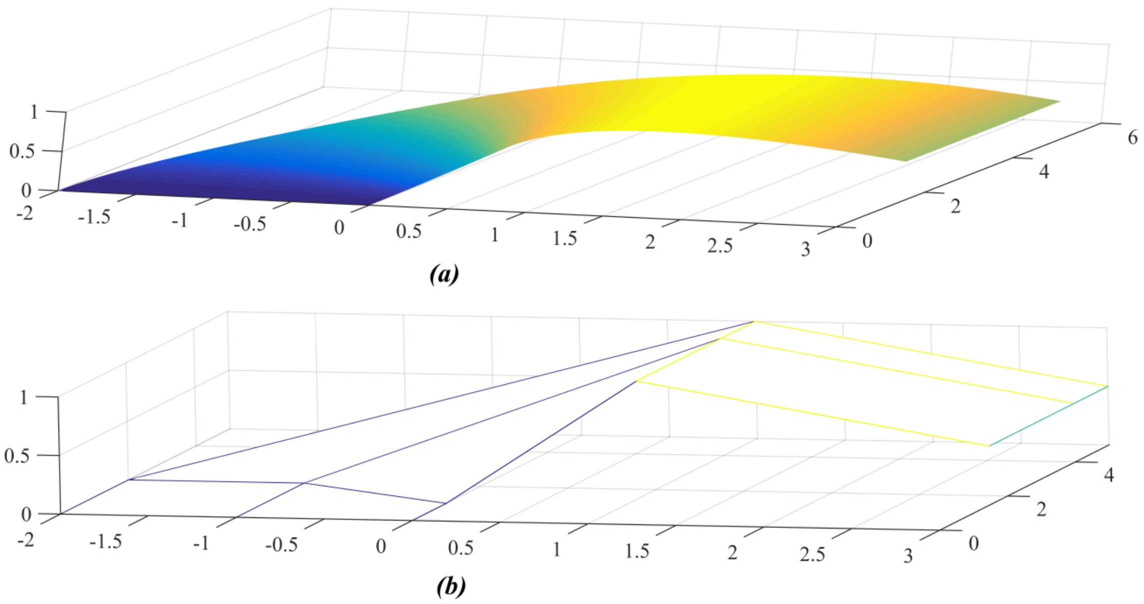

Fig.11. (a): Bi-quadratic B-Spline surface obtained with the Control points network represented in (b) and the knot vectors $\Xi = \{0, 0, 0, 0.5\ 1, 1\ , 1\}$ and $\mathrm{H} = \{0, 0, 0, 1, 1, 1\}$. The control points coordinates are given in Table 3.

For this case, the local support of $\widetilde{N}_{1,1;2,2}(\xi,\eta)$, is $[\xi_1,\xi_4] \times [\eta_1,\eta_4]$. Similarly, the local support of $\widetilde{N}_{3,2;2,2}(\xi,\eta)$, is $[\xi_3,\xi_6] \times [\eta_2,\eta_5]$. The local support of each of these functions is represented in the parametric space in Fig.12.a Now, it is easy to see exactly which nodal interval constitutes the support for each function, including the areas of overlap. We can also present the same information in the parametric space, as shown in Fig.12.b where we reported the current knot values. It is clear that here, we have only two important elements; therefore, two elements for which the calculations must be optimized during the analysis. The function

$\widetilde{N}_{3,2;2,2}(\xi,\eta)$ is supported by each of these elements, while $\widetilde{N}_{1,1;2,2}(\xi,\eta)$ is only supported by only one element.

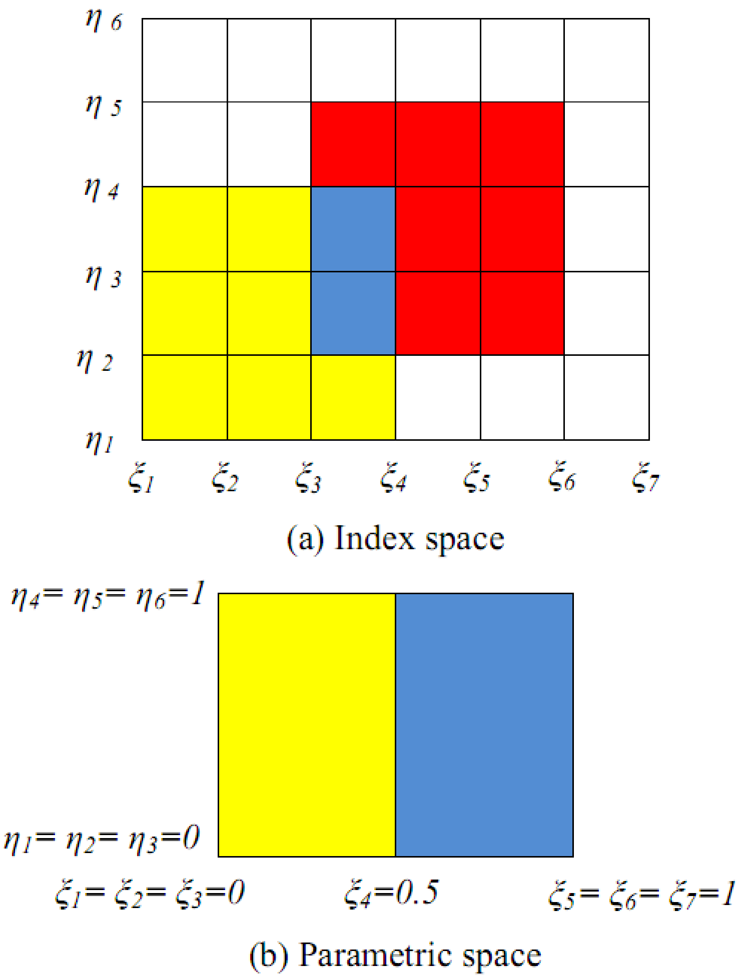

Fig.12. (a) Parametric space, where the support of $\widetilde{N}_{1,1;2,2}(\xi,\eta)$ is colored in gray, while thatof $\widetilde{N}_{3,2;2,2}(\xi,\eta)$, is colored black. The area where they overlap is dark gray. (b) Parametric space, where$\widetilde{N}_{3,2;2,2}(\xi,\eta)$ is supported by both elements, whereas $\widetilde{N}_{1,1;2,2}(\xi,\eta)$ is supported only by one.

2.3.2. NURBS Surfaces

As for polynomial surfaces, the NURBS surface is given by the tensor product (2.15).

$$S(\xi,\eta) = \sum_{i=1}^{n}\sum_{j=1}^{m} R_{i,p}(\xi) T_{j,q}(\eta) B_{i,j} \tag{2.15}$$

$R_{i,p}(\xi) and T_{j,q}(\eta)$are NURBS basis functions (2.16).

$$R_{i,j}^{p,q}(\xi,\eta) = \frac{N_{i,p}(\xi) M_{j,q}(\eta) w_{i,j}}{\sum_{\hat{\imath}=1}^{n}\sum_{\hat{\jmath}=1}^{m} N_{\hat{\imath},p}(\xi) M_{\hat{\jmath},q}(\eta) w_{\hat{\imath},\hat{\jmath}}} \tag{2.16}$$

$B_{i,j}$ is a network of control points and $w_{i,j}$ the weight of the control point.

These rational basis functions inherit the properties of their polynomial predecessors, in particular: the continuity of functions and local support that derive directly from the nodal vector, just as before. The base is always a partition of unity and is positive in every respect

It should be noted that weights play an important role in the definition of the base, but they are not associated with any explicit geometric interpretation in this setting, and we are free to choose the control points regardless of their associated weights. Also, it should be noted that if all the weights are equal, then $R_{i,j}^{p,q}(\xi,\eta) = N_{i,j;p,q}(\xi,\eta)$ and the curve is again apolynomial, so B-Splines are only a special case of NURBS [5].

2.3.3. Some techniques for building NURBS surfaces

2.3.3.a. Extrusion

An extruded surface is generated by a flat curve sliding along a rectilinear trajectory or not, the initial curve remains parallel to itself (pure translation). In the following example Fig.14, the extrusion of a cylindrical surface is made by the translation of a generating sketched circle Fig.13.

Sketch of the generator circle: The circle is one of the most common geometries in engineering design. There are several ways to build a circle using NURBS. In Fig.13, a complete circle was constructed from four 90 ° arcs, but using only one NURBS curve of order $p = 2$. The curve (the circle) is formed of four elements, a continuity of C^0 is ensured by the multiplicity $m=p$ at the boundaries of the elements, in this example the knot vector is Ξ = {0, 0, 0, 1/4, 1/4, 2/4, 2/4, 3/4, 3/4, 1, 1, 1}. It should be noted that the circle has been closed by positioning the first and last control points in the same position. Table 4 shows the coordinates of the control points and their respective weights.

Table 4: Coordinates of control points and their respective weights to the draw of Fig.13.

i	x_i	y_i	w_i
1	4	2	1
2	4	0	$1/\sqrt{2}$
3	2	0	1
4	0	0	$1/\sqrt{2}$
5	0	2	1
6	0	4	$1/\sqrt{2}$
7	2	4	1
8	4	4	$1/\sqrt{2}$
9	4	2	1

Extrusion: The NURBS cylender is extruded by sliding its generator sketched in the z direction, this is done by introducing a second NURBS base of order p=1. The base is thus $R_{i,j}^{2,1}(\xi,\eta) = S_{i,2}(\xi) \times T_{j,1}(\eta)$, such that $S_{i,2}(\xi)$ and $T_{j,1}(\eta)$are NURBS basis functions, respectively of order p = 2 and q = 1. the network of control points is given in Table 5.

Table 5: Coordinates of control points and their respective weights corresponding to Fig.14.

i	j	x	y	z	w_i	w_j
1	1	4	2	0	1	1
1	2	4	0	0	$1/\sqrt{2}$	1
1	3	2	0	0	1	1
1	4	0	0	0	$1/\sqrt{2}$	1
1	5	0	2	0	1	1
1	6	0	4	0	$1/\sqrt{2}$	1
1	7	2	4	0	1	1
1	8	4	4	0	$1/\sqrt{2}$	1
1	9	4	2	0	1	1
2	1	4	2	1	1	1
2	2	4	0	1	$1/\sqrt{2}$	1
2	3	2	0	1	1	1
2	4	0	0	1	$1/\sqrt{2}$	1
2	5	0	2	1	1	1
2	6	0	4	1	$1/\sqrt{2}$	1
2	7	2	4	1	1	1
2	8	4	4	1	$1/\sqrt{2}$	1
2	9	4	2	1	1	1

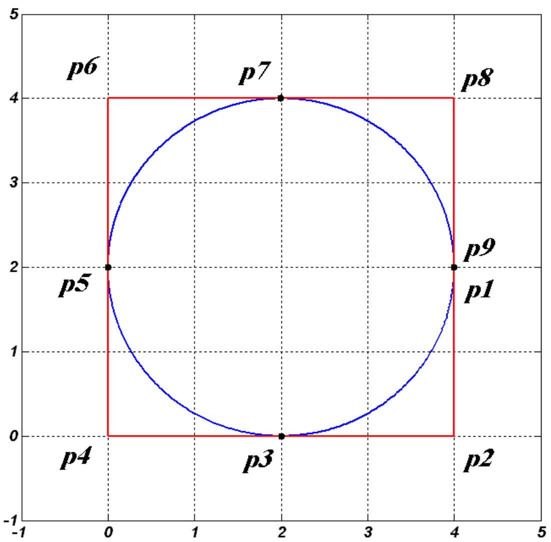

Fig.13. Circle sketched with a quadratic NURBS curve.

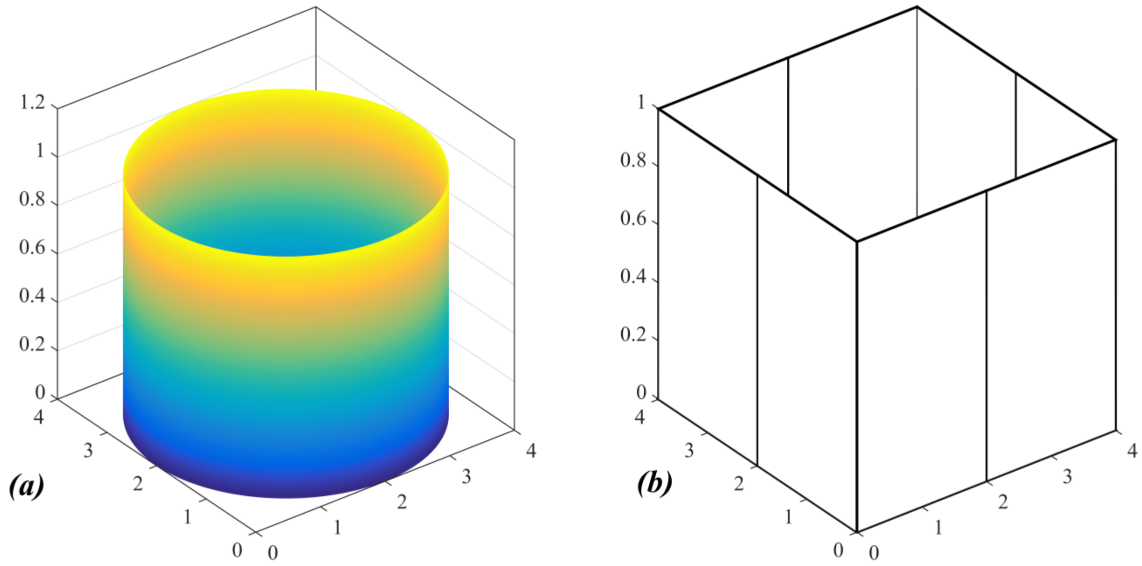

Fig.14. (a) NURBS cylindrical surface constructed from two bases of order p = 2 and q = 1.
(b) Network of control points.

2.3.3.b. Ruled surfaces

Ruled surface is generated from a line called "ruler" sliding along two curves (Fig.15).

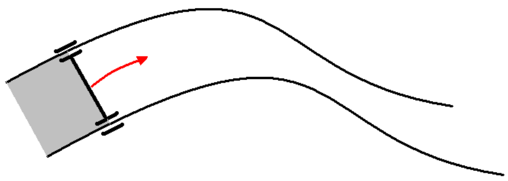

Fig.15. Construction principle of a ruled surface.

From algebraic point of view, a ruled surface is given by the relation (2.17).

$$S(\xi,\eta) = \sum_{i=1}^{p} \sum_{j=1}^{2} R_{i,p}(\xi).R_{j,1}(\eta).B_{ij} \qquad (2.17)$$

where: $R_{i,p}(\xi)$and$R_{j,1}$are NURBS basis functions, respectively of order p and 1.

Fig.17 shows a ruled surface generated by a straight lone sliding along two identical curves shown in Fig.16. Table.6 gives the control points and their respective weights.

Table 6: Coordinates of control points and their respective weights corresponding to the draw of Fig.17.

i	*j*	*x*	*y*	*z*	w_i	w_j
1	**1**	**9**	**0**	**0**	**1**	**1**
1	**2**	**10**	**0**	**0**	**1**	**1**
1	**3**	**10**	**3**	**0**	**1**	**1**
1	**4**	**7**	**3**	**0**	**1**	**1**
1	**5**	**7**	**6**	**0**	**1**	**1**
1	**6**	**0**	**6**	**0**	**1**	**1**
1	**7**	**2**	**4**	**0**	**1**	**1**
1	**8**	**0.5**	**3**	**0**	**1**	**1**
1	**9**	**0.5**	**1**	**0**	**1**	**1**
1	**10**	**1**	**0**	**0**	**1**	**1**
2	**1**	**9**	**0**	**2**	**1**	**1**
2	**2**	**10**	**0**	**2**	**1**	**1**
2	**3**	**10**	**3**	**2**	**1**	**1**
2	**4**	**7**	**3**	**2**	**1**	**1**
2	**5**	**7**	**6**	**2**	**1**	**1**
2	**6**	**0**	**6**	**2**	**1**	**1**
2	**7**	**2**	**4**	**2**	**1**	**1**
2	**8**	**0.5**	**3**	**2**	**1**	**1**
2	**9**	**0.5**	**1**	**2**	**1**	**1**
2	**10**	**1**	**0**	**2**	**1**	**1**

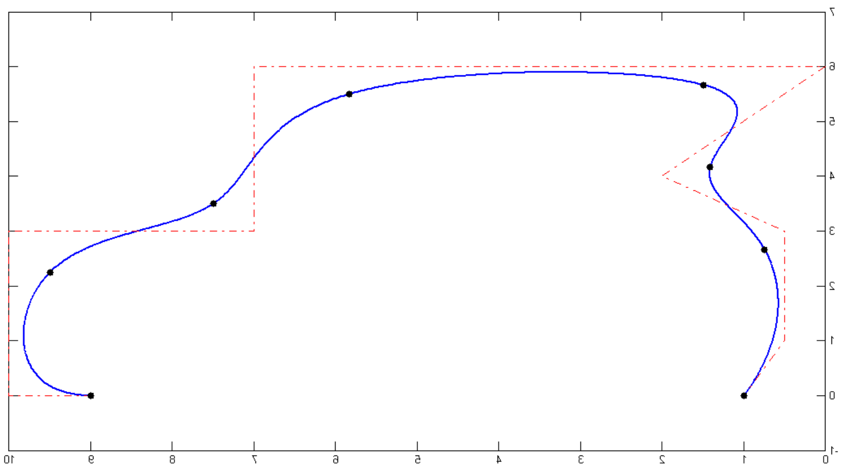

Fig.16. NURBS curve generating the set surface shown in Fig.17.

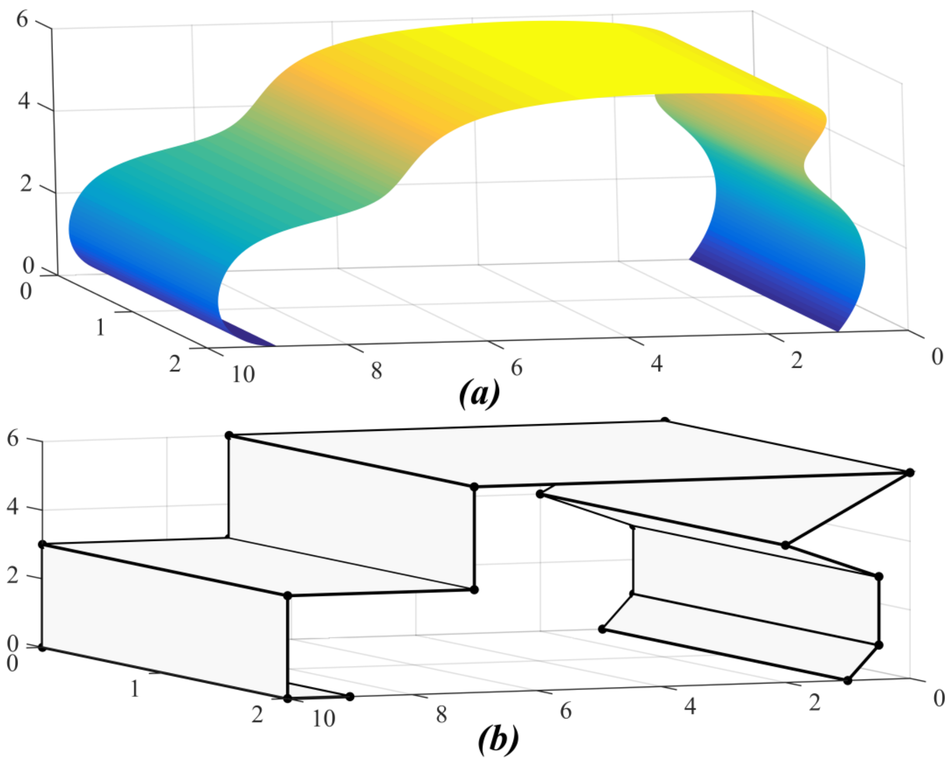

Fig.17. (a).NURBS ruled surface. (b). Network of control points.

2.3.3.c. Surface of revolution

Let a curve C (ξ) in a given plane $(\overrightarrow{Ox}, \overrightarrow{Oz})$ in 3D space. A surface of revolution is generated by the rotation of C (ξ) around a defined axis $\overrightarrow{Oz}$. The control points network must be constructed on planes perpendicular to $\overrightarrow{Oz}$ (See Fig.18).

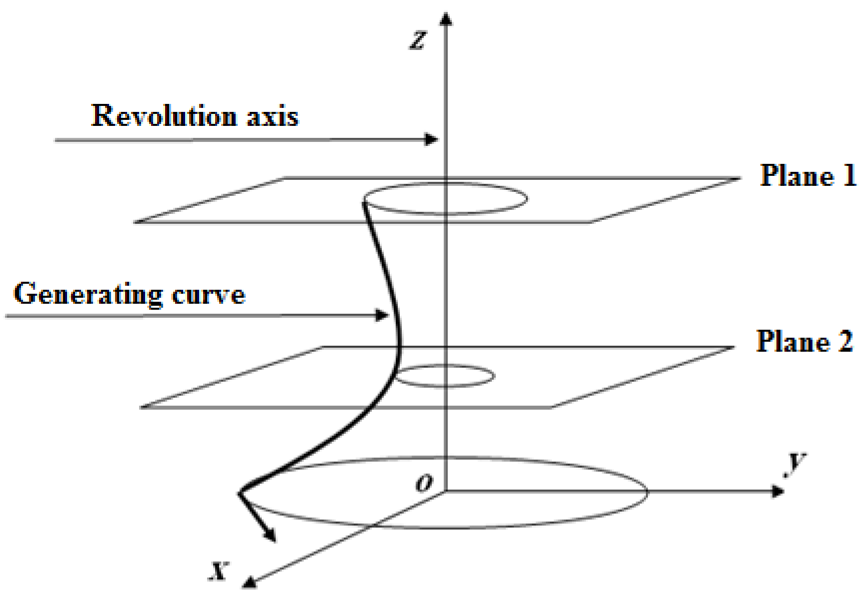

Fig.18. NURBS surface generated by the revolution of the generating curve around $\overrightarrow{\boldsymbol{Oz}}$ axis.

In practice, one of the methods for building a NURBS surface of revolution is given in (2.18).

$$S(\xi,\eta) = \sum_{i=1}^{8}\sum_{j=1}^{q} R_{i,2}(\xi).R_{j,n}(\eta).B_{ij} \tag{2.18}$$

In the above equation:

- $\boldsymbol{R_{i,2}}$ and$\boldsymbol{R_{j,p}}$ are NURBS basis functions of orders 2 and *p*respectively**.**
- In order to ensure the circular revolution, one can choose the weights of the quadratic basis $R_{i,2}$, as follows: $w_i = \left\{1, \frac{\sqrt{2}}{2}, 1, \frac{\sqrt{2}}{2}, 1, \frac{\sqrt{2}}{2}, 1, \frac{\sqrt{2}}{2}, 1\right\}$. and knot vector: $\Xi = \{0,0,0,\frac{1}{4},\frac{1}{4},\frac{2}{4},\frac{2}{4},\frac{3}{4},\frac{3}{4},1,1,1\}$see Fig.14 (sketch of a circle).
- The control points must be carefully chosen so that the characteristic network is symmetrical with respect to the axis of revolution.

As example, we give the case represented in Fig.19 showing a surface of revolution about the axis passing through the point *A* (2, 2, 0) and parallel to the axis $\overrightarrow{Oz}$.

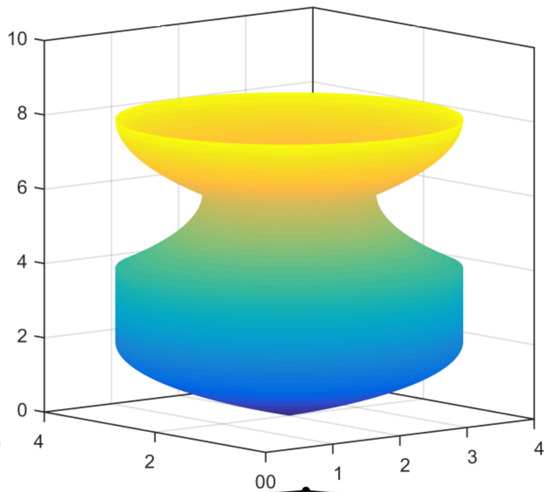

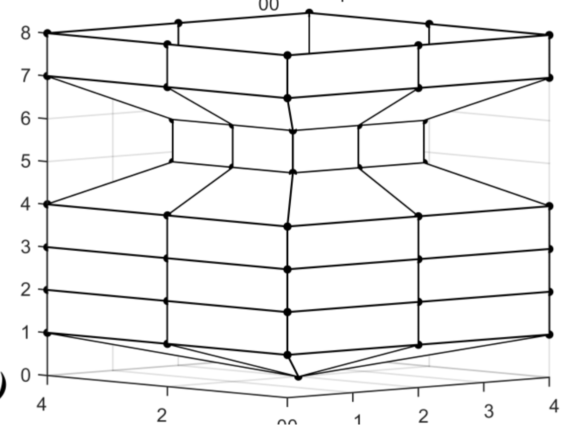

Fig.19. (*a*) Surface of revolution about the axis passing through A and parallel to$\overrightarrow{\boldsymbol{Oz}}$.
(*b*)Characteristic networks.

In the next chapter (chapter 3), we present the theoretical foundations of the isogeometric collocation method followed by a more practical presentation in chapter 4.

Ch3

3. Isogeometric Collocation Method (IGA-C)

The goal of this chapter is to present the Isogeometric collocation method for solving PDEs and more precisely eigenvalue problems modelling the dynamical behaviour of structures.However, imposition of boundary conditions will be dealt with in the next chapter (Chapter 4) with the first application. Indeed, we propose in this work a new formula of injection of boundary conditions.

As is stated in the introduction, the IGA-C is a collocation method that uses NURBS as shape functions. In consequence, we present firstly the theoretical bases of collocation methods (pseudo-spectral methods). Then, we introduce the IGA-C.

3.1. Collocation methods: general principle and foundation

The basic idea is to assume that the unknown $u(x)$ can be approximated by a sum of $N+1$ "basis functions" $R_n(x)$ and $N+1$ coefficients of expansion u_i as in (3.1).

$$u(x) \approx u^p(x) = \sum_{i=0}^{n} u_i R_i(x_j) \tag{3.1}$$

When this series is substituted into equation (3.2).

$$Lu = f(x) \tag{3.2}$$

Where L is the operator of the differential or integral equation, the result defined by (3.3) is called "residual function"

$$R(x; a_0, a_1, \dots, a_N) = Lu - f(x) \tag{3.3}$$

When $R(x;\ a_n)$ is identically equal to zero the solution is exact. The challenge is to choose the series coefficients so that the residual function is minimized. The different spectral and pseudo-spectral methods differ mainly in their minimization strategies.

Example:

To better explain the concept of collocation method, take the case of a simple problem such as the one dimensional linear PDE (3.4).

$$\begin{cases} u_{xx} - (x^6 + 3x^2)u = 0 \\ u(-1) = u(1) = 1 \end{cases} \tag{3.4}$$

The exact solution of (3.4) is (3.5) (see [19]).

$$u(x) = e^{((x^4-1)/4)} \tag{3.5}$$

As polynomial approximations are recommended for most problems, we choose a spectral solution (3.6). In order to satisfy the boundary conditions independently of the unknown spectral coefficients, it is convenient to write the approximation as in (3.6).

$$u_2 = 1 + (1 - x^2)(a_0 + a_1 x + a_2 x^2) \tag{3.6}$$

The decision to keep only three degrees of freedom is arbitrary.

The substitution of the solution (3.6) in equation (3.4) gives (3.7).

$$R(x; a_0, a_1, \dots, a_N) = u_{2,xx} - (x^6 + 3x^2)u_2 \tag{3.7}$$

The residue*R (x, a0, a1, a2)* is given in (3.8).

$$\begin{aligned} R = (2a_2 + 2a_0) - 6a_1 x - (3 + 3a_0 + 12a_2)x^2 - 3a_1 x^3 + 3(a_0 - a_2)x^4 \\ +3a_1 x^5 + (-1 - a_0 + 3a_2)x^6 - a_1 x^7 + (a_0 - a_2)x^8 + a_1 x^9 + 10a_2 x^{10} \end{aligned} \tag{3.8}$$

As error minimization conditions, we choose to make the residual zero at a set of points equal in number to that of the unknowns coefficients in $u_2(x)$. This is called the “collocation” or “pseudo-spectral” method. If we arbitrarily choose the points $x_i=\{-1/2\ ;\ 0;\ 1/2\}$, this gives the three equations (3.9).

$$\begin{cases} -\frac{659}{256}a_0 + \frac{1683}{512}a_1 - \frac{1171}{1024}a_2 - \frac{49}{64} = 0 \\ 2(a_0 - a_2) = 0 \\ -\frac{659}{256}a_0 - \frac{1683}{512}a_1 - \frac{1171}{1024}a_2 - \frac{49}{64} = 0 \end{cases} \tag{3.9}$$

The coefficients (3.10) are then determined by solving (3.9).

$$a_0 = -\frac{784}{3807}, \quad a_1 = 0, \quad a_2 = a_0 \tag{3.10}$$

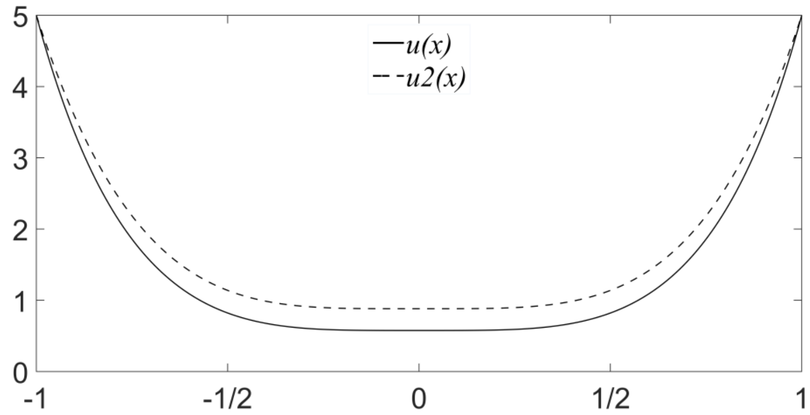

Fig.20. Exact solution *u(x)* and collocated solution $u_2(x)$ of equation (3.4).

Remarks

Choosing powers of *x* as a basis is actually rather dangerous unless *N*, the number of degrees-of-freedom, is small or the calculations are being done in exact arithmetic. In the following, we describe the good choices.

The obtained algebraic equations (3.9)could be written in matrix form to be solved by library software in Matlab, FORTRAN or C…

The method is not necessarily harder to program than finite difference or finite element algorithms.

Collocation methods are not purely numerical. When N is sufficiently small, Chebyshev and Fourier methods yield an analytic answer; that's why it's sometimes called a semi-analytical method.

3.2. Interpolation and collocation principles

The collocation (pseudo-spectral) family of algorithms is closely related to the Galerkin method. To show this and to understand the mechanics of pseudo-spectral methods, it is necessary to review some classical numerical analysis: polynomial interpolation, trigonometric interpolation, and Gaussian integration.

Interpolation

The interpolation of a function *f(x)* consists to an expression $P_{N-1}(x)$ (3.11), usually an ordinary or trigonometric polynomial.whose*N* degrees of freedom are determined by the requirement that the interpolant agree with *f(x)* at each of a set of *N* interpolation points (3.11).

$$P_{N-1}(x_i) = f(x_i) \quad i = 1,2,\dots,N \tag{3.11}$$

In the following, we will discuss the choice of interpolation points and methods for computing the interpolant.

It could be noted that the expressions "interpolation points" and "collocation points" refer identically to the set of points where the function is evaluated in the approximation. However, "interpolation" has the connotation that *f(x)*, the function which is being approximated by a polynomial, is already a known function. "Collocation" and "pseudo-spectral" are applied to interpolatory methods for solving differential equations for an unknown function *f(x)*.

3.3. Polynomial interpolation

Linear interpolation consists to draw a straight line between two known values of *f(x)* situated at the abscissa x_0 and x_1 which bracket the desired x. The value of the linear function at x is then taken as the approximation to *f(x)* see Fig.21.This operation can be represented algebraically by the equation (3.12).

$$P_1(x) \approx \frac{(x-x_1)}{(x_0-x_1)} f(x_0) + \frac{(x-x_0)}{(x_1-x_0)} f(x_1) \tag{3.12}$$

$$\text{where} P_1(x_0) = f(x_0)\,, P_1(x_1) = f(x_1) \tag{3.13}$$

Linear interpolation is not very accurate unless the tabulated points are very close together, but one can extend this idea to higher orders. Fig.21 illustrates quadratic interpolation. A parabola is uniquely specified by giving any three points upon it. Thus, we can alternatively approximate *f(x)* by the quadratic polynomial $P_2(x)$ (3.14) which satisfies the three interpolation conditions (3.15).

$$P_2(x) \approx \frac{(x-x_1)}{(x_0-x_1)} \frac{(x-x_2)}{(x_0-x_2)} f(x_0) + \frac{(x-x_0)}{(x_1-x_0)} \frac{(x-x_2)}{(x_1-x_2)} f(x_1) + \frac{(x-x_0)}{(x_2-x_0)} \frac{(x-x_1)}{(x_2-x_1)} f(x_2) \tag{3.14}$$

$$\text{where} P_2(x_0) = f(x_0)\,,\ P_2(x_1) = f(x_1)\ ,\ P_2(x_2) = f(x_2) \tag{3.15}$$

In general, one may fit any $N+1$points by a polynomial of N^{th}degree via Lagrange interpolation formula (3.16).

$$P_N(x) \equiv \sum_{i=0}^{N} f(x_i) C_i(x) \tag{3.16}$$

where the $C_i(x)$, the "cardinal functions", are polynomials of degree N which satisfy the conditions (3.17).

$$C_i(x_j) = \delta_{ij} \tag{3.17}$$

whereδ_{ij} is the Kroneckerδ function. The cardinal functions are defined in (3.18).

$$C_i(x_j) = \prod_{j=0, j\neq i}^{N} \frac{(x-x_j)}{(x_i-x_j)} \tag{3.18}$$

The N factors of $(x\text{-}x_i)$ insure that $C_i(x)$ vanishes at all the interpolation points except x_i. (Note that we omit the factor $j=i$ so that $C_i(x)$ is a polynomial of degree N, not $(N+1)$) The denominator forces $C_i(x)$ to equal 1 at the interpolation point $x=x_i$; at that point, every factor in the product is $(x_i\text{-}x_j)/(x_i\text{-}x_j)=1$. The cardinal functions are also called the "fundamental polynomials for pointwise interpolation", the "elements of the cardinal basis", the "Lagrange basis", or the "shape functions".

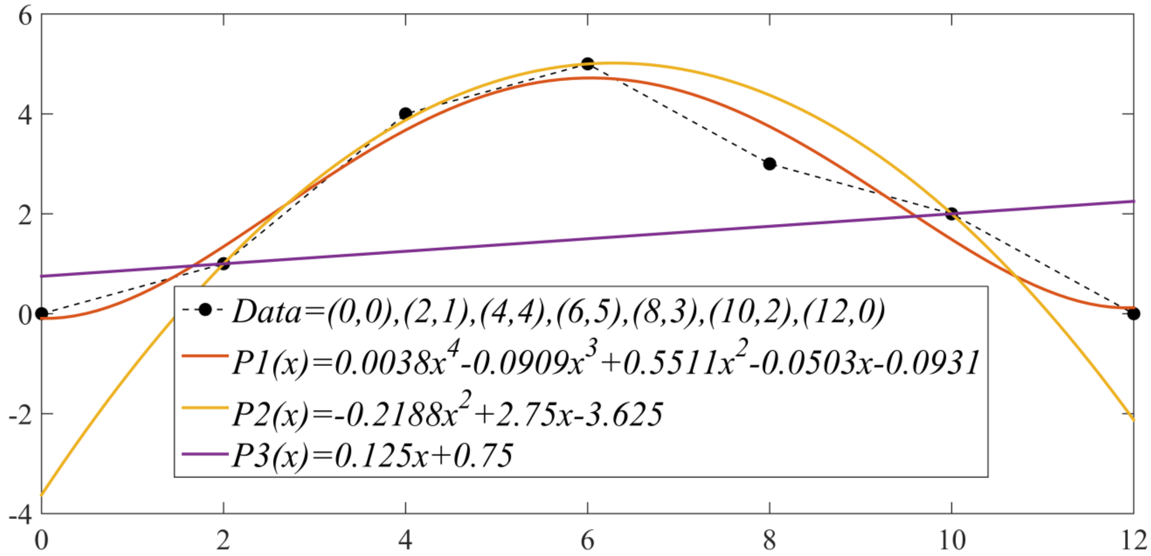

Fig. 21.Linear, quadratic and 4th degree polynomial interpolation of the described set of points. Note that the linear interpolation is performed using two points {(2,1),(10,2)} , the quadratic one with three points {(2,1),(6,5),(10,2)}. Finally the 4th order one with the entire Data base.

3.4. Gaussian Integration & Pseudo-spectral Grids

The reason why "collocation" methods are alternatively labelled "pseudo-spectral" is that the optimum choice of the interpolation points, makes collocation methods identical with the Galerkin method if the inner products are evaluated by a type of numerical quadrature known as "Gaussian integration". Numerical integration and Lagrangian interpolation are very closely related because one obvious method of integration is to fit a polynomial to the integrand $f(x)$ and then integrate $P_N(x)$. Since the interpolant can be integrated exactly, the error comes entirely from the difference between $f(x)$ and $P_N(x)$ (3.19) [1].

$$\int_a^b f(x)\,dx \approx \sum_{i=0}^{N} w_i f(x_i) \tag{3.19}$$

The quadrature weights functions w_i are given by (3.20)

$$w_i = \int_a^b C_i(x)\,dx \tag{3.20}$$

where the $C_i(x)$ are the cardinal functions on the set of fixing points as defined by (3.18) above.

3.5. Collocation points for NURBS basis

The selection of points guaranteeing a stable interpolation is a fundamental issue for a collocation scheme. In NURBS-based collocation literature, the so-called Greville abscissa have been widely adopted as the default choice, given their simple definition and good results from a practical point of view in virtually every situation. The Greville abscissas are defined from the knot vector Ξ as averages of consecutive knots as in (3.21). The Greville abscissas are the maxima of the basis functions.

$$\xi_j = \frac{\xi_{j+1} + \xi_{j+2} + \cdots + \xi_{j+p}}{p}, \qquad j = 1,2,\dots,n \tag{3.21}$$

Note that ξ_j represents elements of the knot vector defined in the previous section.

3.6. Isogeometric collocation method

The limits of the collocation methods come out to be those of the shape functions used for approximating the solutions.

The first step is thus to write the solutions approximating the function *u (x)* and its derivatives as linear combination of *n* NURBS basis functions and *n* control variables as (3.22) and (3.23.a.b).

L is the physical length of the space to interpolate(eg. length of the beam)and$x \in [0, L]$. ξ is the parametric variable defined by : $\xi = \frac{x}{L} \in [0, 1]$.

Thereafter, an algebraic system is built by writing the expression of the solution on a set of collocation points$\xi_j$as in (3.22).

$$u(x_j) \approx u(\xi_j) = \sum_{i=0}^{n} u_i R_i(\xi_j) = \begin{bmatrix} R_1(\xi_1) & R_2(\xi_1) & \dots & R_n(\xi_1) \\ R_1(\xi_2) & R_2(\xi_2) & \cdots & R_n(\xi_2) \\ \vdots & \vdots & \ddots & \vdots \\ R_1(\xi_j) & R_2(\xi_j) & \cdots & R_n(\xi_j) \end{bmatrix} \begin{bmatrix} u_1 \\ u_2 \\ \vdots \\ u_n \end{bmatrix} = [R]\{u\} \tag{3.22}$$

Similarly, one obtains the expression of the successive derivatives with $[R']$, $[R'']$ as described in (3.23.a.b).

$$u'(x_j) \approx \frac{1}{L} u'(\xi_j) = \frac{1}{L}[R']\{u\} \quad (3.23.a) \qquad u''(x_j) \approx \frac{1}{L^2} u''(\xi_j) = \frac{1}{L^2}[R'']\{u\} \quad (3.23.b)$$

where ' stands for the differentiation with respect to ξ.

Substituting the approximate solutions (3.22) and (3.23.a.b) in the considered PDE (3.4) gives (3.24).

$$\frac{1}{L^2}[R'']\{u\} - (x_j^6 + 3x_j^2)[R]\{u\} = \{0_{N\times 1}\}$$

$$\Leftrightarrow \left(\frac{1}{L^2}[R''] - (x_j^6 + 3x_j^2)[R]\right)\{u\} = \{0_{N\times 1}\} \tag{3.24}$$

Equation (3.24) should be written in compact form (3.25).

$$[H]\{u\} = \{0_{N\times 1}\} \tag{3.25}$$

where$\{A\} = \{u_1, u_2, \dots, u_n\}^T$

The developed boundary conditions imposing technique will be presented in the next chapter with the first application.

Ch4

4. In-plane vibration of Timoshenko straight beam

4.1 Equation of motion

To derive the equation of motion of a homogeneous Timoshenko beam of constant rectangular section and unity width, we consider the dynamical equilibrium equation (4.1).

$$\begin{cases} \dfrac{\partial M}{\partial x} + V = \rho I \dfrac{\partial^2 \Theta}{\partial t^2} \\ \dfrac{\partial T}{\partial x} = \rho h \dfrac{\partial^2 \mathrm{V}}{\partial t^2} \end{cases} \tag{4.1}$$

where$V=V\ (x,\ t)$ is the transverse deflection, $\Theta=\Theta\ (x,\ t)$ the rotation of the transverse line about the y axis, ρ the mass density of the beam material, h the thickness of the beam, I the second moment of inertia. $M=M\ (x,\ t)$ the bending moment and $T=T\ (x,\ t)$ the shearing force.

M and T are given by (4.2).

$$\begin{cases} M = EI \dfrac{\partial \Theta}{\partial x} \\ T = \alpha G h (\dfrac{\partial \mathrm{V}}{\partial x} - \Theta) \end{cases} \tag{4.2}$$

where$E$ is the Young modulus, G the shear modulus and α the shear correction factor.

The Fourier method of variables separation is used to find functions satisfying system (4.2). It is assumed that each function *V (x, t)* and *Θ (x, t)* can be represented in the form of product of a function dependent on the spatial coordinate *x* and a function dependent on time coordinate *t* (4.3).

$$\begin{cases} \Theta(x,t) = \theta(x)\cos(\omega t) \\ \mathrm{V}(x,t) = v(x)\cos(\omega t) \end{cases} \tag{4.3}$$

Substituting (4.3) and (4.2) into (4.1) yields (4.4).

$$\begin{cases} EI\dfrac{d^2\theta}{dx^2} + \alpha hG\left(\dfrac{\partial v}{\partial x} - \theta\right) = -\omega^2\rho I\theta \\ -\alpha hG\dfrac{d\theta}{dx} + \alpha hG\dfrac{d^2 v}{dx^2} = -\omega^2\rho h v \end{cases} \tag{4.4}$$

Equation (4.4) is an eigenvalue problem. Its resolution amounts to finding the eigenvalues ω_j and their associated eigenmodes.

4.2 Discretisation of the problem

The first step is thus to write the solutions approximating the functions *v (x)* and *θ (x)* and their derivatives as linear combination of *n* basis functions and *n* control variables as (4.5.a.b).

L is the length of the beam and $x \in [0, L]$. ξ is the parametric variable defined by : $\xi = \frac{x}{L} \in [0, 1]$.

Thereafter, an algebraic system is built by writing the expression of the solution on a set of collocation pointsξ_j.

$$v(x_j) \approx v(\xi_j) = \sum_{i=0}^{n} v_i R_i(\xi_j) = \begin{bmatrix} R_1(\xi_1) & R_2(\xi_1) & \dots & R_n(\xi_1) \\ R_1(\xi_2) & R_2(\xi_2) & \cdots & R_n(\xi_2) \\ \vdots & \vdots & \ddots & \vdots \\ R_1(\xi_j) & R_2(\xi_j) & \cdots & R_n(\xi_j) \end{bmatrix} \begin{bmatrix} w_1 \\ w_2 \\ \vdots \\ w_n \end{bmatrix} = [R]\{v\} \tag{4.5.a}$$

$$\theta(x_j) \approx \theta(\xi_j) = \sum_{i=0}^{n} \theta_i R_i(\xi_j) = \begin{bmatrix} R_1(\xi_1) & R_2(\xi_1) & \dots & R_n(\xi_1) \\ R_1(\xi_2) & R_2(\xi_2) & \cdots & R_n(\xi_2) \\ \vdots & \vdots & \ddots & \vdots \\ R_1(\xi_j) & R_2(\xi_j) & \cdots & R_n(\xi_j) \end{bmatrix} \begin{bmatrix} \theta_1 \\ \theta_2 \\ \vdots \\ \theta_n \end{bmatrix} = [R]\{\theta\} \tag{4.5.b}$$

Similarly, one obtains the expression of the successive derivatives with $[R']$, $[R'']$ as described in (4.6.a.b.c.d).

$$\theta'(x_j) \approx \tfrac{1}{L}\theta'(\xi_j) = \tfrac{1}{L}[R']\{\theta\} \qquad (4.6.a) \qquad \theta''(x_j) \approx \tfrac{1}{L^2}\theta''(\xi_j) = \tfrac{1}{L^2}[R'']\{\theta\} \qquad (4.6.b)$$

$$v'(x_j) \approx \tfrac{1}{L}w'(\xi_j) = \tfrac{1}{L}[R']\{v\} \qquad (4.6.c) \qquad v''(x_j) \approx \tfrac{1}{L^2}w''(\xi_j) = \tfrac{1}{L^2}[R'']\{v\} \qquad (4.6.d)$$

Where ' stands for the differentiation with respect to ξ.

Substituting the approximate solutions (4.5) and (4.6) in the considered problem (4.4) gives (4.7).

$$\begin{cases} \left(\frac{EI}{L^2}[R''] - \alpha hG[R]\right)\{\theta\} + \frac{\alpha hG}{L}[R']\{v\} = -\omega^2\rho I[R]\{\theta\} \\ \qquad -\frac{\alpha hG}{L}[R']\{\theta\} + \frac{\alpha hG}{L^2}[R'']\{v\} = -\omega^2\rho h[R]\{v\} \end{cases} \tag{4.7}$$

The above system can be rewritten in matrix form as given by (4.8).

$$\begin{bmatrix} \left(\frac{EI}{L^2}[R''] - \alpha hG[R]\right) & \frac{\alpha hG}{L}[R'] \\ -\frac{\alpha hG}{L}[R'] & \frac{\alpha hG}{L^2}[R''] \end{bmatrix} \begin{bmatrix} \{\theta\} \\ \{v\} \end{bmatrix} = -\omega^2 \begin{bmatrix} \rho I[R] & 0 \\ 0 & \rho h[R] \end{bmatrix} \begin{bmatrix} \{\theta\} \\ \{v\} \end{bmatrix} \tag{4.8}$$

Equation (4.8) should be written in compact form (4.9).

$$[H]\{A\} = -\omega^2[S]\{A\} \tag{4.9}$$

where$\{A\} = \{\theta_1, \theta_2, \dots, \theta_n, v_1, v_2, \dots, v_n\}^T$

4.3. Imposing the boundary conditions

In this work, we propose a practical way of injecting the boundary conditions in various configurations of structures without operating on the basis functions.This method was developed and published in the frame of this thesis (see [18]).

T. Mikami and J. Yoshimura [20] proposed a method of imposing the boundary conditions for the pseudo-spectral method using Tchebychev polynomials. Its principle is to adopt additional collocation points to beused for the injection of the boundary conditions. That of course works well on Tchebychev base of which each function is defined on the whole definition interval of the base as in Fig 22 *(a)*. However, the nature of NURBS makes impossible the application of this known method. Effectively, a NURBS function of order *p* has significant value only on a domain of *p+1* knot intervals (see chapter 2), in Fig 22 *(b),* it can be observed that $R_n(0)=0$. This mean that the last function of a basis set might have no effect on the boundary of abscissa *x=0*. In what follows, we present an adaptation of the mentioned method for NURBS base.

The boundary conditions are imposed on the system in the following four steps:

a. Each side of the eigenvalues problem (4.9) is decomposed into two expressions as in (4.10). The first one ($[H_r]\{A_r\}$ and $[S_r]\{A_r\}$) contains the matrix elements relative to the internal collocation points and internal physical nodal abscissas. The second one ($[H^+]\{A^+\}$ and $[H^+]\{A^+\}$) contains the matrix elements relative to the internal physical nodal abscissas and the boundaries collocation points (ξ=0 and ξ=1).
b. The boundary conditions equations are approached with a linear combination of the same set of basis functions and collocation points as for the equation of motion. Table 7 illustrates the most common ideal and non ideal boundary condition equations and their respective approximations.
c. The obtained boundary conditions equation system is than decomposed into two expressions as in (4.15). The first one ($[U]\{A_r\}$) contains the matrix elements relative to the internal collocation points and the boundaries physical nodal abscissas ($x=0$ and $x=L$). The second one ($[V]\{A^+\}$) contains the matrix elements relative to boundaries physical nodal abscissas ($x=0$ and $x=L$) and boundaries collocation points (ξ=0 and ξ=1).
d. Finally, the value of $\{A^+\}$ is taken from equation (4.15) and injected to equation (4.10) to obtain the eigenvalues problem (4.16) satisfying the selected boundary conditions.

$$[\boldsymbol{H_r}]\{\boldsymbol{A_r}\} + [\boldsymbol{H}^+]\{\boldsymbol{A}^+\} = -\boldsymbol{\omega}^2([\boldsymbol{S_r}]\{\boldsymbol{A_r}\} + [\boldsymbol{S}^+]\{\boldsymbol{A}^+\}) \tag{4.10}$$

where $\{A_r\} = \{\theta_2\theta_3 \dots \theta_{n-1} w_2 w_3 \dots w_{n-1}\}^T and \{A^+\} = \{\theta_1\theta_n w_1 w_n\}^T$

Note that the size of $[\boldsymbol{H_r}]$ is ***2(n-2)*** × ***2(n-2)*** and that of $[\boldsymbol{H}^+]$ is ***2(n-2)×4***. The full number of unknown factors in $\{\boldsymbol{A}\}$ and $\{\boldsymbol{A}^+\}$ is $\boldsymbol{n}$ while the number of equations is ***n-4***. The remaining four equations are obtained with the boundary conditions.

Let us impose a condition to the j^{th}node. The four ideal boundary conditions mentioned above are represented in the first four lines of table 1 and their effects on the system in the second column. One should represent the effect of the condition associated to the coordinate ξ_j using relations (4.2), (4.5) and (4.6) as in the third column of table 7.

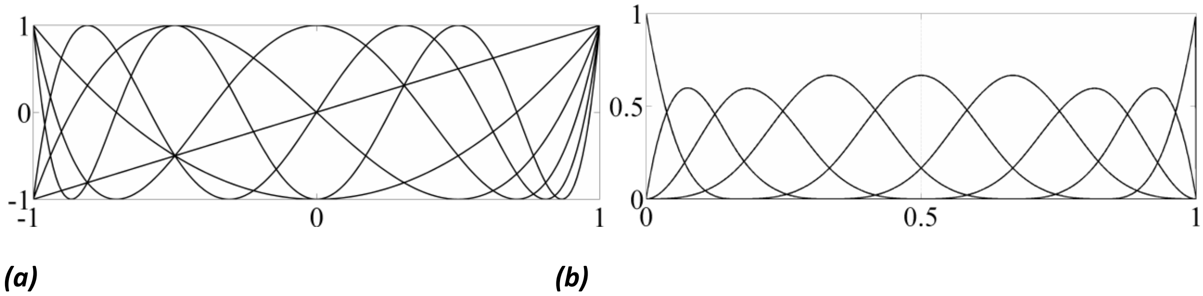

Fig.22. *(a)* first 6 Tchebychev functions of the first kind. (b) Set of n=9 cubic (p=3) NURBS basis functions with knot vector Ξ={0,0,0,0,1/6,1/3,1/2,2/3,5/6,1,1,1,1}.

4.4. Damaged boundary condition

A non ideal boundary condition is modelled as a translational and rotational springs respectively of elastic modules K and K_t at the beams boundary of abscissa $x=L$. see [21], [22] and [23]. The static equilibrium at this limit is given in (4.11) in the non dimensional form and its IGA-C approximation in the last line of table 7.

$$\begin{cases} M(L) = \frac{EI}{L}\theta'(L) = -K_T\theta(L) \\ T(L) = \alpha G h\left(\frac{1}{L}w'(L) - \theta(L)\right) = -Kw(L) \end{cases} \tag{4.11}$$

Note: in reference [23] the authors suggested α and α_t as damage parameters such as: $\alpha=AG/KL$ and $\alpha_t=EI/K_tL$. This appears to me as an anomaly as we don't end to expression of α when a linear parameterisation is used.

Table 7: approximation of the studied boundary conditions.

BC	affects of the BC	approximation of the BC
Clamped **(C)**	$w(\xi_j)=0$	$\sum_{i=1}^{n} w_i R_i(\xi_j)=0$
	$\theta(\xi_j)=0$	$\sum_{i=1}^{n} \theta_i R_i(\xi_j) = 0$
Free **(F)**	$M(\xi_j)=0$	$\frac{1}{L}\sum_{i=1}^{n} \theta_i R'_i(\xi_j) = 0$
	$T(\xi_j)=0$	$\frac{1}{L}\sum_{i=1}^{n} w_i R'_i(\xi_j) - \sum_{i=1}^{n} \theta_i R_i(\xi_j) = 0$
Sliding **(S)**	$\theta(\xi_j)=0$	$\sum_{i=1}^{n} \theta_i R_i(\xi_j) = 0$
	$T(\xi_j)=0$	$\frac{1}{L}\sum_{i=1}^{n} w_i R'_i(\xi_j) - \sum_{i=1}^{n} \theta_i R_i(\xi_j) = 0$
Pinned **(P)**	$w(\xi_j)=0$	$\sum_{i=1}^{n} w_i R_i(\xi_j) = 0$
	$M(\xi_j)=0$	$\frac{1}{L}\sum_{i=1}^{n} \theta_i R'_i(\xi_j) = 0$
Damaged **(D)**	$M(\xi_j)=-K_t\theta(\xi_j)$	$\frac{EI}{L}\sum_{i=1}^{n} \theta_i R'_i(\xi_j) + K_t\theta(\xi_j) = 0$
	$T(\xi_j)=-K\,w(\xi_j)$	$\frac{\alpha Gh}{L}\sum_{i=1}^{n} w_i R'_i(\xi_j) - \alpha Gh\sum_{i=1}^{n} \theta_i R_i(\xi_j) + Kw(\xi_j) = 0$

Now, by considering the two boundaries, one should represent the boundary conditions in term of the nodal variables as in (4.12). This might be clearer through examples (4.12) and (4.14) which represents Clamped-Free and Pinned-Damaged boundary conditions.

Clamped free boundary conditions:

$$\begin{cases} \sum_{i=1}^{n} w_i R_i(0) = 0 \\ \sum_{i=1}^{n} \theta_i R_i(0) = 0 \\ \frac{1}{L}\sum_{i=1}^{n} \theta_i R'_i(1) = 0 \\ \frac{1}{L}\sum_{i=1}^{n} w_i R'_i(1) - \sum_{i=1}^{n} \theta_i R_i(1) = 0 \end{cases} \tag{4.12}$$

$$\begin{bmatrix} \{R_1(0), R_2(0), \dots, R_n(0)\} & \{0_{1\times n}\} \\ \{0_{1\times n}\} & \{R_1(0), R_2(0), \dots, R_n(0)\} \\ \left\{\frac{1}{L}R'_1(1), \frac{1}{L}R'_2(1), \dots, \frac{1}{L}R'_n(1)\right\} & \{0_{1\times n}\} \\ -\{R_1(1), R_2(1), \dots, R_n(1)\} & \left\{\frac{1}{L}R'_1(1), \frac{1}{L}R'_2(1), \dots, \frac{1}{L}R'_n(1)\right\} \end{bmatrix} \begin{Bmatrix} \{\theta\} \\ \{w\} \end{Bmatrix} = \{0_{2n\times 1}\} \tag{4.13}$$

Pinned-Damaged boundary conditions:

$$\begin{cases} \sum_{i=1}^{n} w_i R_i(0) = 0 \\ \sum_{i=1}^{n} \theta_i R'_i(0) = 0 \\ \frac{EI}{L}\sum_{i=1}^{n} \theta'_n R_{in} + K_T \sum_{i=1}^{n} \theta_n R_{in} = 0 \\ \frac{\alpha G h}{L}\sum_{i=1}^{n} w_n R'_{in} - \alpha G h \sum_{i=1}^{n} \theta_n R_{in} + K \sum_{i=1}^{n} w_n R_{in} = 0 \end{cases} \tag{4.14}$$

Expressions (4.12) and (4.14) are than written in term of $\{A^+\}$ and $\{A_r\}$ as in (4.15).

$$[U]\{A^+\} + [V]\{A_r\} = \{0_{4\times 1}\} \tag{4.15}$$

where $\{A_r\} = \{\theta_2\theta_3 \dots \theta_{n-1} v_2 v_3 \dots v_{n-1}\}^T$, $\{A^+\} = \{\theta_1\theta_n w_1 w_n\}^T$ and $\{0_{i\times j}\}$ stands for a matrix of *i* lines and *j* columns with all elements are equal to zero.

Expression (4.15) enables us to draw the values of $\{A^+\}$ which satisfy the boundary conditions. These are then injected into the initial system (4.10) in order to obtain system (4.16).

$$([H_r] - [H^+][U]^{-1}[V])\{A_r\} = -\omega^2\big(([S_r] - [S^+][U]^{-1}[V])\{A_r\}\big) \tag{4.16}$$

4.5 Numerical experiments

In this section, the results obtained from the resolution of Timoshenko equation by isogeometric collocation method are presented. The results are given in terms of the non-dimensional frequency parameter λ defined in (4.17) and this with the aim of taking into account only relationship between the length L of the beam and its width h. In addition, that facilitates the comparison between the results published previously. The results are thus compared with those of previous works, notably, reference [24] obtained with the pseudo-spectral method using the Tchebychev polynomials (PS-C), reference [25] obtained using the isogeometricGalerkin method (IGA-G) and in the same reference [25] obtained using the Timoshenko finite elements method.

$$\lambda_i^2 = \omega_i L^2 \sqrt{\frac{m}{EI}} \tag{4.17}$$

where*m*is the mass per unit of length.

For evaluating the convergence and accuracy of the developed IGA-C element, two preliminary tests are carried out. The first one aims to fix the number of collocation points n=100points and to vary the degree of approximation p (p-refinement) (Table 8). The results are identical with those of references [24] and [25] obtained respectively using the pseudo-spectral method PS-C and isogeometricGalerkin method IGA-G and are in good agreement with the results of reference [25] obtained by Timoshenko finite elements. The results shows a fast convergence of the IGA-C; effectively, on the first 6 eigenvalues, the IGA-C requires a degree of approximation of p=6 to fix 6 significant digits. On the first 15 eigenvalues, the IGA-C requires a degree of approximation of p=8 to fix 6 significant digits. The convergence of the isogeometric collocation method reaches its limit with p=18, with 12 significant digits fixed; this is in agreement with the conclusions of previous works [6] and [7] where it is underlined that interpolation on Greville collocation points become instable for degrees higher than $p=19$.

The second test consists of fixing the degree of approximation at p=14 and vary the number of collocation points (Table 9). As previously the results are identical with those of references [24] and [25] obtained respectively using the pseudo-spectral method PS-C and isogeometricGalerkin method IGA-G and are in good agreement with the results of reference [25] obtained by Timoshenko finite elements. For the first 15 eigenvalues, the IGA-C model requires n=35 collocation points to fix 2 significant digits. The IGA-C reaches the limit of convergence for n=60 with 7 digits and for n=100 with 11 digits.

Tables 10 to 13 represent the results obtained in term of the non-dimensional frequency parameter for various boundary conditions configurations and various thicknesses to lengths ratios of beam; the thickness ratio of the beam is the ratio of its width over its length, i.e. *h/L*. That shows that the results are in good agreement with those of the references [24] and [25].

In Fig. 23, we represent the first three flexural modes obtained for the straight Timoshenko beam for different boundary conditions cases.

Fig 24 and 25 show the decrease of the first three eigenvalues of respectively Clamped-Damaged and Pinned-Damaged beams such as $K=K_t$. It can be seen that the eigenvalues decrease as damage parameters decrease. The high values of damage parameters ($K\to\infty, K_t\to\infty$) correspond to the clamped boundary case and the low values ($K\to 0, K_t\to 0$) to the free boundary case.

According to Fig 26, it should be noted that the values range of the damage parameters that influence the dynamical behaviour of the system varies according to the value of the Young's modulus of the beam. This come from the fact that the damage parameters are nothing else elastic modulus of translational and rotational springs coupled to the beam's end (section 4.4). Consequently, the influence of these springs on the beam's behaviour (and vice-versa) is considerable only when the elastic moduli of those two elements are relatively closes. This last conclusion should be taken into account for an optimal choice of the values of K and K_t.

Fig 27 and Fig 28 show the change of the first three eigenvalues as the two damage parameters K and K_t vary independently. It appears to be rational that the value of each parameter and/or its variation has to be chosen according to the modelled system using above all, the common sense. For instance, the ranges of values of K and K_t have to be chosen close of E and G respectively when looking to model a precocious damage at the clamped end of the beam. On the other hand, it is appropriate to choose a low values of K_t and high values of K ($K_t \to 0$, $K \to \infty$) to model a friction at the pinned end of a propeller blade.

Table 8 : Non-dimensional frequency parameters with increasing polynomial degree p . Case of a clamped-clamped straight Timoshenko beam with rectangular cross section ($\boldsymbol{\nu} = \mathbf{0.3}$, $\boldsymbol{\alpha} = \mathbf{5}/\mathbf{6}$ and $\boldsymbol{h}/\boldsymbol{L} = \mathbf{0.01}$).

Mode	PS-C	FEA	IGA-G	IGA-C			
	p=*n*=35		*p*=5	*p*=4	*p*=6	*p*=8	*p*=10
1	4.7284	4.7330	4.7284	4.7284	4.7284	4.7284	4.7284
2	7.8469	7.8675	7.8469	7.8472	7.8469	7.8469	7.8469
3	10.9800	11.0351	10.9800	10.9808	10.9801	10.9800	10.9800
4	14.1062	14.2218	14.1062	14.1078	14.1062	14.1062	14.1062
5	17.2246	17.4342	17.2246	17.2278	17.2246	17.2246	17.2246
6	20.3338	20.6683	20.3338	20.3392	20.3339	20.3338	20.3338
7	23.4325	23.9600	23.4325	23.4409	23.4325	23.4325	23.4325
8	26.5192	27.2857	26.5192	26.5316	26.5192	26.5192	26.5192
9	29.5926	30.6616	29.5926	29.6102	29.5927	29.5926	29.5926
10	32.6514	34.0944	32.6514	32.6756	32.6516	32.6514	32.6514
11	35.6946	37.5907	35.6946	35.7267	35.6948	35.6946	35.6946
12	38.7209	41.1574	38.7209	38.7627	38.7212	38.7209	38.7209
13	41.7293	44.8016	41.7293	41.7827	41.7298	41.7293	41.7293
14	44.7189	48.5306	44.7189	44.7860	44.7196	44.7189	44.7189
15	47.6888	52.3517	47.6888	47.7718	47.6898	47.6888	47.6888

Table 9: Non-dimensional frequency parameters with increasing collocation points n in the case of a clamped-clamped straight Timoshenko beam with rectangular cross section ($\nu = 0.3$, $\alpha = {}^{5}/_{6}$ and ${}^{h}/_{L} = 0.01$).

Mode	PS-C	FEA	IGA-G	IGA-C			
	p=n=35		n=64	n=35	n=40	n=60	n=80
1	4.7284	4.7330	4.7284	4.7284	4.7284	4.7284	4.7284
2	7.8469	7.8675	7.8469	7.8469	7.8469	7.8469	7.8469
3	10.9800	11.0351	10.9800	10.9801	10.9801	10.9801	10.9801
4	14.1062	14.2218	14.1062	14.1062	14.1062	14.1062	14.1062
5	17.2246	17.4342	17.2246	17.2246	17.2246	17.2246	17.2246
6	20.3338	20.6683	20.3338	20.3338	20.3338	20.3338	20.3338
7	23.4325	23.9600	23.4325	23.4325	23.4325	23.4325	23.4325
8	26.5192	27.2857	26.5192	26.5192	26.5192	26.5192	26.5192
9	29.5926	30.6616	29.5926	29.5926	29.5926	29.5926	29.5926
10	32.6514	34.0944	32.6514	32.6516	32.6514	32.6514	32.6514
11	35.6946	37.5907	35.6946	35.6953	35.6946	35.6946	35.6946
12	38.7209	41.1574	38.7209	38.7242	38.721	38.7209	38.7209
13	41.7293	44.8016	41.7293	41.7428	41.7296	41.7293	41.7293
14	44.7189	48.5306	44.7189	44.7693	44.72	44.7189	44.7189
15	47.6888	52.3517	47.6888	47.8508	47.6922	47.6888	47.6888

Table 10: Non-dimensional frequency parameters of a clamed-clamed straight Timoshenko beam ($\boldsymbol{\nu = 0.3, n = 18}$).

Mode	h/L=0.002			h/L=0.01			h/L=0.2	
	FEA	IGA-G	IGA-C	FEA	IGA-G	IGA-C	IGA-G	IGA-C
1	4.7345	4.7300	4.7300	4.7330	4.7284	4.7284	4.2420	4.2420
2	7.8736	7.8530	7.8530	7.8675	7.8469	7.8469	6.4179	6.4179
3	11.0504	10.9950	10.9950	11.0351	10.9801	10.9801	8.2853	8.2853
4	14.2526	14.1359	14.1359	14.2218	14.1062	14.1062	9.9037	9.9037
5	17.4888	17.2766	17.2766	17.4342	17.2246	17.2246	11.3487	11.3487
6	20.767	20.4169	20.4169	20.6783	20.3338	20.3338	12.6402	12.6402
7	24.0955	23.5567	23.5567	23.9600	23.4325	23.4325	13.4567	13.4567
8	27.4833	26.6960	26.6960	27.2857	26.5192	26.5192	13.8101	13.8101
9	30.9398	29.8348	29.8348	30.6616	29.5926	29.5926	14.4806	14.4806
10	34.4748	32.9729	32.9729	34.0944	32.6514	32.6514	14.9383	14.9383
11	38.0993	36.1103	36.1103	37.5907	35.6946	35.6946	15.6996	15.6996
12	41.8249	39.2470	39.2470	41.1574	38.7209	38.7209	16.0040	16.0040
13	45.6642	42.3829	42.3829	44.8016	41.7293	41.7293	16.9621	16.9621
14	49.6312	45.5178	45.5178	48.5306	44.7189	44.7189	16.9999	16.9999
15	53.7410	48.6519	48.6519	52.3517	47.6888	47.6888	17.9357	17.9357

Table 11: Non-dimensional frequency parameters of a pinned-pinned straight Timoshenko beam ($\boldsymbol{\nu = 0.3, n = 18}$).

Mode	h/L						
	0.002	0.005	0.01	0.02	0.05	0.1	0.2
1	3.1416	3.1415	3.1413	3.1405	3.1350	3.1157	3.0453
2	6.2831	6.2827	6.2811	6.2747	6.2314	6.0907	5.6716
3	9.4245	9.4230	9.4176	9.3963	9.2554	8.8405	7.8395
4	12.5657	12.5621	12.5494	12.4994	12.1813	11.3431	9.6571
5	15.7066	15.6997	15.6749	15.5784	14.9926	13.6132	11.2220
6	18.8473	18.8352	18.7926	18.6282	17.6810	15.6790	12.6022
7	21.9875	21.9684	21.9011	21.6443	20.2447	17.5705	13.0323
8	25.1273	25.0988	24.9988	24.6227	22.6862	19.3142	13.4443
9	28.2666	28.2261	28.0845	27.5599	25.0111	20.9325	13.8433
10	31.4053	31.3498	31.1568	30.4533	27.2263	22.4441	14.4378
11	34.5434	34.4697	34.2145	33.3006	29.3394	23.8639	14.9766
12	37.6807	37.5853	37.2565	36.1001	31.3581	25.2044	15.6676
13	40.8174	40.6962	40.2815	38.8507	33.2896	26.0647	16.0241
14	43.9531	43.8021	43.2886	41.5517	35.1410	26.2814	16.9584
15	47.0881	46.9027	46.2769	44.2026	36.9186	26.4758	17.0019

Table 12: Non-dimensional frequency parameters of a free-free straight Timoshenko beam ($\nu = 0.3, n = 18$).

Mode	h/L						
	0.002	0.005	0.01	0.02	0.05	0.1	0.2
1	4.7300	4.7298	4.7292	4.7266	4.7087	4.6485	4.4496
2	7.8530	7.8522	7.8491	7.8368	7.7540	7.4972	6.8026
3	10.9952	10.9928	10.9843	10.9508	10.7332	10.1255	8.7729
4	14.1362	14.1311	14.1131	14.0426	13.6040	12.5076	10.4094
5	17.2770	17.2678	17.2350	17.1078	16.3550	14.6682	11.7942
6	20.4174	20.4022	20.3483	20.1415	18.9813	16.6358	12.8163
7	23.5575	23.5341	23.4516	23.1394	21.4834	18.4375	13.5584
8	26.6970	26.6630	26.5436	26.0979	23.8654	20.0959	13.6520
9	29.8360	29.7885	29.6228	29.0138	26.1335	21.6283	14.6971
10	32.9744	32.9104	32.6881	31.8846	28.2949	23.0452	14.7384
11	36.1122	36.0282	35.7382	34.7084	30.3571	24.3472	15.8190
12	39.2492	39.1415	38.7719	37.4839	32.3275	25.5006	15.9135
13	42.3854	42.2500	41.7882	40.2099	34.2132	26.2976	16.9742
14	45.5208	45.3534	44.7861	42.8861	36.0205	26.3874	16.9918
15	48.6552	48.4512	47.7647	45.5121	37.7554	27.1340	17.9829

Table 13: Non-dimensional frequency parameters of a pinned-sliding straight Timoshenko beam ($\boldsymbol{\nu = 0.3, n = 18}$).

Mode	h/L						
	0.002	0.005	0.01	0.02	0.05	0.1	0.2
1	1.5708	1.5708	1.5708	1.5707	1.5700	1.5675	1.5578
2	4.7124	4.7122	4.7115	4.7088	4.6903	4.6277	4.4203
3	7.8538	7.8529	7.8498	7.8375	7.7542	7.4963	6.8066
4	10.9951	10.9927	10.9842	10.9505	10.7319	10.1223	8.7852
5	14.1362	14.1311	14.1130	14.0423	13.6020	12.5056	10.4663
6	17.2770	17.2677	17.2348	17.1073	16.3524	14.6697	11.9320
7	20.4174	20.4021	20.3481	20.1408	18.9784	16.6448	13.1407
8	23.5575	23.5340	23.4514	23.1384	21.4804	18.4593	13.2379
9	26.6970	26.6629	26.5432	26.0966	23.8628	20.1378	13.8936
10	29.8360	29.7884	29.6224	29.0123	26.1320	21.7007	14.4219
11	32.9744	32.9103	32.6876	31.8828	28.2952	23.1646	15.0377
12	36.1121	36.0280	35.7375	34.7064	30.3601	24.5434	15.5100
13	39.2492	39.1413	38.7712	37.4816	32.3343	25.8482	16.3112
14	42.3854	42.2498	41.7874	40.2074	34.2249	26.1196	16.5209
15	45.5207	45.3531	44.7852	42.8834	36.0386	26.5417	17.4685

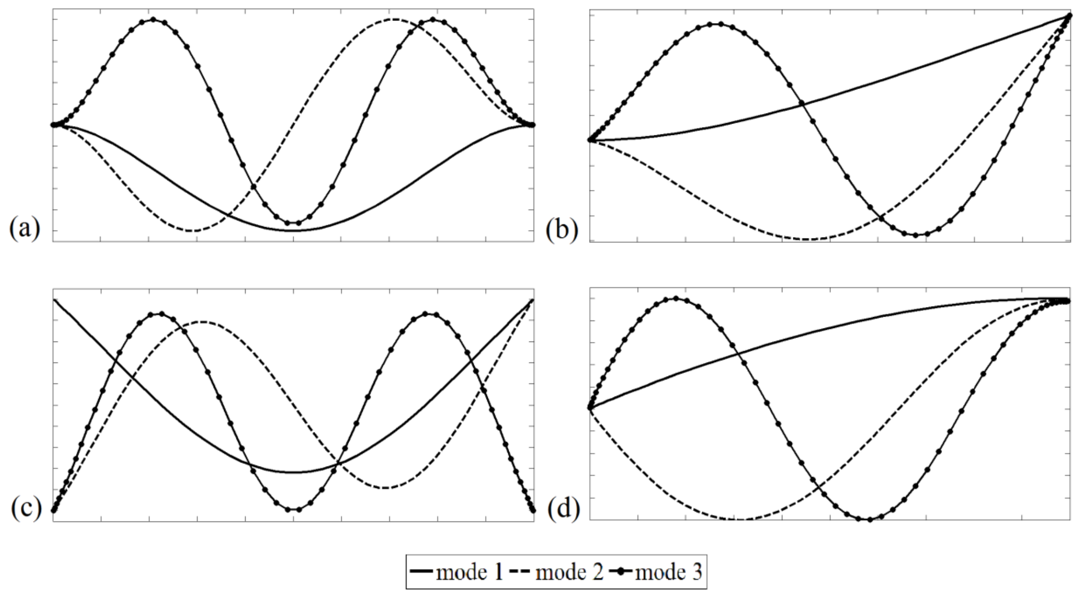

Fig. 23. First three mode shapes of Timoshenko straight Beam in different cases of boundary conditions: (a) Clamped-Clamped. (b) Clamped-Free. (c) Free-Free. (d) Pinned-Sliding.

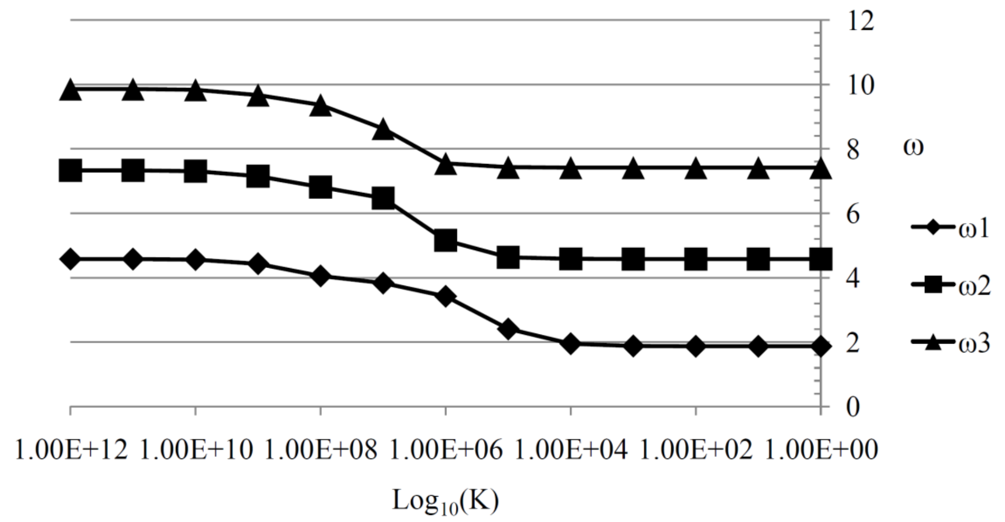

Fig.24: First three eigenvalue versus damage parameters *K*=*Kt* obtained for Clamped-Damaged beam. (ν=0.3, k=5/6, h/L=0.1, *E*=210 000 MPa).

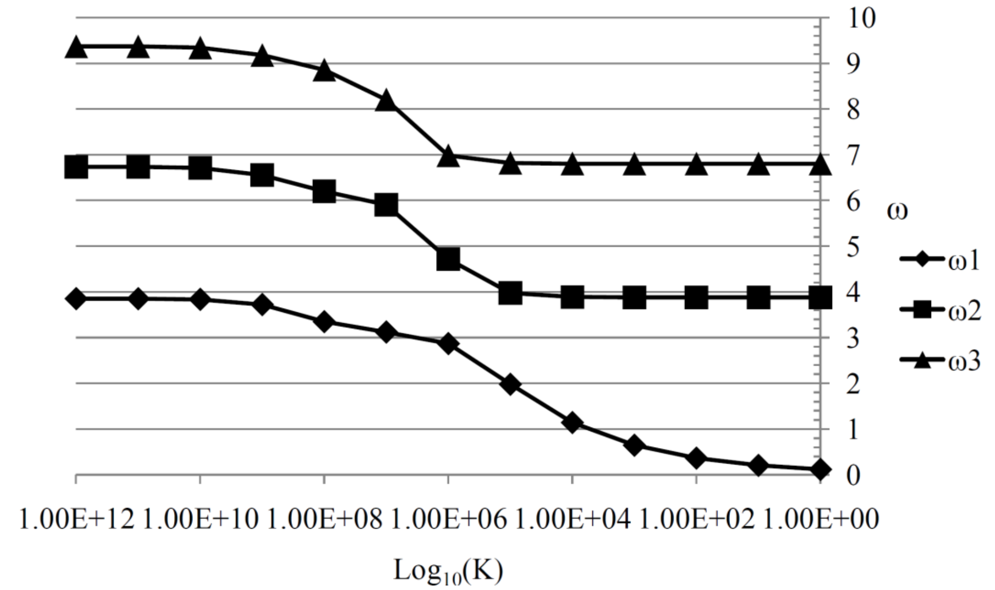

Fig.25: First three eigenvalue versus damage parameters *K*=*Kt* obtained for Pinned-Damaged beam. (*ν*=0.3, *k*=5/6, *h/L*=0.1,*E*=210 000 MPa).

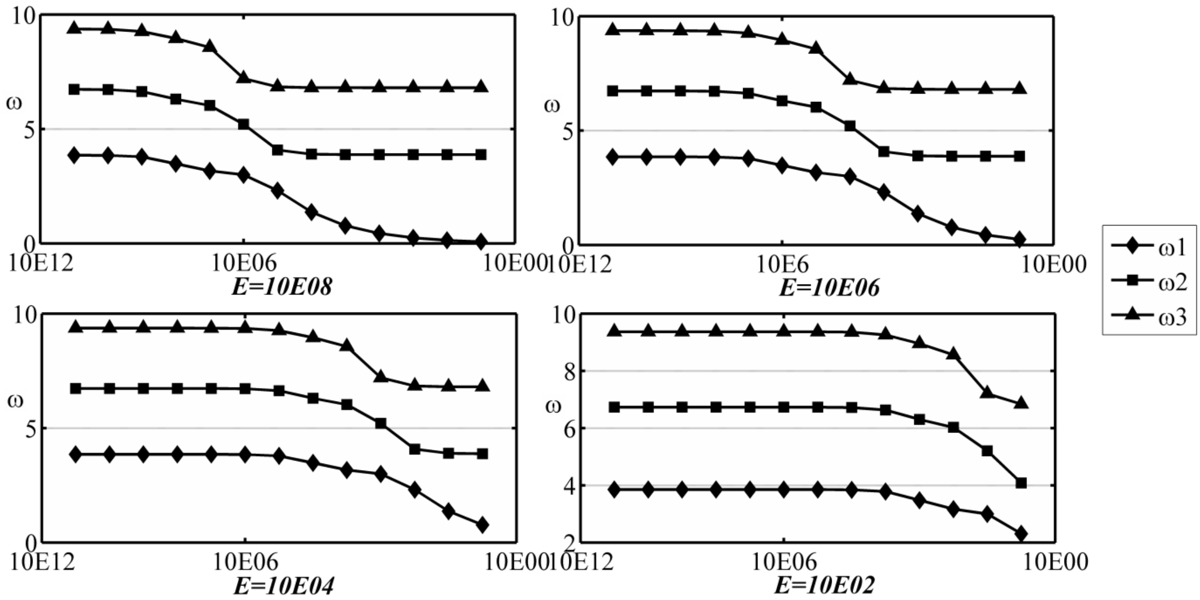

Fig.26: First three eigenvalue versus damage parameters K=Kt obtained for different values of Young's modulus E. (ν=0.3, k=5/6, h/L=0.1, Pinned-Damaged boundary conditions).

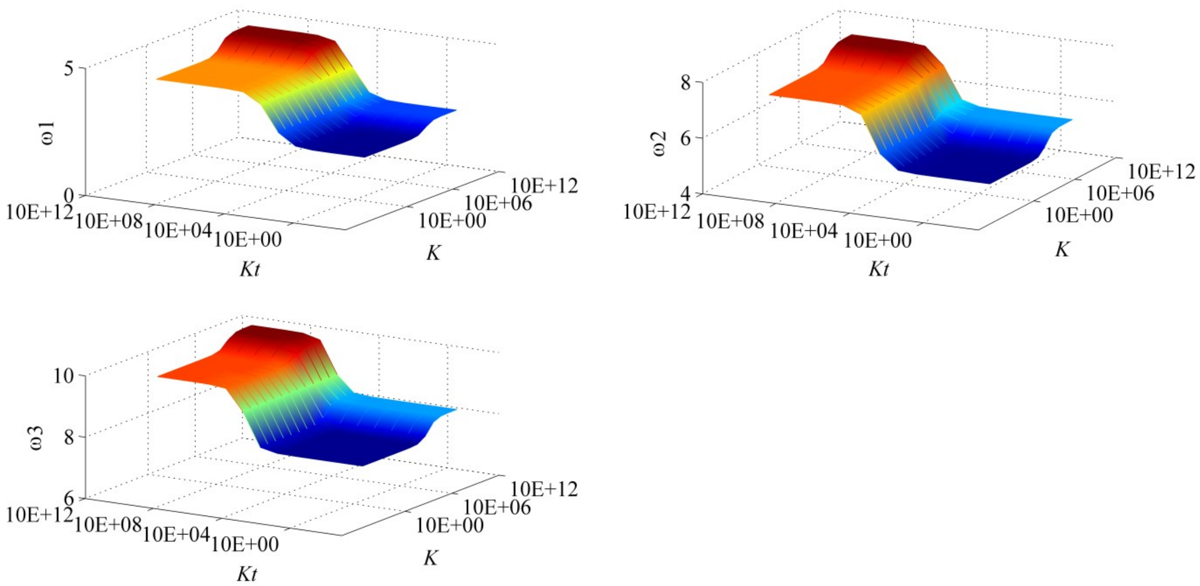

Fig.27: First three natural frequencies versus the two damage parameters for the Clamped-Damaged beam. (ν=0.3, k=5/6, h/L=0.1,E=210 000 MPa).

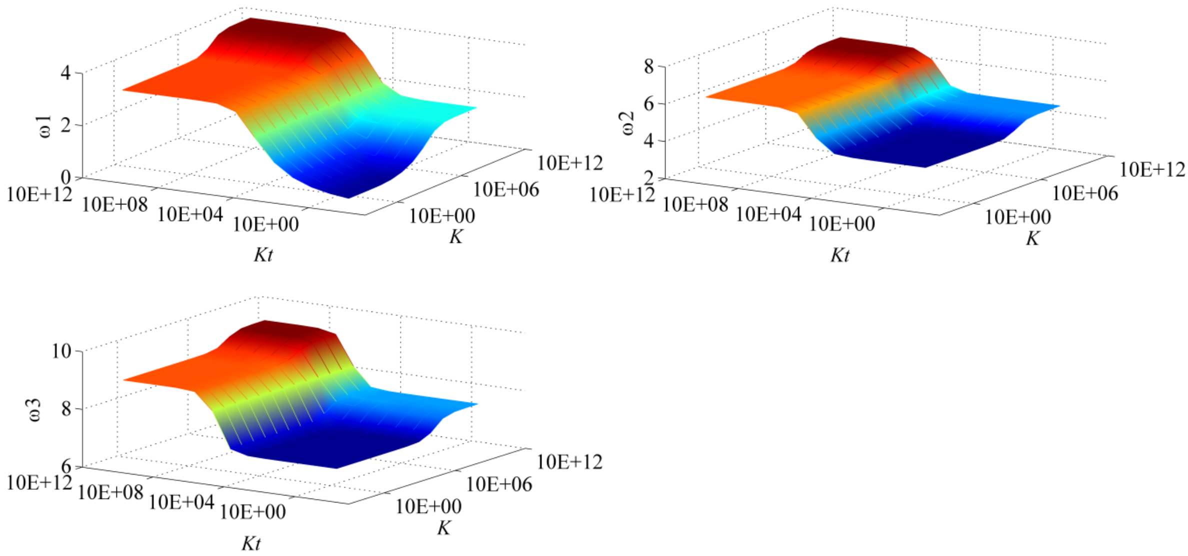

Fig.28: First three natural frequencies versus the two damage parameters for the Pinned-Damaged beam. (*v*=0.3, *k*=5/6, *h/L*=0.1, ,*E*=210 000 MPa).

Ch5

5. In-plane vibration of Timoshenko arched beam

5.1. Equation of Motion

The equation of motion in the plane of an arched beam (Fig. 29) is given by the relation (5.1) [26]. The proceedure of resolution is similar to that for the straight beam.

$$\begin{cases} \frac{1}{R}\frac{\delta N(\phi,t)}{\delta\phi} - \frac{V(\phi,t)}{R} = \rho A\frac{\delta^2 U(\phi,t)}{\delta t^2} \\ \frac{1}{R}\frac{\delta V(\phi,t)}{\delta\phi} + \frac{N(\phi,t)}{R} = \rho A\frac{\delta^2 W(\phi,t)}{\delta t^2} \\ \frac{1}{R}\frac{\delta M(\phi,t)}{\delta\phi} - \frac{V(\phi,t)}{R} = \rho I\frac{\delta^2 \Theta(\phi,t)}{\delta t^2} \end{cases} \quad (5.1)$$

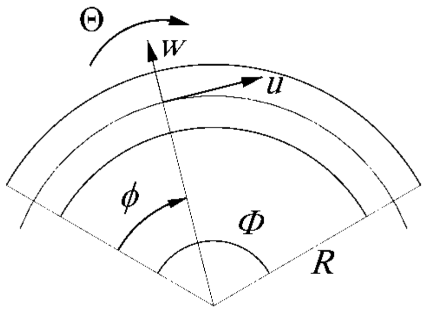

Fig. 29: Arched beam diagram indicating its geometry, degrees of freedom involved in equation of motion (5.1).

where *U(Φ,t)* is the longitudinal displacement, *W(Φ, t)* is the transverse deflection, Θ*(Φ,t)* is the rotation of the transverse line about the transversal axis, *N(Φ,t)* is the longitudinal force, *V(Φ,t)* is the shearing force, *M (Φ, t)* is the bending moment, *R* is the radius of the arch, *ρ* is the mass density of the beam material, *A* is the area of the cross section, *I*the second moment of inertia.

We write the stresses in terms of displacements as follows in (5.2).

$$\begin{cases} M(\phi,t) = \frac{EI}{R}\frac{\delta\Theta(\phi,t)}{\delta\phi} \\ N(\phi,t) = \frac{EA}{R}\left(\frac{\delta U(\phi,t)}{\delta\phi} - W(\phi,t)\right) \\ V(\phi,t) = \alpha AG\left(\frac{1}{R}\frac{\delta W(\phi,t)}{\delta\phi} + \frac{U(\phi,t)}{R} - \Theta(\phi,t)\right) \end{cases} \tag{5.2}$$

We suppose that the movement is periodical in time as in (5.3).

$$\begin{cases} U(\phi,t) = u(\phi)\cos(\omega t) \\ W(\phi,t) = w(\phi)\cos(\omega t) \\ \Theta(\phi,t) = \theta(\phi)\cos(\omega t) \end{cases} \tag{5.3}$$

Substituting (5.2) and then (5.3) into (5.1) yields the (5.4).

$$\begin{cases} \frac{EA}{R^2}\frac{d^2u}{d\phi^2} - \frac{\alpha AG}{R^2}u - \frac{(EA+\alpha AG)}{R^2}\frac{dw}{d\phi} + \frac{\alpha AG}{R}\theta = -\omega^2\rho Au \\ \frac{(EA+\alpha AG)}{R^2}\frac{du}{d\phi} + \frac{\alpha AG}{R^2}\frac{d^2w}{d\phi^2} - \frac{EA}{R^2}w - \frac{\alpha AG}{R}\frac{d\theta}{d\phi} = -\omega^2\rho Aw \\ \frac{\alpha AG}{R}u + \frac{\alpha AG}{R}\frac{dw}{d\phi} + \frac{EI}{R^2}\frac{d^2\theta}{d\phi^2} - \alpha AG\theta = -\omega^2\rho I\theta \end{cases} \tag{5.4}$$

with $u=u(\Phi)$, $w=w(\Phi)$ and $\theta=\theta(\Phi)$.

5.2. Discretisation of the problem

The discretization of the problem is done by expressing the functions of the system (5.4) in the form of linear combination of n NURBS basis functions of order p noted $R_i^p(\xi)$ and n coefficients of expansion as in (5.5. a ,b ,c). These shape functions are written on the collocation points of Greville ξ_j.

$$u(\phi_j) \approx u(\xi_j) = \sum_{i=0}^{N} u_i R_i(\xi_j) = [R]\{a\} \tag{5.5.a}$$

$$w(\phi_j) \approx w(\xi_j) = \sum_{i=0}^{N} w_i R_i(\xi_j) = [R]\{b\} \tag{5.5.b}$$

$$\theta(\phi_j) \approx \theta(\xi_j) = \sum_{i=0}^{N} \theta_i R_i(\xi_j) = [R]\{c\} \tag{5.5.c}$$

Where $\{a\}=\{u_1,u_2,\dots,u_n\}^T$, $\{b\}=\{w_1,w_2,\dots,w_n\}^T$, $\{c\}=\{\theta_1,\theta_2,\dots,\theta_n\}^T$.

Linear normalisation of the parametric variable ξ is performed using the relation (5.6).

$$\xi = \frac{\phi}{\Phi}, \qquad \phi \in [0, \Phi], \qquad \xi \in [0,1] \tag{5.6}$$

Substituting the physical variable Φ with the parametric one ξ and the solutions functions with their approximation in (5.5.a.b.c) into equation (5.4) yields the eigenvalues (5.7), which should be written in the compact form (5.8).

$$\begin{bmatrix} \frac{EA}{R^2\Phi^2}[R''] - \frac{\alpha AG}{R^2}[R] & -\frac{EA+\alpha AG}{R^2\Phi}[R'] & \frac{\alpha AG}{R}[R] \\ \frac{EA+\alpha AG}{R^2\Phi}[R'] & \frac{\alpha AG}{R^2\Phi^2}[R''] - \frac{EA}{R^2}[R] & -\frac{\alpha AG}{R\Phi}[R'] \\ \frac{\alpha AG}{R}[R] & \frac{\alpha AG}{R\Phi}[R'] & \frac{EI}{R^2\Phi^2}[R''] - \alpha AG[R] \end{bmatrix} \begin{bmatrix} \{a\} \\ \{b\} \\ \{c\} \end{bmatrix}$$
$$= -\omega^2 \begin{bmatrix} \rho A[R] & 0 & 0 \\ 0 & \rho A[R] & 0 \\ 0 & 0 & \rho I[R] \end{bmatrix} \begin{bmatrix} \{a\} \\ \{b\} \\ \{c\} \end{bmatrix} \tag{5.7}$$

$$[\boldsymbol{H}]\{\boldsymbol{A}\} = -\boldsymbol{\omega}^2[\boldsymbol{S}]\{\boldsymbol{A}\} \tag{5.8}$$

5.3. Imposing the boundary conditions

Let us rewrite first the expression of the eigenvalue problem (5.8) as in (5.9)

$$[\boldsymbol{H_r}]\{\boldsymbol{A_r}\} + [\boldsymbol{H^+}]\{\boldsymbol{A^+}\} = -\boldsymbol{\omega}^2([\boldsymbol{S_r}]\{\boldsymbol{A_r}\} + [\boldsymbol{S^+}]\{\boldsymbol{A^+}\}) \tag{5.9}$$

where$\{A_r\} = \{u_2 u_3 \dots u_{n-1} w_2 w_3 \dots w_{n-1} \theta_2 \theta_3 \dots \theta_{n-1}\}^T$

and$\{A^+\} = \{u_1 u_n w_1 w_n \theta_1 \theta_n\}^T$

The size of $[H]$ is $3\ (n\text{-}2) \times 3\ (n\text{-}2)$ and that of $[H^+]$ is $3\ (n\text{-}2) \times 4$. The full number of unknown factors in {A} and $\{A^+\}$ is n while the number of equations is n-6. The six remaining equations are obtained thanks to the boundary conditions as follows.

We will restrict this study to the most current boundary conditions namely case: clamped, free, and pinned.

Let us impose a condition to the j^{th}node. The three possibilities studied here are represented in the first column of table 14 and their effects on the system in the second column. One should represent the effect of the condition associated to the coordinate ξ_j using relations (5.2) and (5.5) as in the third column of table 14.

Now, by considering the two boundaries, one should represent the boundary conditions in term of the nodal variables as in the relation (5.10). This might seem clearer through the example (5.11) and (5.12) which represents Clamped-free boundary conditions at ξ=0 and ξ=1.

Table 14: Approximation of the studied boundary conditions.

BC	affects of the BC	approximation of the BC
Clamped (**C**)	*u(ξ_j) =0*	$\sum_{i=1}^{n} u_i R_i(\xi_j) = 0$
	w(ξ_j) =0	$\sum_{i=1}^{n} w_i R_i(\xi_j) = 0$
	θ (ξ_j) =0	$\sum_{i=1}^{n} \theta_i R_i(\xi_j) = 0$
Free (**F**)	*N(ξ_j) =0*	$\frac{1}{\Phi}\sum_{i=1}^{n} u_i R'_i(\xi_j) - \sum_{i=1}^{n} w_i R_i(\xi_j) = 0$
	Q(ξ_j) =0	$\frac{1}{R}\sum_{i=1}^{n} u_i R_i(\xi_j) + \frac{1}{R\Phi}\sum_{i=1}^{n} w_i R'_i(\xi_j) - \sum_{i=1}^{n} \theta_i R_i(\xi_j) = 0$
	M(ξ_j) =0	$\sum_{i=1}^{n} \theta_i R'_i(\xi_j) = 0$
Pinned (**P**)	*u(ξ_j) =0*	$\sum_{i=1}^{n} u_i R_i(\xi_j) = 0$
	v(ξ_j) =0	$\sum_{i=1}^{n} w_i R_i(\xi_j) = 0$
	M(ξ_j) =0	$\sum_{i=1}^{n} \theta_i R'_i(\xi_j) = 0$

$$[U]\{A^{+}\} + [V]\{A_r\} = \{0_{3n\times 1}\} \tag{5.10}$$

Clamped free boundary conditions:

$$\begin{cases} \sum_{i=1}^{n} u_i R_i(0) = 0 \\ \sum_{i=1}^{n} w_i R_i(0) = 0 \\ \sum_{i=1}^{n} \theta_i R_i(0) = 0 \\ \frac{1}{\Phi}\sum_{i=1}^{n} u_i R'_i(1) - \sum_{i=1}^{n} w_i R_i(1) = 0 \\ \frac{1}{R}\sum_{i=1}^{n} u_i R_i(1) + \frac{1}{R\Phi}\sum_{i=1}^{n} w_i R'_i(1) - \sum_{i=1}^{n} \theta_i R_i(1) = 0 \\ \sum_{i=1}^{n} \theta_i R'_i(1) = 0 \end{cases} \tag{5.11}$$

$$\begin{bmatrix} \{R_1(0),R_2(0),\dots,R_n(0)\} & \{0_{1\times n}\} & \{0_{1\times n}\} \\ \{0_{1\times n}\} & \{R_1(0),R_2(0),\dots,R_n(0)\} & \{0_{1\times n}\} \\ \{0_{1\times n}\} & \{0_{1\times n}\} & \{R_1(0),R_2(0),\dots,R_n(0)\} \\ \frac{1}{\Phi}\{R'_1(1),R'_2(1),\dots,R'_n(1)\} & -\{R_1(1),R_2(1),\dots,R_n(1)\} & \{0_{1\times n}\} \\ \frac{1}{R}\{R_1(1),R_2(1),\dots,R_n(1)\} & \frac{1}{R\Phi}\{R'_1(1),R'_2(1),\dots,R'_n(1)\} & -\{R_1(1),R_2(1),\dots,R_n(1)\} \\ \{0_{1\times n}\} & \{0_{1\times n}\} & \{R'_1(1),R'_2(1),\dots,R'_n(1)\} \end{bmatrix} \begin{Bmatrix} \{a\} \\ \{b\} \\ \{c\} \end{Bmatrix} = \{0_{3n\times 1}\} \tag{5.12}$$

Expression (5.10) enables us to draw the values of $\{A^+\}$ which satisfy the boundary conditions. These are then injected into the initial system (5.9) in order to obtain system (5.13).

$$([H_r]-[H^+][U]^{-1}[V])\{A_r\} = -\omega^2\big(([S_r]-[S^+][U]^{-1}[V])\{A_r\}\big) \tag{5.13}$$

5.4. Numerical experiments

In this work, we limit ourselves to the study of arched Timoshenko beam with circular section of radius r.

The results are presented in terms of the non-dimensional frequency parameter λ_i defined by (5.14) and compared to those obtained by the pseudo-spectral method based on the Tchebyshev polynomials published by Jinhee Lee [26].

$$\lambda_i = \sqrt{\frac{\rho A R^4 \omega_i^2}{EI}} \tag{5.14}$$

As for the preceding straight beam application, two preliminary tests are carried out. The first test consists in fixing the number of collocation points to *n=100* and varying the degree of approximation *p* (table 15). for the first 4 eigenvalues, this shows that *9* significant digits are fixed with *p=8* and *10* significant digits with *p=10*. This shows the fast convergence of the IGA-C. It should be noted that by varying the degree of approximation from *p=10* to *18*, the results continue to converge.

The second test consists in fixing the degree of approximation at *p=14* and varying the number of collocation points (table 16). This shows that for the first *9* eigenvalues, *5* digits are fixed with *n=30* and *10* significant digits with *n=60*.

Tables 17 to 19 represent the results obtained in terms of the non-dimensional frequency parameter for various cases of figures of boundary conditions and various thickness of beams; the thickness of the beam symbolized by S_t is defined in (5.15). The results are in agreement with those published previously [26].

$$S_t = \sqrt{\frac{AR^2}{I}} \tag{5.15}$$

In Fig.30, we represent the first three mode shapes obtained for the arched Timoshenko beam for different boundary conditions configurations.

Table 15: Non-dimensional frequency parameters with increasing polynomial degree p. Case of claped-clamped Timoshenko arched beam ($n = 100,\ \nu = 0.9, \alpha = 0.89, \Theta = 120°$ and $S_t = 100$).

Mode	PS-C	IGA-C				
	n=*p*=30	*p*=4	*p*=10	*p*=12	*p*=14	*p*=16
1	11.79	11.7907	11.7903	11.7903	11.7903	11.7903
2	23.249	23.2504	23.2490	23.2490	23.2490	23.2490
3	42.367	42.3716	42.3673	42.3673	42.3673	42.3673
4	61.424	61.4329	61.4244	61.4244	61.4244	61.4244
5	89.872	89.8913	89.8720	89.8720	89.8720	89.8720
6	94.074	94.0797	94.0739	94.0739	94.0739	94.0739
7	124.2	124.2299	124.1958	124.1958	124.1958	124.1958
8	150.94	150.9874	150.9380	150.9380	150.9380	150.9380
9	179.06	179.0778	179.0606	179.0606	179.0606	179.0606
10	193.18	193.2751	193.1805	193.1805	193.1805	193.1805

Table 16: Non-dimensional frequency parameters with increasing number of collocation points p. Case of clamped-clamped Timoshenko arched beam with circular section ($p = 16,\ \nu = 0.3$, $\alpha = 0.89, \Theta = 120° et S_t = 100$).

Mode	PS-C	IGA-C				
		n=30	n=40	n=60	n=80	n=100
1	11.79	11.7903	11.7903	11.7903	11.7903	11.7903
2	23.249	23.2490	23.2490	23.2490	23.2490	23.2490
3	42.367	42.3673	42.3673	42.3673	42.3673	42.3673
4	61.424	61.4244	61.4244	61.4244	61.4244	61.4244
5	89.872	89.8720	89.8720	89.8720	89.8720	89.8720
6	94.074	94.0739	94.0739	94.0739	94.0739	94.0739
7	124.2	124.1959	124.1958	124.1958	124.1958	124.1958
8	150.94	150.9385	150.9380	150.9380	150.9380	150.9380
9	179.06	179.0612	179.0606	179.0606	179.0606	179.0606
10	193.18	193.1874	193.1805	193.1805	193.1805	193.1805

Table 17: Non-dimensional frequency parameters of clamped-clamped Timoshenko arched beam ($n = 100, \nu = 0.3, p = 16, \alpha = 0.89$).

Mode	St	Θ=60°		Θ=120°		Θ=180°	
		PS-C	IGA-C	PS-C	IGA-C	PS-C	IGA-C
1	10	15.384	15.3838	8.3526	8.3526	3.6367	3.6367
2		24.546	24.5464	8.7515	8.7515	6.3571	6.3571
3		32.902	32.9016	17.0700	17.0699	10.5980	10.5981
4		43.344	43.3435	17.3540	17.3544	10.9760	10.9762
5		60.015	60.0150	25.6310	25.6309	15.3420	15.3421
1	20	23.772	23.7723	10.6120	10.6122	4.1570	4.1570
2		38.988	38.9884	15.1820	15.1822	8.5354	8.5354
3		62.958	62.9581	24.7160	24.7163	15.4550	15.4552
4		70.676	70.6760	30.5530	30.5530	17.9130	17.9132
5		103.410	103.4097	39.0760	39.0757	25.5130	25.5134
1	50	44.746	44.7464	11.6230	11.6229	4.3456	4.3456
2		50.298	50.2980	22.1150	22.1146	9.4576	9.4576
3		100.100	100.1030	40.7210	40.7212	17.4770	17.4772
4		145.110	145.1110	45.1790	45.1794	26.2290	26.2294
5		165.670	165.6742	64.6830	64.6828	37.8440	37.8435
1	100	15.384	15.3838	8.3526	8.3526	3.6367	3.6367
2		24.546	24.5464	8.7515	8.7515	6.3571	6.3571
3		32.902	32.9016	17.0700	17.0699	10.5980	10.5981
4		43.344	43.3435	17.3540	17.3544	10.9760	10.9762
5		60.015	60.0150	25.6310	25.6309	15.3420	15.3421

Table 18: Non-dimensional frequency parameters of pinned-pinned Timoshenko arched beam ($\boldsymbol{n = 100, \nu = 0.3, p = 16, \alpha = 0.89}$).

Mode	St	Θ =60°		Θ =120°		Θ =180°	
		PS-C	IGA-C	PS-C	IGA-C	PS-C	IGA-C
1	10	11.548	11.5481	5.8117	5.8116	2.0773	2.0773
2		21.288	21.2879	8.6209	8.6210	5.6267	5.6266
3		32.527	32.5271	14.6220	14.6219	9.8229	9.8229
4		41.114	41.1130	17.0620	17.0619	10.3500	10.3503
5		58.809	58.8107	23.5210	23.5208	14.3980	14.3982
1	20	19.564	19.5643	6.5895	6.5894	2.2146	2.2146
2		28.691	28.6909	14.4090	14.4088	6.5425	6.5425
3		60.51	60.5096	20.9530	20.9532	12.8300	12.8295
4		62.75	62.7495	28.0230	28.0229	17.8740	17.8738
5		95.409	95.4080	36.5750	36.5748	22.1980	22.1981
1	50	32.65	32.6503	6.8693	6.8693	2.2582	2.2582
2		44.205	44.2052	17.0420	17.0415	6.8591	6.8591
3		77.116	77.1155	32.7380	32.7383	13.7770	13.7765
4		126.69	126.6919	45.0060	45.0062	22.2380	22.2384
5		158.76	158.7554	55.3390	55.3392	32.8600	32.8598
1	100	33.373	33.3731	6.9122	6.9122	2.2646	2.2646
2		69.013	69.0132	17.3840	17.3835	6.9071	6.9071
3		101.51	101.5120	33.5080	33.5077	13.9270	13.9266
4		137.56	137.5618	52.4560	52.4556	22.6750	22.6753
5		215.02	215.0222	77.3770	77.3772	33.6580	33.6576
1	200	33.562	33.5622	6.9231	6.9240	2.2662	2.2664
2		74.004	74.0038	17.4680	17.4681	6.9192	6.9191
3		140.55	140.5468	33.7070	33.7070	13.9650	13.9649
4		183.65	183.6542	53.2410	53.2408	22.7840	22.7835
5		230.01	230.0906	78.4060	78.4064	33.8610	33.8612

Table 19: Non-dimensional frequency parameters of clamped-pinned Timoshenko arched beam ($\boldsymbol{n = 100, \nu = 0.3, p = 16, \alpha = 0.89}$).

Mode	St	Θ =60°		Θ =120°		Θ =180°	
		PS-C	IGA-C	PS-C	IGA-C	PS-C	IGA-C
1	10	13.224	13.2238	6.9561	6.9561	2.8342	2.8342
2		23.183	23.1831	8.7388	8.7388	6.0670	6.0670
3		32.684	32.6839	16.0030	16.0033	10.0120	10.0116
4		42.211	42.2112	17.0710	17.0709	10.8590	10.8594
5		59.803	59.8026	24.6140	24.6137	14.7660	14.7662
1	20	20.952	20.9518	8.4860	8.4860	3.1326	3.1326
2		34.152	34.1522	14.9520	14.9520	7.5689	7.5689
3		62.68	62.6802	22.5680	22.5684	14.1130	14.1127
4		65.863	65.8628	29.6440	29.6437	17.9030	17.9029
5		99.557	99.5568	37.4810	37.4812	23.7860	23.7860
1	50	39.981	39.9809	9.8300	9.0830	3.2336	3.2336
2		45.006	45.0063	19.6170	19.6166	8.1344	8.1344
3		88.415	88.4150	36.5410	36.5405	15.5700	15.5703
4		137.48	137.4796	45.1450	45.1446	24.2420	24.2419
5		160.58	160.5764	59.7760	59.7764	35.3000	35.2995
1	100	42.351	42.3514	9.1775	9.1775	3.2488	3.2488
2		73.76	73.7602	20.2640	20.2641	8.2217	8.2217
3		107.62	107.6165	37.7760	37.7756	15.8020	15.8022
4		154.17	154.1713	57.0200	57.0203	24.9090	24.9088
5		235.06	235.0589	83.3460	83.3455	36.4210	36.4212
1	200	42.794	42.7943	9.2015	9.2015	3.2526	3.2526
2		84.728	84.7281	20.4220	20.4223	8.2438	8.2438
3		157.76	157.7585	38.0840	38.0840	15.8610	15.8613
4		183.75	183.7519	58.3340	58.3341	25.0710	25.0705
5		250.94	250.9351	84.8900	84.8896	36.7010	36.7007

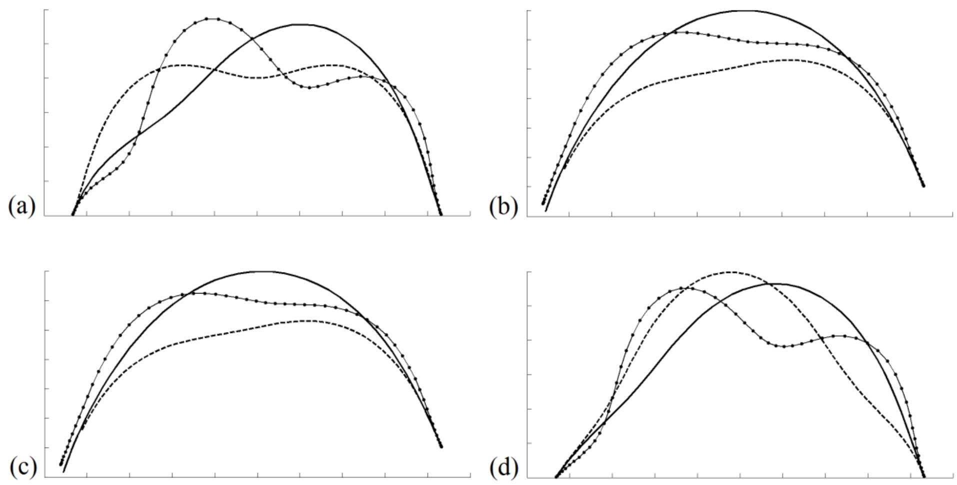

Fig. 30: The first three mode shapes of Timoshenko arched Beam (Θ=120°) in different cases of boundary conditions: (a) Clamped-Clamped. (b) Free-Clamped. (c) Free-Free. (d) Pinned-Clamped.

Ch6

6. In-plane vibration of Two layer beams

In this session, we study the dynamic behaviour of a composite two-layer beam modelled by mean of two connected Timoshenko beams (Fig 31). The connection between these beams are represented by uniformly distributed tangential and normal forces respectively F_T and F_N of values given by relations (6.3.a.b), the elastic proprieties of the connection is ensured by the introduction of two parameters K_T and K_N respectively shear and normal elastic modulus of the connection. This technique is used to model composite beams structure [27] and [28]. Comparatively to other methods like homogenization, it has the advantage of saving all the structure's data which making the possibility of getting information about the behaviour of the interface and ones of each beam separately as has been demonstrated in reference [29]. Consequently, this model is specially used to represent local effects such as interlaminar stress distribution, delamination. anisotropic materials, damage identification [29].

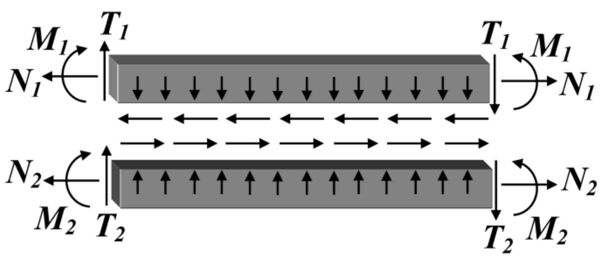

Fig.31: two layer beams.

The equilibrium equation of each beam is given in (6.1.ab), the constitutive relations in (6.2.ab) and the interface relation in (6.3.a.b).

$$\begin{cases} N_1' - F_T = \rho_1 A_1 \ddot{w}_1 \\ T_1' + F_N = \rho_1 A_1 \ddot{v}_1 \\ M_1' - T_1 + h_1 F_T = \rho_1 J_1 \ddot{\theta}_1 \end{cases} \quad (6.1.a) \qquad \begin{cases} N_2' + F_T = \rho_2 A_2 \ddot{w}_2 \\ T_2' + F_N = \rho_2 A_2 \ddot{v}_1 \\ M_2' - T_2 + h_2 F_T = \rho_2 J_2 \ddot{\theta}_2 \end{cases} \quad (6.1.b)$$

Constitutive relations: $$\begin{cases} N_1 = E_1 A_1 w_1' \\ T_1 = \chi_1 G_1 A_1 (v_1' + \theta_1) \\ M_1 = E_1 J_1 \theta_1' \end{cases} \quad (6.2.a) \begin{cases} N_2 = E_2 A_2 w_2' \\ T_2 = \chi_2 G_2 A_2 (v_2' + \theta_2) \\ M_2 = E_2 J_2 \theta_2' \end{cases} \quad (6.2.b)$$

Interface relations: $$\begin{cases} S_T = w_1 - w_2 - h_1\theta_1 - h_2\theta_2 \\ S_N = v_1 - v_2 \end{cases} \quad (6.3.a) \qquad \begin{cases} F_T = K_T S_T \\ F_N = K_N S_N \end{cases} \quad (6.3.b)$$

Eigenvalues problem for the studied beam is derived by substituting (6.2.a.b) then (6.3.a.b) in (6.1.a.b) and considering a sinusoidal motion through time. It is given in (6.4).

$$\begin{cases} -K_T w_1 + E_1 A_1 w_1'' + K_T h_1 \theta_1 + K_T w_2 + K_T h_2 \theta_2 = -\omega^2 \rho_1 A_1 w_1 \\ K_N v_1 + \chi_1 G_1 A_1 v_1'' + \chi_1 G_1 A_1 \theta_1' - K_N v_2 = -\omega^2 \rho_1 A_1 v_1 \\ h_1 K_T w_1 - \chi_1 G_1 A_1 v_1' - (h_1 K_T h_1 + \chi_1 G_1 A_1)\theta_1 + E_1 J_1 \theta_1'' - h_1 K_T w_2 - h_1 K_T h_2 \theta_2 = -\omega^2 \rho_1 J_1 \theta_1 \end{cases}$$

(6.4)

$$\begin{cases} K_T w_1 - K_T h_1 \theta_1 - K_T w_2 + E_2 A_2 w_2'' - K_T h_2 \theta_2 = -\omega^2 \rho_2 A_2 w_2 \\ K_N v_1 - K_N v_2 + \chi_2 G_2 A_2 v_2'' + \chi_2 G_2 A_2 \theta_2' = -\omega^2 \rho_2 A_2 v_2 \\ h_2 K_T w_1 - h_2 K_T h_1 \theta_1 - h_2 K_T w_2 - \chi_2 G_2 A_2 v_2' - (h_2 K_T h_2 + \chi_2 G_2 A_2)\theta_2 + E_2 J_2 \theta_2'' = -\omega^2 \rho_2 J_2 \theta_2 \end{cases}$$

6.1. Discretisation of the problem

The solution functions of system (6.4) are approximated with a linear combination of *n* NURBS shape functions of order *p* noted $R_i^p(\xi)$ and *n* coefficients of expansion. These shape functions are written on the collocation points of Grevilleξ_j as in (6.5.a.b.c.d.e.f).

$$w_1(x) \approx w_1(\xi_j) = \sum_{i=0}^{n} w_{1_i} R_i(\xi_j) = [R]\{w_1\} \quad (6.5.a)$$

$$v_1(x) \approx v_1(\xi_j) = \sum_{i=0}^{n} v_{1_i} R_i(\xi_j) = [R]\{v_1\} \quad (6.5.b)$$

$$\theta_1(x) \approx \theta_1(\xi_j) = \sum_{i=0}^{n} \theta_{1_i} R_i(\xi_j) = [R]\{\theta_1\} \tag{6.5.c}$$

$$w_2(x) \approx w_2(\xi_j) = \sum_{i=0}^{n} w_{2_i} R_i(\xi_j) = [R]\{w_2\} \tag{6.5.d}$$

$$v_2(x) \approx v_2(\xi_j) = \sum_{i=0}^{n} v_{2_i} R_i(\xi_j) = [R]\{v_2\} \tag{6.5.e}$$

$$\theta_2(x) \approx \theta_2(\xi_j) = \sum_{i=0}^{n} \theta_{2_i} R_i(\xi_j) = [R]\{\theta_2\} \tag{6.5.f}$$

where $\{w_i\}=\{w_{i1},w_{i2},\ldots,w_{in}\}^T$, $\{v_i\}=\{v_{i1},v_{i2},\ldots,v_{in}\}^T$, $\{w_i\}=\{\theta_{i1}, \theta_{i2},\ldots, \theta_{in}\}^T$, $i=1,2$

By substituting (6.5.a-f) in (6.4) we obtain the eigenvalues problem (6.6)

$$\begin{bmatrix} h_{11} & [0] & h_{13} & h_{14} & [0] & h_{16} \\ [0] & h_{22} & h_{23} & [0] & h_{25} & [0] \\ h_{31} & h_{32} & h_{33} & h_{34} & [0] & h_{36} \\ h_{41} & [0] & h_{43} & h_{44} & [0] & h_{46} \\ [0] & h_{52} & [0] & [0] & h_{55} & h_{56} \\ h_{61} & [0] & h_{63} & h_{64} & h_{65} & h_{66} \end{bmatrix} \begin{Bmatrix} \{w_1\} \\ \{v_1\} \\ \{\theta_1\} \\ \{w_2\} \\ \{v_2\} \\ \{\theta_2\} \end{Bmatrix} = \omega^2 \begin{bmatrix} s_{11} & [0] & [0] & [0] & [0] & [0] \\ [0] & s_{22} & [0] & [0] & [0] & [0] \\ [0] & [0] & s_{33} & [0] & [0] & [0] \\ [0] & [0] & [0] & s_{44} & [0] & [0] \\ [0] & [0] & [0] & [0] & s_{55} & [0] \\ [0] & [0] & [0] & [0] & [0] & s_{66} \end{bmatrix} \begin{Bmatrix} \{w_1\} \\ \{v_1\} \\ \{\theta_1\} \\ \{w_2\} \\ \{v_2\} \\ \{\theta_2\} \end{Bmatrix} \tag{6.6}$$

Equation (6.6) should be written in compact form (6.7).

$$[H]\{A\} = \omega^2 [S]\{A\} \tag{6.7}$$

where :

$$h_{11} = \frac{E_1 A_1}{L^2}[R''] - K_T[R]$$
$$h_{13} = K_T h_1 [R]$$
$$h_{14} = K_T[R]$$
$$h_{16} = K_T h_2 [R]$$

$$h_{22} = K_N[R] + \frac{\chi_1 G_1 A_1}{L^2}[R'']$$
$$h_{23} = \frac{\chi_1 G_1 A_1}{L}[R']$$
$$h_{25} = -K_N[R]$$

$$h_{31} = h_1 K_T[R]$$
$$h_{32} = -\frac{\chi_1 G_1 A_1}{L}[R']$$
$$h_{33} = \frac{E_1 J_1}{L^2}[R''] - (h_1 K_T h_1 + \chi_1 G_1 A_1)[R]$$
$$h_{34} = -h_1 K_T[R]$$
$$h_{36} = -h_1 K_T h_2 [R]$$

$$h_{41} = K_T[R]$$
$$h_{43} = -K_T h_1[R]$$
$$h_{44} = \frac{E_2 A_2}{L^2}[R''] - K_T[R]$$
$$h_{46} = -K_T h_2[R]$$

$$h_{52} = K_N[R]$$
$$h_{55} = \frac{\chi_2 G_2 A_2}{L^2}[R''] - K_N[R]$$
$$h_{56} = \frac{\chi_2 G_2 A_2}{L}[R']$$

$$h_{61} = h_2 K_T[R]$$
$$h_{63} = -h_2 K_T h_1[R]$$
$$h_{64} = -h_2 K_T[R]\{w_2\}$$
$$h_{65} = -\frac{\chi_2 G_2 A_2}{L}[R']$$
$$h_{66} = \frac{E_2 J_2}{L^2}[R''] - (h_2 K_T h_2 + \chi_2 G_2 A_2)[R]$$

$$s_{11} = -\rho_1 A_1[R]$$
$$s_{22} = -\rho_1 A_1[R]$$
$$s_{33} = -\rho_1 J_1[R]$$

$$s_{44} = -\rho_2 A_2[R]$$
$$s_{55} = -\rho_2 A_2[R]$$
$$s_{66} = -\rho_2 J_2[R]$$

6.2. Imposing the boundary conditions

In the aim of comparing our results with experimental and analytical published ones [27] and [28], we will impose the free-free F-F boundary conditions to the considered problem. Nevertheless the proposed method should be followed to impose any other boundary condition.

Let us before rewrite equation (6.7) as in (6.8).

$$[\boldsymbol{H_r}]\{\boldsymbol{A_r}\} + [\boldsymbol{H^+}]\{\boldsymbol{A^+}\} = -\boldsymbol{\omega}^2([\boldsymbol{S_r}]\{\boldsymbol{A_r}\} + [\boldsymbol{S^+}]\{\boldsymbol{A^+}\}) \tag{6.8}$$

Where $\{A_r\} = \{\{w_1\}_r, \{v_1\}_r, \{\theta_1\}_r, \{w_2\}_r, \{v_2\}_r, \{\theta_2\}_r\}^T$,
$\{w_1\}_r = \{w_{12}, w_{13}, \dots, w_{1(n-1)}\}T$

Idem for $\{v_1\}_r, \{\theta_1\}_r, \{w_2\}_r, \{v_2\}_r and \{\theta_2\}_r$

and$\{A^+\} = \{w_{11}, w_{1n}, v_{11}, v_{1n}, \theta_{11}, \theta_{1n}, w_{21}, w_{2n}, v_{21}, v_{2n}, \theta_{21}, \theta_{12n},\}^T$

The free boundary condition is satisfied when all efforts are reduced to zero. The approximation of this boundary condition is given in Table 20

Table 20: Approximation of the studied boundary conditions.

BC	effets of the BC	approximation of the BC
Free **(F)**	$N_1(\xi_j) = 0$	$\frac{E_1A_1}{L}\sum_{i=0}^{n} w_{1_i} R_i(\xi_j)$=0
	$T_1(\xi_j) = 0$	$\chi_1 G_1 A_1 \left(\frac{1}{L}\sum_{i=0}^{n} v_{1_i} R_i(\xi_j) + \sum_{i=0}^{n} \theta_{1_i} R_i(\xi_j)\right)$=0
	$M_1(\xi_j) = 0$	$M_1 = \frac{E_1J_1}{L}\sum_{i=0}^{n} \theta_{1_i} R_i(\xi_j)$=0
	$N_2(\xi_j) = 0$	$N_2 = \frac{E_2A_2}{L}\sum_{i=0}^{n} w_{2_i} R_i(\xi_j)$=0
	$T_2(\xi_j) = 0$	$T_2 = \chi_2 G_2 A_2 \left(\frac{1}{L}\sum_{i=0}^{n} v_{2_i} R_i(\xi_j) + \sum_{i=0}^{n} \theta_{2_i} R_i(\xi_j)\right)$=0
	$M_2(\xi_j) = 0$	$M_2 = \frac{E_2J_2}{L}\sum_{i=0}^{n} \theta_{2_i} R_i(\xi_j)$=0

Now, by considering the two boundaries, one should represent the boundary conditions in term of the nodal variables using expressions of Table 20 as in (6.9).

$$[U]\{A^+\} + [V]\{A_r\} = \{0_{6\times1}\} \tag{6.9}$$

Expression (6.9) enables us to draw the values of $\{A^{+}\}$ which satisfy the boundary conditions. These are then injected into the initial system (6.8) in order to obtain system (6.10).

$$([H_r] - [H^+][U]^{-1}[V])\{A_r\} = -\omega^2\big(([S_r] - [S^+][U]^{-1}[V])\{A_r\}\big) \tag{6.10}$$

6.3. Numerical experiment

Natural frequencies of concrete-steel composite beam studied in references [27] and [28] are evaluated using the developed IGA-C model. The beams parameters are taken from reference [28] and given in Table 21, where the subscript s refers to steel and c to concrete. The model has been updated using minimum problem (95), the nominal and optimal values of coefficients K_T and K_N are given in Table 22.

First seven natural frequencies of the two studied specimens of beams named T1PR and T1CR are given in (Tables 23-26) and error are evaluated for each frequency. Results are compared to experiment and published ones.

In Tables 23 and 24, the polynomial order p is fixed and the number of collocation points$n$ is varied. A maximum error of 0.6% for T1PR and 3.1% for T1CR is reached with $p=5$ and $n=40$.

In Tables 25 and 26, the number of collocation points$n$ is fixed and the polynomial order p is varied. This shows that the results are accurate from $p=5$.

It should be noted that the superior accuracy of the presented IGA-C model than the analytical one for the high frequencies is simply due to the fact that we have taken into account the first 7 frequencies to update our model (6.11) contrary to reference [28] where the model has been updated according to the first frequency.

$$\text{To find } K_T and K_N \text{such that } A = \min_{\substack{0<K_T\leq 3K_{T\,0} \\ 0<K_N\leq 3K_{N\,0}}} F(\mu, k), \tag{6.11}$$

Where

$$F(K_T, K_N) = \sum_{i=1}^{7} \sqrt{\left(\left(f_i - f_{exp\,i}\right)/f_{exp\,i}\right)^2}.$$

f and f_{exp} are respectively the analytical and experimental values of the natural frequencies, i is the mode number. The optimal values of K_T and K_N are given in Table 22.

Table 21 : Physical parameters of the composite beams T1PR and T1CR, taken from reference [18]

Parameter	Value
Concrete slab	
Length L	3.5 m
Cross-sectional area A_c	3.00 10^{-2} m^2
Moment of inertia J_c	9.00 10^{-6} m^4
Linear mass density ρ_c (T1PR)	73.2 kg/m
Linear mass density ρ_c (T1CR)	77.2 kg/m
Young's modulus E_c	42 863 MPa
Steel beam	
Length L	3.5 m
Cross-sectional area A_s	1.64 10^{-3} m^2
Moment of inertia J_s	5.41 10^{-6} m^4
Linear mass density ρ_s	12.9 kg/m
Young's modulus E_s	210 000 MPa

Table 22: Nominal and optimal values of elastic coeficients for stadied beams connections.

coefficient	T1PR (N/m^2)	T1CR (N/m^2)
K_{T0}	9.3600 10^8	1.3460 10^9
K_T	1.8720 10^9	4.0380 10^9
K_{N0}	5.5909 10^9	8.2000 10^9
K_N	7.7714 10^8	9.5120 10^8

Table 23: Comparison of natural frequecies of T1PR beam ander free-free boundary conditions by the analytical Euler-Bernoulli beam model, Timoshenko finite elements beam model and Timoshenko IGA-C with experimental results. Results are presented as the number of collocation points n increases.

Mode	exp	ref 1		ref 2		IGA-C p=5					
		freq	Δ%	freq	Δ%	n=20	Δ%	n=30	Δ%	n=40	Δ%
1	60.68	60.68	0.0	60.68	0.0	60.63	0.1	60.60	0.1	60.59	0.1
2	145.46	149.55	2.8	147.66	1.5	146.58	0.8	146.24	0.5	146.20	0.5
3	247.11	265.25	7.3	253.75	2.7	249.12	0.8	247.51	0.2	247.35	0.1
4	351.08	401.87	14.5	369.95	5.4	358.89	2.2	353.55	0.7	353.05	0.6
5	461.38	553.89	20.1	492.89	6.8	475.92	3.2	461.76	0.1	460.44	0.2
6	570.77	713.32	25.0	620.95	8.8	606.65	6.3	574.75	0.7	571.65	0.2
7	691.48	873.28	26.3	754.31	9.1	762.25	10.2	698.30	1.0	691.76	0.0

Ref1 and Ref2: respectively analytical solution with Euler-Bernoulli and Timoshenko models [18]. $\boldsymbol{\Delta = 100\left(\left(f - f_{exp}\right)/f_{exp}\right)}$

Table 24: Comparison of natural frequecies of T1CR beam ander free-free boundary conditions by the analytical Euler-Bernoulli beam model, Timoshenko finite elements beam model and Timoshenko IGA-C with experimental results. Results are presented as the number of collocation points n increases.

Mode	Exp	ref 1		ref 2		IGA-C	p=5				
		freq	Δ%	freq	Δ%	n=20	Δ%	n=30	Δ%	n=40	Δ%
1	60.49	60.49	0.0	60.49	0.0	60.44	0.1	60.42	0.1	60.41	0.1
2	146.34	153.23	4.7	152.04	3.9	150.66	3.0	150.37	2.8	150.33	2.7
3	250.82	275.03	9.7	266.34	6.2	260.08	3.7	258.66	3.1	258.51	3.1
4	361.26	418.23	15.8	391.16	8.3	375.83	4.0	370.97	2.7	370.51	2.6
5	473.88	577.13	21.8	521.11	10.0	496.08	4.7	482.93	1.9	481.71	1.7
6	588.38	745.49	26.7	654.48	11.2	607.11	3.2	597.10	1.5	594.24	1.0
7	709.04	915.75	29.2	791.41	11.6	780.08	10.0	719.38	1.5	713.30	0.6

Ref1 and Ref2: respectively analytical solution with Euler-Bernoulli and Tmoshenko models [18]. $\boldsymbol{\Delta = 100((f - f_{exp})/f_{exp})}$

Table 25: Comparison of natural frequecies of T1PR beam ander free-free boundary conditions by the analytical Euler-Bernoulli beam model, Timoshenko finite elements beam model and Timoshenko IGA-C with experimental results. Results are presented as the polynomial order p increases.

Mode	Exp	ref 1		ref 2		IGA-C	n=40				
		freq	Δ %	freq	Δ %	p=3	Δ %	p=5	Δ %	p=6	Δ %
1	60.68	60.68	0.0	60.68	0.0	64.22	5.8	60.59	0.1	60.59	0.1
2	145.46	149.55	2.8	147.66	1.5	156.14	7.3	146.20	0.5	146.18	0.5
3	247.11	265.25	7.3	253.75	2.7	268.26	8.6	247.35	0.1	247.30	0.1
4	351.08	401.87	14.5	369.95	5.4	391.38	11.5	353.05	0.6	352.89	0.5
5	461.38	553.89	20.1	492.89	6.8	524.84	13.8	460.44	0.2	460.05	0.3
6	570.77	713.32	25.0	620.95	8.8	620.91	8.8	571.65	0.2	570.79	0.0
7	691.48	873.28	26.3	754.31	9.1	842.28	21.8	691.76	0.0	690.03	0.2

Ref1 and Ref2: respectively analytical solution with Euler-Bernoulli and Tmoshenko models [18]. $\boldsymbol{\Delta = 100((f - f_{exp})/f_{exp})}$

Table 26: Comparison of natural frequecies of T1CR beam ander free-free boundary conditions by the analytical Euler-Bernoulli beam model, Timoshenko finite elements beam model and Timoshenko IGA-C with experimental results. Results are presented as the polynomial order p increases.

Mode	Exp	ref 1		ref 2		IGA-C		n=40			
		freq	Δ %	freq	Δ %	p=3	Δ %	p=5	Δ %	p=6	Δ %
1	60.49	60.49	0.0	60.49	0.0	63.64	5.2	60.41	0.1	60.41	0.1
2	146.34	153.23	4.7	152.04	3.9	159.46	9.0	150.33	2.7	150.32	2.7
3	250.82	275.03	9.7	266.34	6.2	277.86	10.8	258.51	3.1	258.46	3.0
4	361.26	418.23	15.8	391.16	8.3	406.09	12.4	370.51	2.6	370.36	2.5
5	473.88	577.13	21.8	521.11	10.0	541.53	14.3	481.71	1.7	481.35	1.6
6	588.38	745.49	26.7	654.48	11.2	607.32	3.2	594.24	1.0	593.44	0.9
7	709.04	915.75	29.2	791.41	11.6	853.94	20.4	713.30	0.6	711.69	0.4

Ref1 and Ref2: respectively analytical solution with Euler-Bernoulli and Tmoshenko models [18]. $\boldsymbol{\Delta = 100\left(\left(f - f_{exp}\right)/f_{exp}\right)}$

Ch7

7. Out-of-plane vibration of helical spring

7.1 Equation of motion

The geometry of interest and the notation used are shown in the Fig. 32. Consider the helical spring with a constant circular cross-section. R and ψ are the centerline radius of the helix, and the pitch angle of the helix, respectively. s is the curvilinear abscissa along the spring and S is the total length of the spring.

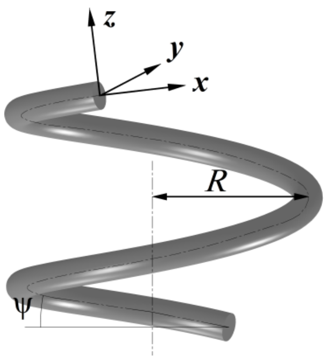

Fig.32: helical spring with a constant circular cross-section.

Yildirim [30, 31] derived the equation of motion of the described spring under the assumption of coincidence of the centroid of the cross-section and the shear centerline and neglecting the warping of the cross-section due to torsion. The mentioned equation is given in (7.1.a.b.c.d.e.f).

$$\frac{dT_x}{ds} - \chi T_y = -\omega^2 \rho A U_x \tag{7.1.a}$$

$$\frac{dT_y}{ds} + \chi T_x - \tau T_z = -\omega^2 \rho A U_y \tag{7.1.b}$$

$$\frac{dT_z}{ds} + \tau T_y = -\omega^2 \rho A U_z \tag{7.1.c}$$

$$\frac{dM_x}{ds} - \chi M_y = -\omega^2 \rho J \Theta_z \tag{7.1.d}$$

$$\frac{dM_y}{ds} - T_z + \chi M_x - \tau M_z = -\omega^2 \rho I_y \Theta_y \tag{7.1.e}$$

$$\frac{dM_z}{ds} + T_y + \tau M_y = -\omega^2 \rho I_z \Theta_z \tag{7.1.f}$$

Subscripts x, y and z stand for the tangential direction, the normal direction and the binormal direction.$U_j=U_j(s)$ represents the displacement in the direction j and $\Theta_j = \Theta_j(s)$ the rotation about the axis j. ρ is the density, A is the cross sectional area, I_n and I_b are the second moments of area with respect to the normal axis and to the binormal axis and J is the torsional moment of inertia of the cross section.

$\chi = \cos^2\psi/R$ and $\tau = \cos\psi \sin\psi/R$ are the curvature and the tortuosity of the helix, respectively.

$T_j=T_j(s)$ represents the internal force in the j direction, and $M_j=M_j(s)$ represents the internal moment acting on the axis j. Their expressions are given by (7.2.a.b.c.d.e.f).

$$T_x = EA\left(\frac{dU_x}{ds} - \chi U_y\right) \tag{7.2.a}$$

$$T_y = \alpha_y GA\left(\frac{dU_y}{ds} + \chi U_x - \tau U_z - \Theta_z\right) \tag{7.2.b}$$

$$T_z = \alpha_z GA\left(\frac{dU_z}{ds} + \tau U_z + \Theta_z\right) \tag{7.2.c}$$

$$M_x = GJ\left(\frac{d\Theta_x}{ds} - \chi \Theta_y\right) \tag{7.2.d}$$

$$M_y = EI_y\left(\frac{d\Theta_y}{ds} + \chi \Theta_x - \tau \Theta_z\right) \tag{7.2.e}$$

$$M_z = EI_z\left(\frac{d\Theta_z}{ds} + \tau \Theta_y\right) \tag{7.2.f}$$

E and G are Young's modulus and the shear modulus. α_y and α_z are the shear correction factors.

Substituting (7.2.a.b.c.d.e.f) into (7.1.a.b.c.d.e.f) yields (7.3.a.b.c.d.e.f).

$$EA\frac{d^2U_x}{ds^2}-\chi^2\alpha_y GAU_x-\chi A(E+\alpha_y G)\frac{dU_y}{ds}+\alpha_y\chi\tau GAU_z+\alpha_n\chi GA\Theta_z=-\omega^2\rho AU_x \tag{7.3.a}$$

$$\chi A(E+\alpha_y G)\frac{dU_x}{ds}+\alpha_y GA\frac{d^2U_y}{ds^2}-A(\chi^2E+\alpha_z\tau^2G)U_y-\tau GA(\alpha_y+\alpha_z)\frac{dU_z}{ds}-\alpha_z\tau GA\Theta_y$$
$$-\alpha_y GA\frac{d\Theta_z}{ds}=-\omega^2\rho AU_y \tag{7.3.b}$$

$$\alpha_y\chi\tau GAU_x+\tau GA(\alpha_y+\alpha_z)\frac{dU_y}{ds}+\alpha_z GA\frac{d^2U_z}{ds^2}-\tau^2\alpha_y GA\mathrm{U}_z+\alpha_z GA\frac{d\Theta_y}{ds}-\alpha_y\tau GA\Theta_z=$$
$$-\omega^2\rho AU_z \tag{7.3.c}$$

$$GJ\frac{d^2\Theta_x}{ds^2}-\chi^2EI_y\Theta_x-\chi(EI_y+GJ)\frac{d\Theta_y}{ds}+\chi\tau EI_y\Theta_z=-\omega^2\rho J\Theta_x \tag{7.3.d}$$

$$-\tau\alpha_z GAU_y-\alpha_z GA\frac{dU_z}{ds}+\chi(EI_y+GJ)\frac{d\Theta_x}{ds}+EI_y\frac{d^2\Theta_y}{ds^2}-(\alpha_z GA+\chi^2GJ+\tau^2EI_z)\Theta_y$$
$$-\tau E(I_y+I_z)\frac{d\Theta_b}{ds}=-\omega^2\rho I_y\Theta_y \tag{7.3.e}$$

$$\chi\alpha_y GAU_x+\alpha_y GA\frac{dU_y}{ds}-\alpha_y\tau GA\mathrm{U}_z+\chi\tau EI_y\Theta_x+\tau E(I_y+I_z)\frac{d\Theta_y}{ds}+EI_z\frac{d^2\Theta_z}{ds^2}$$
$$-(\alpha_y GA+\tau^2EI_y)\Theta_z=-\omega^2\rho I_z\Theta_z \tag{7.3.f}$$

7.2 Discretisation of the problem

As for the preceding examples, the solutions functions of system (98) are approximated with a linear combination of n NURBS shape functions of order p noted $R_i^p(\xi)$ and n coefficients of expansion as in (7.4.a.b.c.d.e.f). These shape functions are written on the collocation points of Grevilleξ_j.

$$U_x(\theta_j)\approx u_x(\xi_j)=\textstyle\sum_{i=0}^{n}u_{x_i}R_i(\xi_j)=[R]\{u_x\} \tag{7.4.a}$$
$$U_y(\theta_j)\approx u_y(\xi_j)=\textstyle\sum_{i=0}^{n}u_{y_i}R_i(\xi_j)=[R]\{u_y\} \tag{7.4.b}$$
$$U_z(\theta_j)\approx u_z(\xi_j)=\textstyle\sum_{i=0}^{n}u_{z_i}R_i(\xi_j)=[R]\{u_z\} \tag{7.4.c}$$

$$\Theta_x(\theta_j)\approx\theta_x(\xi_j)=\textstyle\sum_{i=0}^{n}\theta_{x_i}R_i(\xi_j)=[R]\{\theta_x\} \tag{7.4.d}$$
$$\Theta_y(\theta_j)\approx\theta_y(\xi_j)=\textstyle\sum_{i=0}^{n}\theta_{y_i}R_i(\xi_j)=[R]\{\theta_y\} \tag{7.4.e}$$
$$\Theta_z(\theta_j)\approx\theta_z(\xi_j)=\textstyle\sum_{i=0}^{n}\theta_{z_i}R_i(\xi_j)=[R]\{\theta_z\} \tag{7.4.f}$$

where $\{u_x\}=\{u_{x1},u_{x2},\dots,u_{xn}\}^T$, $\{u_y\}=\{u_{y1},u_{y2},\dots,u_{yn}\}^T$, $\{u_z\}=\{u_{z1},u_{z2},\dots,u_{zn}\}^T$, $\{\theta_x\}=\{\theta_{x1},\theta_{x2},\dots,\theta_{xn}\}^T$, $\{\theta_y\}=\{\theta_{y1},\theta_{y2},\dots,\theta_{yn}\}^T$ and $\{\theta_z\}=\{\theta_{z1},\theta_{z2},\dots,\theta_{zn}\}^T$

Substituting (7.4) into equation (7.3) yields the eigenvalues (7.5), which should be written in the compact form (7.6).

$$\begin{bmatrix} B_1 & B_2 & B_3 & [0] & [0] & B_4 \\ B_5 & B_6 & B_7 & [0] & B_8 & B_9 \\ B_{10} & B_{11} & B_{12} & [0] & B_{13} & B_{14} \\ [0] & [0] & [0] & B_{15} & B_{16} & B_{17} \\ [0] & B_{18} & B_{19} & B_{20} & B_{21} & B_{22} \\ B_{23} & B_{24} & B_{25} & B_{26} & B_{27} & B_{28} \end{bmatrix} \begin{Bmatrix} \{u_x\} \\ \{u_y\} \\ \{u_z\} \\ \{\theta_x\} \\ \{\theta_y\} \\ \{\theta_z\} \end{Bmatrix} = \omega^2 \begin{bmatrix} C_1 & [0] & [0] & [0] & [0] & [0] \\ [0] & C_2 & [0] & [0] & [0] & [0] \\ [0] & [0] & C_3 & [0] & [0] & [0] \\ [0] & [0] & [0] & C_4 & [0] & [0] \\ [0] & [0] & [0] & [0] & C_5 & [0] \\ [0] & [0] & [0] & [0] & [0] & C_6 \end{bmatrix} \begin{Bmatrix} \{u_x\} \\ \{u_y\} \\ \{u_z\} \\ \{\theta_x\} \\ \{\theta_y\} \\ \{\theta_z\} \end{Bmatrix} \quad (7.5)$$

where

$$B_1 = \frac{EA}{S^2}[\boldsymbol{R''}] - \alpha_y\chi^2 GA[\boldsymbol{R}] \qquad B_2 = -\frac{\chi}{S}\left(EA + \alpha_y GA\right)[\boldsymbol{R'}]$$
$$B_3 = \alpha_y\chi\tau GA[\boldsymbol{R}] \qquad B_4 = \alpha_y\chi GA[\boldsymbol{R}]$$
$$B_5 = \frac{\chi}{S}\left(EA + \alpha_y GA\right)[\boldsymbol{R'}] \qquad B_6 = \frac{\alpha_y GA}{S^2}[\boldsymbol{R''}] - (\chi^2 EA + \alpha_z\tau^2 GA)[\boldsymbol{R}]$$
$$B_7 = -\frac{\tau GA}{S}\left(\alpha_y + \alpha_z\right)[\boldsymbol{R'}] \qquad B_8 = -\tau\alpha_z GA[\boldsymbol{R}]$$
$$B_9 = -\frac{\alpha_y GA}{S}[\boldsymbol{R'}] \qquad B_{10} = \alpha_y\chi\tau GA[\boldsymbol{R}]$$
$$B_{11} = \frac{\tau GA}{S}\left(\alpha_y + \alpha_z\right)[\boldsymbol{R'}] \qquad B_{12} = \frac{\alpha_z GA}{S^2}[\boldsymbol{R''}] - \alpha_y\tau^2 GA[\boldsymbol{R}]$$
$$B_{13} = \frac{\alpha_z GA}{S}[\boldsymbol{R'}] \qquad B_{14} = -\alpha_y\tau GA[\boldsymbol{R}]$$
$$B_{15} = \frac{GJ}{S^2}[\boldsymbol{R''}] - \chi^2 EI_y[\boldsymbol{R}] \qquad B_{16} = -\frac{\chi}{S}\left(EI_y + GJ\right)[\boldsymbol{R'}]$$
$$B_{17} = \chi\tau EI_y[\boldsymbol{R}] \qquad B_{18} = -\alpha_z\tau GA[\boldsymbol{R}]$$
$$B_{19} = -\frac{\alpha_z GA}{S}[\boldsymbol{R'}] \qquad B_{20} = \frac{\chi}{S}\left(EI_y + GJ\right)[\boldsymbol{R'}]$$
$$B_{21} = \frac{EI_y}{S^2}[\boldsymbol{R''}] - (\alpha_z GA + \chi^2 GJ + \tau^2 EI_z)[\boldsymbol{R}] \qquad B_{22} = -\frac{\tau E}{S}\left(I_y + I_z\right)[\boldsymbol{R'}]$$
$$B_{23} = \alpha_y\chi GA[\boldsymbol{R}] \qquad B_{24} = \frac{\alpha_y GA}{S}[\boldsymbol{R'}]$$
$$B_{25} = -\alpha_y\tau GA[\boldsymbol{R}] \qquad B_{26} = \chi\tau EI_y[\boldsymbol{R}]$$
$$B_{27} = \frac{\tau E}{S}\left(I_y + I_z\right)[\boldsymbol{R'}] \qquad B_{28} = \frac{EI_z}{S^2}[\boldsymbol{R''}] - \left(\alpha_y GA + \tau^2 EI_y\right)[\boldsymbol{R}]$$

$$C_1 = -\rho A[R] \qquad C_2 = -\rho A[R]$$
$$C_3 = -\rho A[R] \qquad C_4 = -\rho J[R]$$
$$C_5 = -\rho I_y[R] \qquad C_6 = -\rho I_z[R]$$

[0] stands for a matrix of n lines and n columns with all elements are equal to zero.

$$[\boldsymbol{H}]\{\boldsymbol{A}\} = -\boldsymbol{\omega}^2[\boldsymbol{S}]\{\boldsymbol{A}\} \tag{7.6}$$

7.3 Imposing the boundary conditions

The eigenvalue problem (7.6) is written as in (7.7).

$$[\boldsymbol{H_r}]\{\boldsymbol{A_r}\} + [\boldsymbol{H^+}]\{\boldsymbol{A^+}\} = -\boldsymbol{\omega}^2([\boldsymbol{S_r}]\{\boldsymbol{A_r}\} + [\boldsymbol{S^+}]\{\boldsymbol{A^+}\}) \tag{7.7}$$

where$\{A_r\} = \Big\{{u_x}_2{u_x}_3 \dots {u_x}_{n-1}{u_y}_2{u_y}_3 \dots {u_y}_{n-1}{u_z}_2{u_z}_3 \dots {u_z}_{n-1}{\theta_x}_2{\theta_x}_3 \dots {\theta_x}_{n-1} \dots$

$\dots {\theta_y}_2{\theta_y}_3 \dots {\theta_y}_{n-1}{\theta_z}_2{\theta_z}_3 \dots {\theta_z}_{n-1}\Big\}^T$

and$\{A^+\} = \{{u_x}_1{u_x}_n{u_y}_1{u_y}_n{u_z}_1{u_z}_n{\theta_x}_1{\theta_x}_n{\theta_y}_1{\theta_y}_n{\theta_z}_1{\theta_z}_n\}^T$

The size of $[H]$ is $6(n\text{-}2)\times6(n\text{-}2)$ and that of $[H^+]$ is $6(n\text{-}2)\times12$. The full number of unknown factors in {A} and $\{A^+\}$ is n while the number of equations is $n\text{-}12$.

We will restrict this study to the most current boundary conditions namely case: clamped, free, and pinned.

Let us impose a condition to the j^{th}node. The three possibilities studied here are represented in the first column of Table 27 and their effects on the system in the second column. One should approximate the efforts associated to the coordinate ξ_j using relations (2.a.b.c.d.e.f) and (4.a.b.c.d.e.f) as in the third column of Table 27.

Now, by considering the two boundaries, one should represent the boundary conditions in term of the nodal variables as in the relation (7.8). This might seem clearer through the example (7.9.a.b) which represents Clamped-free boundary conditions at ξ=0 and ξ=1 respectively.

Table 27: Approximation of the studied boundary conditions.

BC	affects of the BC	approximation of the BC
Clamped (**C**)	$u_x(\xi_j)=0$	$\sum_{i=1}^{n} u_{x\,i} R_i(\xi_j) = 0$
	$u_y(\xi_j)=0$	$\sum_{i=1}^{n} u_{y\,i} R_i(\xi_j) = 0$
	$u_z(\xi_j)=0$	$\sum_{i=1}^{n} u_{z\,i} R_i(\xi_j) = 0$
	$\theta_x(\xi_j)=0$	$\sum_{i=1}^{n} \theta_{x\,i} R_i(\xi_j) = 0$
	$\theta_y(\xi_j)=0$	$\sum_{i=1}^{n} \theta_{y\,i} R_i(\xi_j) = 0$
	$\theta_z(\xi_j)=0$	$\sum_{i=1}^{n} \theta_{z\,i} R_i(\xi_j) = 0$
Free (**F**)	$T_x(\xi_j)=0$	$\frac{1}{S}\sum_{i=1}^{n} u_{x\,i} R'_i(\xi_j) - \chi\sum_{i=1}^{n} u_{y\,i} R_i(\xi_j) = 0$
	$T_y(\xi_j)=0$	$\chi\sum_{i=1}^{n} u_{x\,i} R_i(\xi_j) + \frac{1}{S}\sum_{i=1}^{n} u_{y\,i} R'_i(\xi_j) - \tau\sum_{i=1}^{n} u_{z\,i} R_i(\xi_j) -$ $\sum_{i=1}^{n} \theta_{y\,i} R_i(\xi_j) = 0$
	$T_z(\xi_j)=0$	$\tau\sum_{i=1}^{n} u_{y\,i} R_i(\xi_j) + \frac{1}{S}\sum_{i=1}^{n} u_{z\,i} R'_i(\xi_j) + \sum_{i=1}^{n} \theta_{y\,i} R_i(\xi_j) = 0$
	$M_x(\xi_j)=0$	$\frac{1}{S}\sum_{i=1}^{n} \theta_{x\,i} R'_i(\xi_j) - \chi\sum_{i=1}^{n} \theta_{y\,i} R_i(\xi_j) = 0$
	$M_y(\xi_j)=0$	$\chi\sum_{i=1}^{n} \theta_{x\,i} R_i(\xi_j) + \frac{1}{S}\sum_{i=1}^{n} \theta_{y\,i} R'_i(\xi_j) - \tau\sum_{i=1}^{n} \theta_{z\,i} R_i(\xi_j) = 0$
	$M_z(\xi_j)=0$	$\tau\sum_{i=1}^{n} \theta_{y\,i} R_i(\xi_j) + \frac{1}{S}\sum_{i=1}^{n} \theta_{z\,i} R'_i(\xi_j) = 0$
Pinned (**P**)	$u_x(\xi_j)=0$	$\sum_{i=1}^{n} u_{x\,i} R_i(\xi_j) = 0$
	$u_y(\xi_j)=0$	$\sum_{i=1}^{n} u_{y\,i} R_i(\xi_j) = 0$
	$u_z(\xi_j)=0$	$\sum_{i=1}^{n} u_{z\,i} R_i(\xi_j) = 0$
	$M_x(\xi_j)=0$	$\frac{1}{S}\sum_{i=1}^{n} \theta_{x\,i} R'_i(\xi_j) - \chi\sum_{i=1}^{n} \theta_{y\,i} R_i(\xi_j) = 0$
	$M_y(\xi_j)=0$	$\chi\sum_{i=1}^{n} \theta_{x\,i} R_i(\xi_j) + \frac{1}{S}\sum_{i=1}^{n} \theta_{y\,i} R'_i(\xi_j) - \tau\sum_{i=1}^{n} \theta_{z\,i} R_i(\xi_j) = 0$
	$M_z(\xi_j)=0$	$\tau\sum_{i=1}^{n} \theta_{y\,i} R_i(\xi_j) + \frac{1}{S}\sum_{i=1}^{n} \theta_{z\,i} R'_i(\xi_j) = 0$

Each set of the boundary conditions taken from the Table 27 could be written in the matrix form (103).

$$[U]\{A^+\} + [V]\{A_r\} = \{0_{12\times1}\} \tag{7.8}$$

Clamped free boundary conditions:

$$\begin{cases} \sum_{i=1}^{n} u_{x_i} R_i(0) = 0 \\ \sum_{i=1}^{n} u_{y_i} R_i(0) = 0 \\ \sum_{i=1}^{n} u_{z_i} R_i(0) = 0 \\ \sum_{i=1}^{n} \theta_{x_i} R_i(0) = 0 \\ \sum_{i=1}^{n} \theta_{y_i} R_i(0) = 0 \\ \sum_{i=1}^{n} \theta_{z_i} R_i(0) = 0 \end{cases} \tag{7.9.a}$$

$$\begin{cases} \frac{1}{S}\sum_{i=1}^{n} u_{x_i} R'_i(1) - \chi \sum_{i=1}^{n} u_{y_i} R_i(1) = 0 \\ \chi \sum_{i=1}^{n} u_{x_i} R_i(1) + \frac{1}{S}\sum_{i=1}^{n} u_{y_i} R'_i(1) - \tau \sum_{i=1}^{n} u_{z_i} R_i(1) - \sum_{i=1}^{n} \theta_{y_i} R_i(1) = 0 \\ \tau \sum_{i=1}^{n} u_{y_i} R_i(1) + \frac{1}{S}\sum_{i=1}^{n} u_{z_i} R'_i(1) + \sum_{i=1}^{n} \theta_{y_i} R_i(1) = 0 \\ \frac{1}{S}\sum_{i=1}^{n} \theta_{x_i} R'_i(1) - \chi \sum_{i=1}^{n} \theta_{y_i} R_i(1) = 0 \\ \chi \sum_{i=1}^{n} \theta_{x_i} R_i(1) + \frac{1}{S}\sum_{i=1}^{n} \theta_{y_i} R'_i(1) - \tau \sum_{i=1}^{n} \theta_{z_i} R_i(1) = 0 \\ \tau \sum_{i=1}^{n} \theta_{y_i} R_i(1) + \frac{1}{S}\sum_{i=1}^{n} \theta_{z_i} R'_i(1) = 0 \end{cases} \tag{7.9.b}$$

Expression (7.8) enables us to draw the values of $\{A^+\}$ which satisfy the boundary conditions. These are then injected into the initial system (7.7) in order to obtain system (7.10).

$$([H_r] - [H^+][U]^{-1}[V])\{A_r\} = -\omega^2\big(([S_r] - [S^+][U]^{-1}[V])\{A_r\}\big) \tag{7.10}$$

7.4 Numerical experiments

In this section, different numerical experiments are shown to test the accuracy of the IGA-C method. In order to assess the present work, the results obtained are presented in term of natural frequencies (*Hz*) and compared with those of previous works, including reference [32] in which the author used the dynamic stiffness method (DS) and the reference [33] in which the author used pseudo-spectral method with Chebyshev polynomials (PS-C).

The geometrical and material parameters of the tested model are presented in the (Table 28).

Table 28: Geometric and material parameters of the tested model.

Parameter	Value
r	6 mm
R	65 mm
ψ	7.44°
n	6
α_N	10/11
α_B	10/11
E	$2.09*10^{11}$ N/m^2
ν	0.28

To investigate the convergence and accuracy of the results obtained in the present work, two tests are carried out. The first test consists in fixing the number of collocation points to n=100and varying the degree of approximation p (Table 29). The results are in excellent agreement with those obtained by the dynamic stiffness method (DS) and they are identical to those obtained by the PS-C from the polynomial order p=12. (Fig. 33) shows the convergence of the solution by tracing the variation of the logarithm of the error function defined in (7.11) with respect to the polynomial order p.

$$e_{f_i}(p) = \frac{|f_i(p) - f_i(p=19)|}{f_i(p=19)} \tag{7.11}$$

The second test consists in fixing the degree of approximation to p=19and varying the number of collocation points (Table 30). The results are in excellent agreement with those obtained by the dynamic stiffness method (DS) and they are identical to those obtained by the PS-C from n=50. (Fig. 34) shows the convergence of the solution by tracing the variation of the logarithm of the error function defined in (7.12) with respect to the number of collocation points n.

$$e_{f_i}(n) = \frac{|f_i(n) - f_i(n=100)|}{f_i(n=100)} \tag{7.12}$$

Table 29 : Natural frequencies in (Hz) with increasing polynomial degree p . n=100. Clamped-Clamped boundary conditions.

Mode	DS [22]	PS-C [23]	IGA_C						
			p=3	p=6	p=9	p=12	p=15	n=17	n=19
1	40.994	40.993	46.355	41.275	40.993	40.993	40.993	40.993	40.993
2	45.135	45.134	56.807	46.303	45.135	45.134	45.134	45.134	45.134
3	46.951	46.950	93.034	47.592	46.951	46.950	46.950	46.950	46.950
4	47.726	47.725	117.214	48.028	47.725	47.725	47.725	47.725	47.725
5	81.091	81.089	140.792	81.167	81.089	81.089	81.089	81.089	81.089
6	88.976	88.974	184.391	89.556	88.975	88.974	88.974	88.974	88.974
7	91.586	91.585	191.108	91.739	91.585	91.585	91.585	91.585	91.585
8	93.173	93.171	246.190	93.670	93.172	93.171	93.171	93.171	93.171

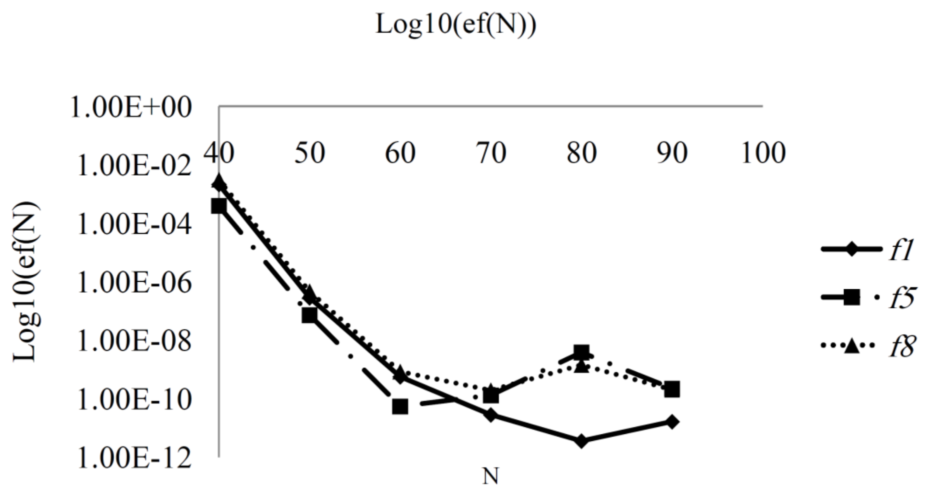

Fig. 33: Error function with respect to the number of collocation points n: $Log_{10}(e_f(n))$.

Table 30: Natural frequencies in (Hz) with increasing number of collocation points *n* .*p*=19. Clamped-Clamped boundary conditions.

Mode	DS [22]	PS-C [23]	IGA_C						
			n=40	*n* =50	*n* =60	*n* =70	*n* =80	*n* =90	*n* =100
1	40.994	40.993	41.079	40.993	40.993	40.993	40.993	40.993	40.993
2	45.135	45.134	45.507	45.134	45.134	45.134	45.134	45.134	45.134
3	46.951	46.950	47.231	46.950	46.950	46.950	46.950	46.950	46.950
4	47.726	47.725	47.751	47.725	47.725	47.725	47.725	47.725	47.725
5	81.091	81.089	81.120	81.089	81.089	81.089	81.089	81.089	81.089
6	88.976	88.974	89.254	88.974	88.974	88.974	88.974	88.974	88.974
7	91.586	91.585	91.663	91.585	91.585	91.585	91.585	91.585	91.585
8	93.173	93.171	93.457	93.171	93.171	93.171	93.171	93.171	93.171

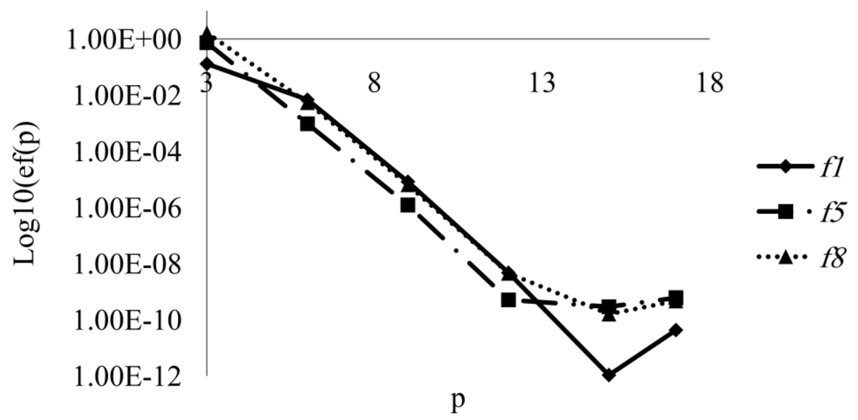

Fig. 34: Error function with respect to the polynomial order p: $Log_{10}(e_f(p))$.

(Table 32) represents the natural frequencies obtained for various boundary conditions.

Table 31: Natural frequencies in (Hz) obtained for different boundary conditions. FF: free-free, C-F: clamped-free and P-P: Pinned-Pinned. n=100 and p=19.

BC	F-F			C-F			P-P		
Mode	DS [22]	PS-C [23]	IGA-C	DS [22]	PS-C [23]	IGA-C	DS [22]	PS-C [23]	IGA-C
1	41.962	41.961	41.961	9.4719	9.4718	9.472	28.516	28.516	28.516
2	43.309	43.309	43.309	9.4998	9.4997	9.500	29.171	29.171	29.171
3	44.106	44.106	44.106	21.359	21.358	21.358	31.162	31.161	31.161
4	49.384	49.384	49.384	24.17	24.17	24.170	33.784	33.784	33.784
5	81.178	81.176	81.176	42.101	42.1	42.100	70.125	70.124	70.124
6	86.721	86.72	86.720	42.857	42.857	42.857	74.721	74.721	74.721
7	88.303	88.302	88.302	63.109	63.107	63.107	78.099	78.098	78.098
8	94.927	94.926	94.926	71.205	71.205	71.205	79.63	79.629	79.629

Finally, we present in (Fig. 35) the first five mode shapes under clamped-clamped boundary conditions; we verify thatthey arein agreement withthose ofreferences[32] and [33].

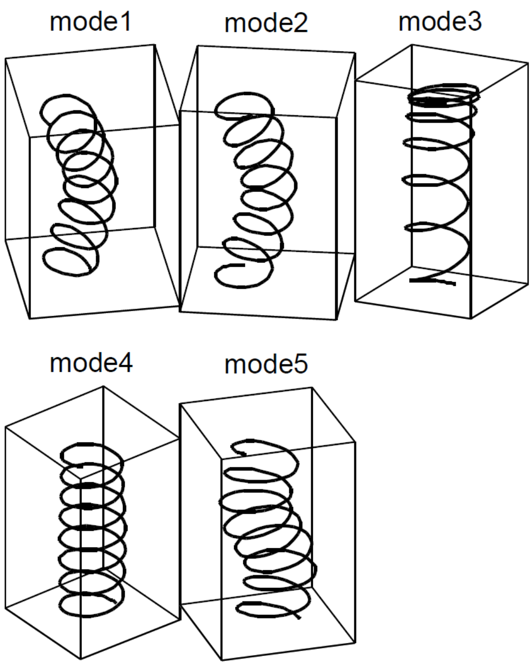

Fig. 35: First five mode shapes. The boundary conditions are clamped-clamped.

Ch8

8. Vibration analysis of a cracked Timoshenko beam

8.1. Crack modelling

In order to model the effects of stress concentration close to the crack location, Christides and Barr [34] have considered that the bending stiffness (*EI*) close to the crack location decreases according to an exponential function; they established this function and calibrated it using experimental results. Meanwhile J. K. SINHA and al [35], considered that the bending stiffness decreases linearly close to the crack location. The two previously mentioned works considered the Euler-Bernoulli beam and developed finite elements models of cracked beams. But, when Timoshenko beam model is used, the shear stiffnessAG intervenes, the variation of this last close to the crack location should be deduced from the bending stiffness as shown in (8.1) and (8.2). In this work, the crack effect on the beam stiffness is approximated by a linear variation in the bending stiffness (*EI*) (8.1) and the shear stiffness (*GA*) (8.2) a long of the beam.

Let us write a distribution function for the bending stiffness along the beam as described in (8.1). This function ensures the decrease of rigidity close the cracked zone as indicated in Fig.36. It also has the advantage of being calibrated using the variable *lc*.

$$EI(x) = \begin{cases} EI - (E(I - I_c))\dfrac{x - (x_c - l_c)}{l_c}, & for x \in [0; x_c] \\ EI - (E(I - I_c))\dfrac{(x_c + l_c) - x}{l_c}, & for x \in [x_c; L] \end{cases} \tag{8.1}$$

where$I = bh^3/12$, $I_c = b(h-d)^3/12$. $x_c$is the crack abscissa. l_c is a constant relative to the beam's thickness *h,* its value is determinate from experimental results by the use of optimisation process.

Then, one deduces simply the function of distribution of the shear stiffness with the relations (8.2).

$$\begin{cases} I = \dfrac{bh^3}{12} = bh\dfrac{h^2}{12} = A\dfrac{h^2}{12} \\ E = G2(1+\nu). \end{cases} \quad \Rightarrow AG(x) = \frac{6}{h^2(1+\nu)}EI(x) \tag{8.2}$$

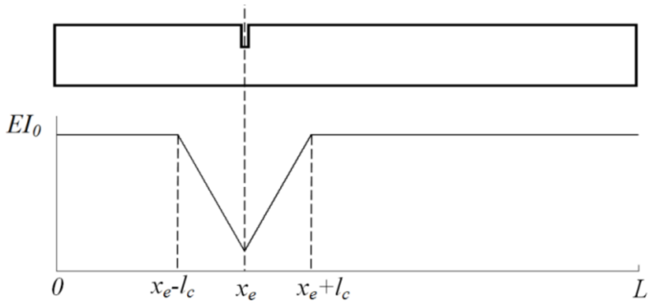

Fig. 36.Distribution of bending stiffness according to equation (8.1) along a damaged beam. The cracked zone is situated in abscissa x_e.

Now the stress-strain relations*M(x)* and *T(x)* should be written as in (8.3) such as the stiffness in depending on *x*.

$$\begin{cases} M(x) = EI(x)\dfrac{\partial\theta}{\partial x} \\ T(x) = \alpha GA(x)\left(\dfrac{\partial v}{\partial x} - \theta\right) \end{cases} \tag{8.3}$$

The substitution of (8.3) in the Timoshenko beam equation described in (4.1) gives equation (8.4) representing a mathematical model of cracked beam.

$$\begin{cases} -\alpha GA\theta + EI'\theta' + EI\theta'' + \alpha GAv' = -\omega^2\rho I\theta \\ -\alpha GA'\theta - \alpha GA\theta' + \alpha GA'v' + \alpha GAv'' = -\omega^2\rho Av \end{cases} \tag{8.4}$$

8.2. Discretisation of the problem

The first step is thus to write the solutions approximating the functions *w (x)* and *θ (x)* and their derivatives as linear combination of *n* basis functions and *n* control variables as in (8.5).

$$\begin{gathered} w(x) \approx w_n(\xi) = \textstyle\sum_{i=0}^{n} w_i R_i(\xi)\ \theta(x) \approx \theta_n(\xi) = \sum_{i=0}^{n} \theta_i R_i(\xi) \\ w'^{(x)} \approx \frac{1}{L}w'_n(\xi) = \frac{1}{L}\textstyle\sum_{i=0}^{n} w_i R'_i(\xi)\ \theta'(x) \approx \frac{1}{L}\theta'_n(\xi) = \frac{1}{L}\sum_{i=0}^{n} \theta_i R'_i(\xi) \\ w''(x) \approx \frac{1}{L^2}w''_n(\xi) = \frac{1}{L^2}\textstyle\sum_{i=0}^{n} w_i R''_i(\xi)\ \theta''(x) \approx \frac{1}{L^2}\theta''_n(\xi) = \frac{1}{L^2}\sum_{i=0}^{n} \theta_i R''_i(\xi) \end{gathered} \tag{8.5}$$

L is the length of the field of investigation and $x \in [0, L]$. ξ is the parametric variable defined by : $\xi = \frac{x}{L} \in [0, 1]$.

Thereafter, an algebraic system is built by writing the expression of the solution on a set of nGreville'scollocation points.

Substituting the approximate solutions (8.5) in the considered problem (8.4) gives (8.6).

$$\begin{cases} \left(-\alpha GA[\mathrm{R}] + \frac{EI'}{L''}[R'] + \frac{EI}{L''}[R'']\right)\{\boldsymbol{\theta}\} + \frac{\alpha GA}{L}[R']\{\boldsymbol{w}\} = -\omega^2 \rho I[R]\{\boldsymbol{\theta}\} \\ \left(-\frac{\alpha GA'}{L}[\mathrm{R}] - \frac{\alpha GA}{L}[\mathrm{R}']\right)\{\boldsymbol{\theta}\} + \left(\frac{\alpha GA'}{L''}[R'] + \frac{\alpha GA}{L''}[R'']\right)\{\boldsymbol{w}\} = -\omega^2 \rho A[R]\{\boldsymbol{w}\} \end{cases} \tag{8.6}$$

The system (8.6) could be rewritten in matrix form (8.7).

$$\begin{bmatrix} \left(-\alpha GA[\mathrm{R}] + \frac{EI'}{L''}[R'] + \frac{EI}{L''}[R'']\right) & \frac{\alpha GA}{L}[R'] \\ \left(-\frac{\alpha GA'}{L}[\mathrm{R}] - \frac{\alpha GA}{L}[\mathrm{R}']\right) & \left(\frac{\alpha GA'}{L''}[R'] + \frac{\alpha GA}{L''}[R'']\right) \end{bmatrix} \begin{bmatrix} \{\boldsymbol{\theta}\} \\ \{\boldsymbol{w}\} \end{bmatrix} = -\omega^2 \begin{bmatrix} \rho I[R] & 0 \\ 0 & \rho h[R] \end{bmatrix} \begin{bmatrix} \{\boldsymbol{\theta}\} \\ \{\boldsymbol{w}\} \end{bmatrix} \tag{8.7}$$

Equation (8.7) could be written in compact form as in (8.8).

$$[H]\{A\} = -\omega^2 [S]\{A\} \tag{8.8}$$

where:$\{A\} = \{\theta_1, \theta_2, \dots, \theta_n, w_1, w_2, \dots, w_n\}$

8.3. Imposing the boundary conditions

Let us rewrite first the expression (8.8) as in (8.9).

$$[\boldsymbol{H_r}]\{\boldsymbol{A_r}\} + [\boldsymbol{H^+}]\{\boldsymbol{A^+}\} = -\boldsymbol{\omega}^2([\boldsymbol{S_r}]\{\boldsymbol{A_r}\} + [\boldsymbol{S^+}]\{\boldsymbol{A^+}\}) \tag{8.9}$$

where $\{A_r\} = \{\theta_2 \theta_3 \dots \theta_{n-1} w_2 w_3 \dots w_{n-1}\}^T$ *and* $\{A^+\} = \{\theta_1 \theta_n w_1 w_n\}^T$

The size of **[*H*]** is **2(n-2) × 2(n-2)** while that of **[H+]** is **2n×4**. The full number of unknown factors in **{*A*}** and **{*A*⁺}** is ***n*** while the number of equations is ***n-4***. The remaining four equations are obtained with the boundary conditions.

<u>Free-free boundary conditions:</u>

Let us consider the case of free-free boundary conditions which is characterized by the absence of external efforts (8.10).

$$\begin{cases} T(0) = M(0) = 0 \\ T(L) = M(L) = 0 \end{cases} \tag{8.10}$$

By the use of expressions (8.3) and (8.5), one can express efforts at the extreme nodes as in (8.11).

$$\begin{array}{l} T(0) = \frac{\alpha GA(0)}{L} \sum_{i=1}^{n} R_i^{'}(0) v_i - \alpha GA(0) \sum_{i=1}^{n} R_i(0)\theta_i \;\;,\;\; M(0) = \frac{EI(0)}{L} \sum_{i=1}^{n} R_i^{'}(0)\theta_i \\ T(L) = \frac{\alpha GA(L)}{L} \sum_{i=1}^{n} R_i^{'}(1) v_i - \alpha GA(0) \sum_{i=1}^{n} R_i(1)\theta_i \;\;,\;\; M(L) = \frac{EI(L)}{L} \sum_{i=1}^{n} R_i^{'}(1)\theta_i \end{array} \tag{8.11}$$

Equations (8.11) can be rearranged in matrix form (8.12).

$$[V]\{A_r\} + [U]\{A^+\} = \{0\} \tag{8.12}$$

Then, the expression of $\{A^+\}$ is derived from (8.12) and injected in the initial system(8.9) to yield (8.13)

$$([\boldsymbol{H_r}] - [\boldsymbol{H^+}][\boldsymbol{U}]^{-1}[\boldsymbol{V}])\{\boldsymbol{A_r}\} = -\boldsymbol{\omega}^2([\boldsymbol{S_r}] - [\boldsymbol{S^+}][\boldsymbol{U}]^{-1}[\boldsymbol{V}])\{\boldsymbol{A_r}\} \tag{8.13}$$

The eigenvalues problem (8.13) describes the dynamic behaviour of a steel–concrete composite beam under free-free boundary conditions.

8.4. Updating the model

Starting from given nominal value $E_0$of the uncracked beam, the optimal value of the Young's modulus is evaluated by solving the minimum problem (8.14).

$$\text{To find } E \text{ such that } A = \min_{0.8E_0 < E \leq 1.2E_0} F(E), \tag{8.14}$$

where:

$$F(\mu, k) = \sum_{i=1}^{4} \sqrt{\left(\left(f_i - f_{exp\,i}\right)/f_{exp\,i}\right)^2}.$$

f and f_{exp} are respectively the analytical and experimental values of the natural frequencies, i being the mode number. Experimental results are taken from reference [35].

8.5. Calibrating the cracked beam model

As for updating the model, we propose to assess the value of l_c by minimisation of the error function F for different cases of damages. Experimental results are taken from reference

[35]. Figure 37 represents the graph of the error function (8.15). The optimal value of l_c is $l_c=h$.

$$F(l_c) = \sum_{j=1}^{3} \sum_{i=1}^{4} \sqrt{\left(\left((f_i)_j - \left(f_{exp\ i}\right)_j\right) / \left(f_{exp\ i}\right)_j\right)^2} \tag{8.15}$$

where $j=1,2,3$ represents the three cases of experimental cracked beams models available in reference [35], these refer to beams with cracks represented by cuts depths 4, 8 and 12 mm all located at 430 cm from the beams edges.

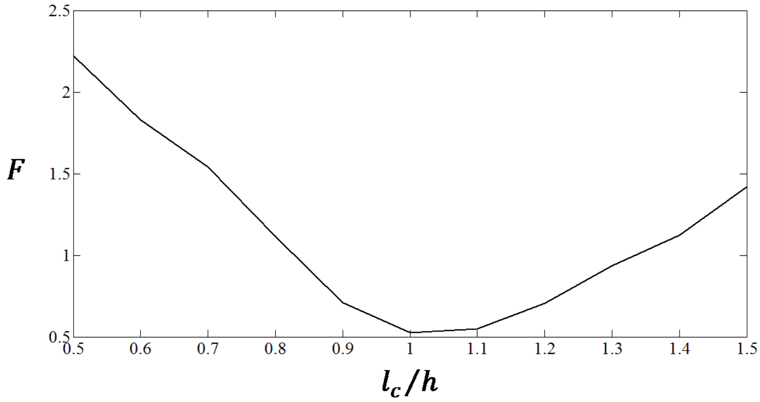

Fig.37. Error function F versus l_c as described in (8.15).

8.6. Local refinement

A good approximation of the stiffness's distribution across a small portion of the beam requires a fine refinement. Indeed, the results deteriorate considerably when the model is not sufficiently refined; nevertheless, the refinement of the entire model increases the computation cost. In this work, we propose to locally refine the beam model by acting on the knot vector defined in chapter 2; we proceed by inserting knots nearly the damaged zone; these act directly by inserting new basis functions and new collocation points. Fig.38 shows a locally refined NURBS basis composed of 11 cubic basis functions.

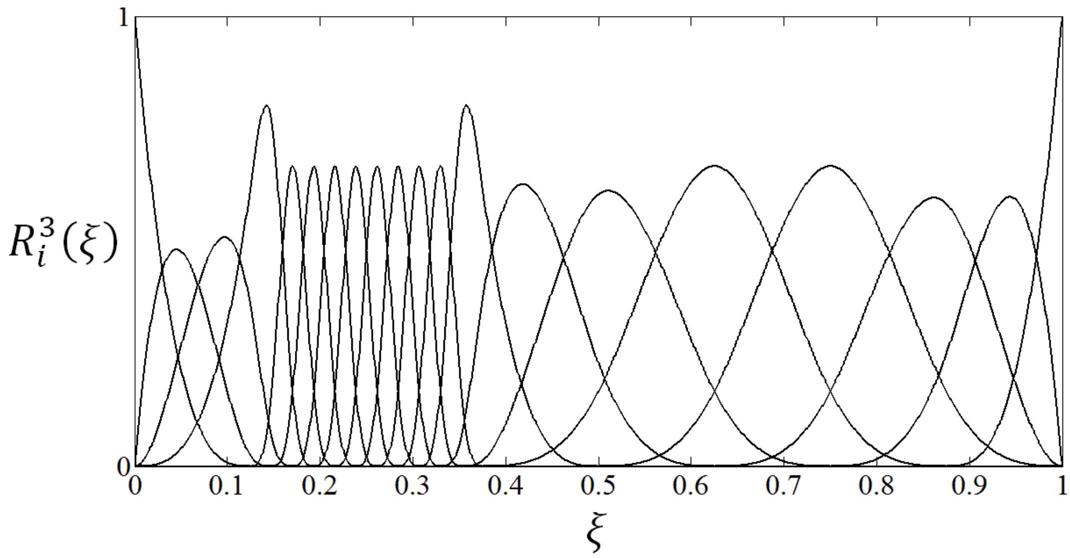

Fig. 38.NURBS cubic base locally refined by knots insertion close to the damaged zone.

8.7. Numerical tests

Natural frequencies of the steel cracked beams studied in references [35] are evaluated using the developed IGA-C model. The beams parameters are taken from reference [35] and reported in Table 32.

Table.32. Steel beams parameters taken from reference [35].

Beam's parameters	
Material	Steel
Young's modulus E	203.91 GN/m^2
Mass density ρ	7800 kg/m^3
Poisson's ratio v	0.33
Beam's length L	1330 mm
Beam's width b	25.30 mm
Beam's depth h	25.30 mm

The first four natural frequencies of the studied beamsspecimens are given in (Tables 33 to 36) and errors are evaluated for each frequency. Results are compared to experimental and analytical published ones from reference [35].

In Table 33, the first four natural frequencies of the studied steel beam with no crack are presented and compared with those of reference [35]. The results are in good agreement with those of reference [35] obtained experimentally andfinite element method computations.

Tables 34, 35 and 36, show the first four natural frequencies of the studied steel beam with the respective crack depths of 4, 8 and 12 mm. All the cracks are situated at the abscissa x_c=430 mm. The results are in good agreement with those of reference [35] obtained by experiment and finite element method.

It should be noted that the precision scale of these experimental results makes them unsuitable as a basis for comparing the accuracy of the two numerical methods.

Fig 39 shows the decrease of the first four eigenvalues of the studied beam with respect to crack depth. We observe that the influence of the crack depth is different from a frequency to another. This could be explained by the crack location. Indeed, we remark in Fig.40 that the damaged zone undergoes a greater displacement by vibrating in the first and the second modes. The displacement is however less important when it vibrates in the fourth mode. The damaged zone is located close to a node of third mode (zero displacement), which explains the fact that the frequency of the latter reacts very little.

This last result shows the importance of using the maximum number of vibratory modes for the localization and the characterisation of the damages in the structures.

Table.33. Natural frequencies in (*Hz*) of the steel Free-Free beam with no Crack.

Mode	no crack				
	exp	ref [35]	error %	IGA-C	error %
1	75,313	75,171	0,189	75,558	0,326
2	207,188	207,212	0,012	207,265	0,037
3	406,250	406,225	0,006	404,673	0,388
4	667,813	671,536	0,557	665,708	0,315

Table.34. Natural frequencies in (Hz) of the steel Free-Free cracked beam.

Mode	d = 4 mm x = 430 mm				
	exp	ref 1	error %	IGA-C	error %
1	74,688	74,406	0,378	75,031	0,460
2	205,625	204,183	0,701	205,410	0,105
3	405,625	405,368	0,063	404,154	0,363
4	666,250	668,429	0,327	663,705	0,382

Table.35. Natural frequencies in (Hz) of the steel Free-Free cracked beam.

Mode	d = 8 mm x = 430 mm				
	exp	ref 1	error %	IGA-C	error %
1	74,063	73,628	0,587	74,260	0,266
2	202,500	201,283	0,601	202,913	0,204
3	404,688	404,557	0,032	403,456	0,304
4	662,813	665,356	0,384	661,095	0,259

Table.36.Natural frequencies in (Hz) of the steel Free-Free cracked beam.

Mode	d = 12 mm		x = 430 mm		
	exp	ref 1	error %	IGA-C	error %
1	72,813	72,958	0,199	72,898	0,116
2	197,188	198,928	0,882	197,958	0,390
3	403,125	403,916	0,196	402,049	0,267
4	655,938	662,874	1,057	655,552	0,059

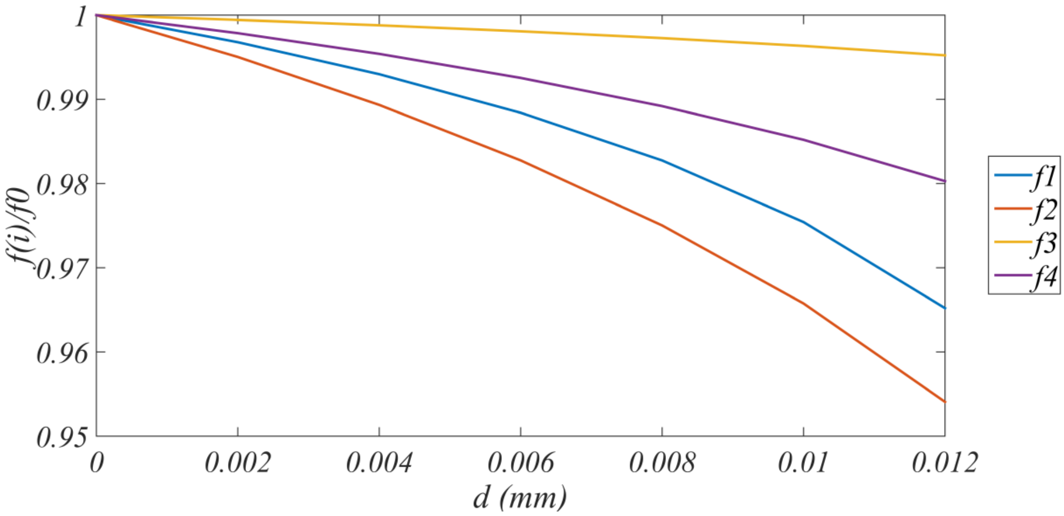

Fig.39. First fournormalized natural frequencies versus damage depth *d*.

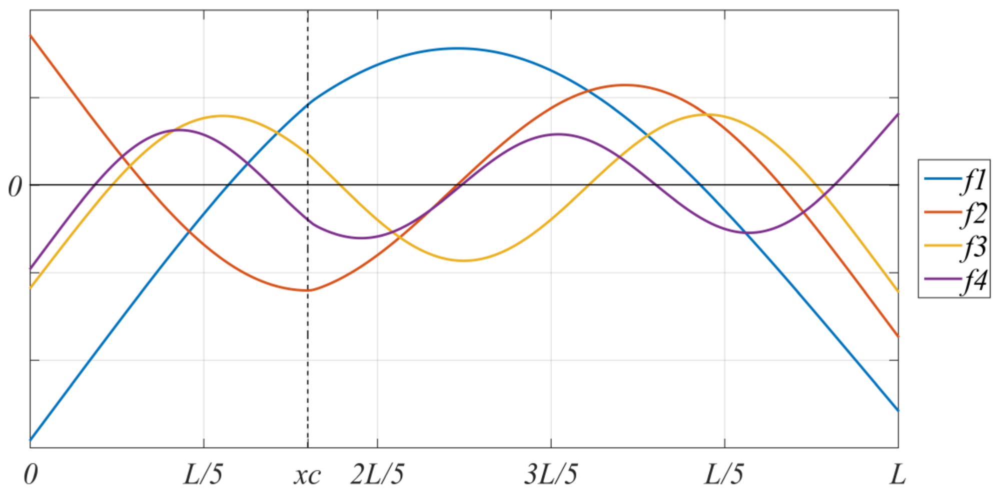

Fig. 40.First four mode shapes of Timoshenko cracked beam

Ch9

9. Reisner-Mindlin plate

Let us consider the eigenvalue problem (9.1.a.b.c) derived from the Reisner-Mindlin's plate equation described in chapter 1 (1.9.a.b.c).

$$k^2 Gh\Theta_x - D\frac{\delta^2\Theta_x}{\delta x^2} - \frac{D}{2}(1-\nu)\frac{\delta^2\Theta_x}{\delta y^2} - D\left(\frac{\nu+1}{2}\right)\frac{\delta^2\Theta_y}{\delta y\delta x} - k^2 Gh\frac{\delta V_z}{\delta x} = \frac{1}{12}\rho h^3\omega^2\Theta_x \tag{9.1.a}$$

$$-D\left(\frac{\nu+1}{2}\right)\frac{\delta^2\Theta_x}{\delta x\delta y} + k^2 Gh\Theta_y - \frac{D}{2}(1-\nu)\frac{\delta^2\Theta_y}{\delta^2 x} - D\frac{\delta^2\Theta_y}{\delta y^2} - k^2 Gh\frac{\delta V_z}{\delta y} = \frac{1}{12}\rho h^3\omega^2\Theta_y \tag{9.1.b}$$

$$-k^2 Gh\frac{\delta\Theta_x}{\delta x} - k^2 Gh\frac{\delta\Theta_y}{\delta y} + k^2 Gh\frac{\delta^2 V_z}{\delta x^2} + k^2 Gh\frac{\delta^2 V_z}{\delta y^2} = -\rho h\omega^2 V_z \tag{9.1.c}$$

where:

$V_z=V_z(x,y,t)$ is the transverse deflection in the z direction.

$\Theta_x=\Theta_x(x,y,t)$ and $\Theta_y=\Theta_y(x,y,t)$are the rotations of the transverse line about the the$x$ and y axis respectively.

$\rho$is the mass density of the beam material, h the thickness of the plate, E the Young modulus, $G=E/(2(1+\nu))$ the shear modulus and α the shear correction factor and $D=Eh^3/(12(1-\nu^2))$.

9.1.Discretisation of the problem

Now, the solutions functions of (9.1.a.b.c) are approximated by the bilinear product (9.2) of two NURBS Basis$R_i(\xi)$ and $R_j(\mu)$and the network of nodal variables v_{ij}.

Let us start by the approximation of the transverse deflection in the z direction as in (9.2).

$$V_z(x,y) \approx V_z(\xi,\mu) = \sum_{i=1}^{n}\sum_{j=1}^{m} v_{ij} R_i(\xi) R_j(\mu) = \{R_1(\xi) \quad R_2(\xi) \quad \dots \quad R_n(\xi)\} \begin{bmatrix} v_{11} & v_{12} & \cdots & v_{1n} \\ v_{21} & v_{22} & \cdots & v_{2n} \\ \vdots & \vdots & \ddots & \vdots \\ v_{n1} & v_{n2} & \cdots & v_{nn} \end{bmatrix} \begin{Bmatrix} R_1(\mu) \\ R_2(\mu) \\ \vdots \\ R_n(\mu) \end{Bmatrix} \tag{9.2}$$

In order to achieve a comfortable algebraic equation system to be easily programmed and solved with standard tools, we proceed to the following transformation of the bilinear system (9.2) as described in (9.3) and expanded in (9.4).

$$V_z(x,y) \approx V_z(\xi,\mu) = \sum_{i=1}^{n} R_i(\xi) \left(\sum_{j=1}^{m} v_{ij} R_j(\mu) \right) \tag{9.3}$$

$$V_z = \{R_1(\mu)R_1(\xi) \quad R_2(\mu)R_1(\xi) \quad \dots \quad R_n(\mu)R_1(\xi)R_1(\mu)R_2(\xi) \quad R_2(\mu)R_2(\xi) \quad \dots \quad R_n(\mu)R_2(\xi)R_1(\mu)R_n(\xi) \quad R_2(\mu)R_n(\xi) \quad \dots \quad R_n(\mu)R_n(\xi)\} \begin{Bmatrix} u_{11} \\ u_{12} \\ \vdots \\ u_{1n} \\ u_{21} \\ u_{22} \\ \vdots \\ u_{2n} \\ u_{n1} \\ u_{n2} \\ \vdots \\ u_{nn} \end{Bmatrix} \tag{9.4}$$

Now, one could write solution function approximation on a network of collocation points as in (9.5). Index n and m are respectively the total number of collocation points in the x and y directions.

$$V_z(\xi_k,\mu_l)=\sum_{i=1}^{n}\sum_{j=1}^{m} v_{ij}\,R_i(\xi_k)R_j(\mu_l) \tag{9.5}$$

Equation (9.5) could be written in the matrix form (9.6).

$$V_z(\xi_k,\mu_l)=\begin{bmatrix} R_1(\xi_1)R_1(\mu_1) & R_1(\xi_1)R_2(\mu_1) & \dots & R_1(\xi_1)R_n(\mu_1) & \dots & R_n(\xi_1)R_1(\mu_1) & R_n(\xi_1)R_2(\mu_1) & \dots & R_n(\xi_1)R_n(\mu_1) \\ R_1(\xi_1)R_1(\mu_2) & R_1(\xi_1)R_2(\mu_2) & \dots & R_1(\xi_1)R_n(\mu_2) & \dots & R_n(\xi_1)R_1(\mu_2) & R_n(\xi_1)R_2(\mu_2) & \dots & R_n(\xi_1)R_n(\mu_2) \\ \vdots & \vdots & \ddots & \vdots & \ddots & \vdots & \vdots & \dots & \vdots \\ R_1(\xi_1)R_1(\mu_n) & R_1(\xi_1)R_2(\mu_n) & \dots & R_1(\xi_1)R_n(\mu_n) & \dots & R_n(\xi_1)R_1(\mu_n) & R_n(\xi_1)R_2(\mu_n) & \dots & R_n(\xi_1)R_n(\mu_n) \\ \vdots & \vdots & \ddots & \vdots & \dots & \vdots & \vdots & \ddots & \vdots \\ R_1(\xi_n)R_1(\mu_1) & R_1(\xi_n)R_2(\mu_1) & \dots & R_1(\xi_n)R_n(\mu_1) & \dots & R_n(\xi_n)R_1(\mu_1) & R_n(\xi_n)R_2(\mu_1) & \dots & R_n(\xi_n)R_n(\mu_1) \\ R_1(\xi_n)R_1(\mu_2) & R_1(\xi_n)R_2(\mu_2) & \dots & R_1(\xi_n)R_n(\mu_2) & \dots & R_n(\xi_n)R_1(\mu_2) & R_n(\xi_n)R_2(\mu_2) & \dots & R_n(\xi_n)R_n(\mu_2) \\ \vdots & \vdots & \ddots & \vdots & \ddots & \vdots & \vdots & \ddots & \vdots \\ R_1(\xi_n)R_1(\mu_n) & R_1(\xi_n)R_2(\mu_n) & \dots & R_1(\xi_n)R_n(\mu_n) & \dots & R_n(\xi_n)R_1(\mu_n) & R_n(\xi_n)R_2(\mu_n) & \dots & R_n(\xi_n)R_n(\mu_n) \end{bmatrix}\begin{Bmatrix} v_{11} \\ v_{12} \\ \vdots \\ v_{1n} \\ \vdots \\ v_{n1} \\ v_{n2} \\ \vdots \\ v_{nn} \end{Bmatrix} \tag{9.6}$$

In compact form: $\boldsymbol{V_z(\xi_k,\mu_l)}=[\boldsymbol{R}]\{\boldsymbol{v}\}$ (9.7)

where:

$$\{v\}=\{v_{11}\quad v_{12}\quad \dots\quad v_{1n}\quad v_{21}\quad v_{22}\quad \dots\quad v_{2n}\quad \dots\quad v_{n1}\quad v_{n2}\quad \dots\quad v_{nn}\}^T$$

In the same way, one could derive NURBS approximations of $\Theta_x(x,y)$, $\Theta_y(x,y)$ and their respective derivatives. The results are presented in Table.37.

Table.37. NURBS approximation of displacement fields as well as their derivatives for a plate element.

$V_z = [R]\{v\}$	$\Theta_x = [R]\{\theta_x\}$	$\Theta_y = [R]\{\theta_x\}$
$\frac{\delta V_z}{\delta x} = \frac{1}{L_x}[R_{,\xi}]\{v\}$	$\frac{\delta \Theta_x}{\delta x} = \frac{1}{L_x}[R_{,\xi}]\{\theta_x\}$	
$\frac{\delta V_z}{\delta y} = \frac{1}{L_y}[R_{,\mu}]\{v\}$		$\frac{\delta \Theta_y}{\delta y} = \frac{1}{L_y}[R_{,\mu}]\{\theta_y\}$
$\frac{\delta^2 V_z}{\delta x^2} = \frac{1}{L_x^2}[R_{,\xi\xi}]\{v\}$	$\frac{\delta^2 \Theta_x}{\delta x^2} = \frac{1}{L_x^2}[R_{,\xi\xi}]\{\theta_x\}$	$\frac{\delta^2 \Theta_y}{\delta x^2} = \frac{1}{L_x^2}[R_{,\xi\xi}]\{\theta_y\}$
$\frac{\delta^2 V_z}{\delta y^2} = \frac{1}{L_y^2}[R_{,\mu\mu}]\{v\}$	$\frac{\delta^2 \Theta_x}{\delta y^2} = \frac{1}{L_y^2}[R_{,\mu\mu}]\{\theta_x\}$	$\frac{\delta^2 \Theta_y}{\delta y^2} = \frac{1}{L_y^2}[R_{,\mu\mu}]\{\theta_y\}$
$\frac{\delta^2 V_z}{\delta x \delta y} = \frac{1}{L_x L_y}[R_{,\xi\mu}]\{v\}$	$\frac{\delta^2 \Theta_x}{\delta x \delta y} = \frac{1}{L_x L_y}[R_{,\xi\mu}]\{\theta_x\}$	$\frac{\delta^2 \Theta_y}{\delta x \delta y} = \frac{1}{L_x L_y}[R_{,\xi\mu}]\{\theta_y\}$

Substituting displacements approximations and their derivatives from Table.37 in equation (9.1.a.b.c) yields the eigenvalue problem (9.8).

$$\begin{bmatrix} \left(k^2Gh[R] - \frac{D}{L_x^2}[R_{,\xi\xi}] - \frac{D(1-\nu)}{2L_y^2}[R_{,\mu\mu}]\right) & -\left(\frac{D(\nu+1)}{2L_xL_y}[R_{,\xi\mu}]\right) & -\left(\frac{k^2Gh}{L_x}[R_{,\xi}]\right) \\ -\left(\frac{D(\nu+1)}{2L_xL_y}[R_{,\xi\mu}]\right) & \left(k^2Gh[R] - \frac{D(1-\nu)}{2L_x^2}[R_{,\xi\xi}] - \frac{D}{L_y^2}[R_{,\mu\mu}]\right) & -\left(\frac{k^2Gh}{L_y}[R_{,\mu}]\right) \\ -\left(\frac{k^2Gh}{L_x}[R_{,\xi}]\right) & -\left(\frac{k^2Gh}{L_y}[R_{,\mu}]\right) & \left(k^2Gh\left(\frac{1}{L_x^2}[R_{,\xi\xi}] + \frac{1}{L_y^2}[R_{,\mu\mu}]\right)\right) \end{bmatrix} \begin{Bmatrix} \{\theta_x\} \\ \{\theta_y\} \\ \{v\} \end{Bmatrix} = \omega^2 \begin{bmatrix} \frac{1}{12}\rho h^3[R] & [0] & [0] \\ [0] & \frac{1}{12}\rho h^3[R]\{b\} & [0] \\ [0] & [0] & -\rho h[R] \end{bmatrix} \begin{Bmatrix} \{\theta_x\} \\ \{\theta_y\} \\ \{v\} \end{Bmatrix} \quad (9.8)$$

At the present stage of the development of the thesis, the generalization of the proposed method of imposing boundary conditions for plates is still underway. Instead, for the moment we are content to strongly impose the boundary conditions for the fully clamped plate case. This is done by removing the degrees of freedom relative to the displacements of the plate's edges and their respective matrix elements.

9.2. Numerical tests

The results obtained from the resolution of Reisner-Mindlinplate equation by the developed IGA-C method are presented. they are given in terms of the non-dimensional frequency parameter λ defined in (9.9) and thus compared with those of previous works, notably, reference [36] obtained with the isogeometricGalerkin method (IGA-G) and in the same reference [37] obtained using finite elements method.

$$\lambda_i = \sqrt{\frac{\rho h \omega_i^2 b^4}{\pi^4 D}} \quad (9.9)$$

In the aim of presenting the obtained results in the same format of the previously published ones [36] (with 3 digits fixed), IGA-C is performed in the present test with $n \times n$=39×39 collocation points and polynomial order p=9 for the two NURBS basis. The results are in good agreement with those obtained by theisogeometricGalerkin method IGA-G and finite elements method [35] and [36]. However, a better accuracy is reached when using IGA-C.

In Fig. 41, we represent the first three flexural modes obtained for the studied Reisner-Mindlin plate for the fully clamped boundary conditions case.

Table.38. Non-dimensional frequency parameters. Case of a fully clamped Reisner-Mindlin square plate C-C-C-C.

CCCC							
mode	exact	FEM	err	IGA-G	err	IGA-C	err
1	5,999	6,017	0,300	5,999	0,000	5,999	0,007
2	8,567	8,606	0,455	8,568	0,012	8,566	0,006
3	8,567	8,606	0,455	8,568	0,012	8,566	0,006
4	10,402	10,439	0,356	10,404	0,019	10,402	0,002
5	11,486	11,533	0,409	11,477	0,078	11,497	0,094
6	11,486	11,562	0,662	11,504	0,157	11,470	0,143
7	12,845	12,893	0,374	12,851	0,047	12,843	0,012
8	12,847	12,896	0,381	12,851	0,031	12,843	0,027
9	-	14,605	-	14,535	-	14,507	-
10	-	14,606	-	14,535	-	14,507	-

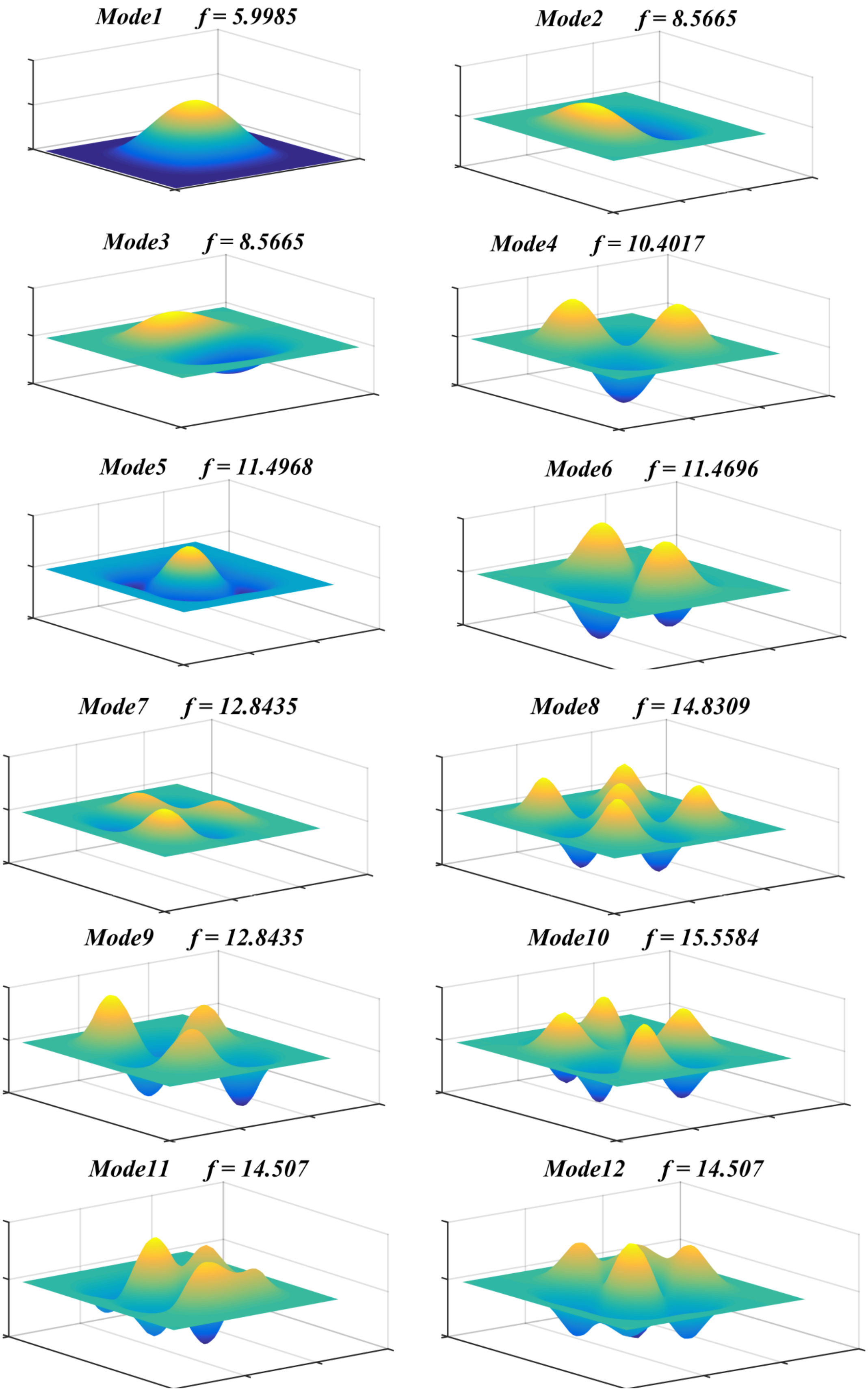

Fig. 41.First twelve mode shapes of a fully clamped C-C-C-C Reisner-Mindlin plate.

Ch 10

10. Conclusion

The first part of this work (bibliographic research and state of the art), has been devoted to selecting and investigating the most efficient analytical models of mechanical structures as well as the most efficient numerical resolution methods. Timoshenko beam models and ReisnerMindlin's platehave been selected because of their simplicity and performance. On the side of numerical methods, the isogeometric collocation method seemed to be the most promising.

The isogeometric collocation method is studied for the analysis of six selected models, namely, the in-plane vibrations of Timoshenko straight and arched beamsin the cases of ideal and non ideal boundary conditions, in-plane vibration of two layer composite beams, out-of-plane vibrations of helical springs,damaged Timoshenko beam and Reisner-Mindlin plate. A new method of imposing boundary conditions is proposed. A new method of damage modelling is proposed. Results are presented in tabular and graphical forms according to the published works in the literature that we used as references.

The obtained results are in good agreements with the recently published ones. A fast convergence and high accuracy are observed.

Higher vibration modes are obtained with much higher accuracy, due to the geometrical performance of NURBS. Logarithmic rate of convergence with h and P refinement (respectively knots insertion and polynomial order elevation) is observed and illustrated in Fig 10 and Fig 11 for helical sprig application. This result bears conclusions in references [7] and [10].

This improved formulation of the isogeometric collocation method comes out to be easy to use, precise, rapidly convergent and particularly having the potential of being able to treat a large variety of problems. In addition, the isogeometric collocation method has the advantage of making it possible to refine the polynomial degree independently of the increment contrarily to usual shape functions where these are dependant. This constitutes a major advantage in many applications, e.g. the detection of damages in the great structures not requiring inevitably a high degree of approximation but a fine increment.

In comparison with other methods, IGA-C has the advantage of using the same shape functions as CAD software, which in practice eliminates the error on the interpolation of the analyzed geometry (according to the reference [5], this constitute 80% of the total computation cost of analysis). IGA-C also has the advantage of not using numerical quadratures which are inertial in computation cost and source of error. A detailed mathematical study showing the high performance of IGA-C according to its convergence and computational properties is presented in references [7] and [10].

In this work, in each application case,particular emphasis is directed towarddetermination of the optimal parameterisation of the IGA-C and the damage modelling in order to establish a helpful database for the use of these methods in other application cases.

The results presented in chapters 4, 6 and 7 have been published in references [18] and [38]. A manuscript dealing with a new method of modelling damages in plates and shells is under development and will soon be submitted for publication.

Further improvements of IGA-C analysis are still under developments for the generalisation of its use in the case of more complex structures that may be of concern for designers such as shells, cracked structures, discontinuity and non linearity modelling.

References

[1] J.P. Boyd. Chebyshev& Fourier Spectral Methods, Lecture Notes in Engineering, Vol. 49, Springer, Berlin, 1989.

[2] Herman H. Goldstine and John Von Neumann, Numerical inverting of matrices of high order, Bull. Amer.Math.Soc.vol. 53 (1947) pp. 1021-1099.

[3] VON NEUMANN, John. & GOLDSTINE, Herman H.Numerical Inverting of Matrices of High Order.The American Mathematical Society, 1947.First edition.

[4] Von Neumann J. (1982) First Draft of a Report on the EDVAC. In: Randell B. (eds) The Origins of Digital Computers. Texts and Monographs in Computer Science. Springer, Berlin, Heidelberg.

[5] J. A. Cottrell, T. J. R. Hughes, Y. Bazilevs. Isogeometric Analysis. Towards Integration of CAD and FEA (Wiley, 2009).

[6] F. Auricchio, L. Beirão Da Veiga,T. J. R. Hughes, A. Reali, G. Sangalli. Isogeometric Collocation Methods. Mathematical Models and Methods in Applied Sciences 20 (2010) 2075–2107.

[7] T.J.R. Hughes, A. Reali, G. Sangalli. Efficient quadrature for NURBS-based isogeometric analysis, Computer Methods in Applied Mechanics and Engineering. 199 (2010) 301–313.

[8] F. Auricchio, L. Beirão da Veiga, T.J.R. Hughes, A. Reali, G. Sangalli.Isogeometric collocation for elastostatics and explicit dynamics.Comput.Methods Appl. Mech. Engrg. 249–252 (2012) 2–14.

[9] L. Beirão da Veiga, C. Lovadina, A. Reali. Avoiding shear locking for the Timoshenko beam problem via Isogeometric collocation methods.Computer Methods in Applied Mechanics and Engineering.Comput.Methods Appl. Mech. Engrg. 241–244 (2012) 38–51.

[10] DominikSchillinger, John A. Evans, Alessandro Reali, Michael A. Scott, Thomas J.R. Hughes. Isogeometric collocation: Cost comparison with Galerkin methods and extension to adaptive hierarchical NURBS discretizations. Comput.Methods Appl. Mech. Engrg. 267 (2013) 170–232.

[11] L. De Lorenzis, J.A. Evans, T.J.R. Hughes, A. Reali. Isogeometric collocation: Neumann boundary conditions and contact. Comput.Methods Appl. Mech. Engrg. 284 (2015) 21–54.

[12] F. Auricchio, L. Beirão da Veiga, J. Kiendl, C. Lovadina, A. Reali. Locking-free isogeometric collocation methods for spatial Timoshenko rods.Comput.Methods Appl. Mech. Engrg. 263 (2013) 113–126.

[13] Hongwei Lin, Qianqian Hu, YunyangXiong. Consistency and convergence properties of the isogeometric collocation method.Comput.Methods Appl. Mech. Engrg. 267 (2013) 471–486.

[14] Timoshenko, S. P., 1921, On the correction factor for shear of the differential equation for transverse vibrations of bars of uniform cross-section, Philosophical Magazine, p. 744.

[15] Timoshenko, S. P., 1922, On the transverse vibrations of bars of uniform cross-section, Philosophical Magazine, p. 125.

[16] R. D. Mindlin, 1951, Influence of rotatory inertia and shear on flexural motions of isotropic, elastic plates, ASME Journal of Applied Mechanics, Vol. 18 pp. 31–38.

[17] E. Reissner, 1945, The effect of transverse shear deformation on the bending of elastic plates, ASME Journal of Applied Mechanics, Vol. 12, pp. A68–77.

[18] HocineBelgaid, Amar Bouazzouni, Vibration analysis of mechanical structures with a new formulation of theisogeometric collocation method, European Journal of Mechanics / A Solids 68 (2018) 88–103.

[19] R.E. Scraton (1965). The solution of linear differential equations in Chebyshev series, Comput, J, 8, P. 57.

[20] T. Mikami, J. Yoshimura, Application of the collocation method to vibration analysis of rectangular Mindlin plates. Computers and Structures 18 (3) (1984) 425–431

[21] Pakdemirli M, Bayaci H. Effects of non-ideal boundary conditions on the vibrations of continuous systems. J Sound Vib2002; 249(4):815–23.

[22] Abbas BAH. Vibrations of Timoshenko beams with elastically restrained ends. J Sound Vib1984;97(4):541–8.

[23] Ma'enS.Sari n, EricA.Butcher. Free vibration analysis of non-rotating and rotating Timoshenko beams with damaged boundaries using the Chebyshev collocation method. International Journal of Mechanical Sciences 60(2012)1–11.

[24] J. Lee, W.W. Schultz. Eigenvalue analysis of Timoshenko beams and axisymmetric Mindlin plates by the pseudospectral method. Journal of Sound and Vibration 269 (2004) 609–621.

.[25] Sang Jin Lee, Kyoung Sub Park, Vibrations of Timoshenko beams with isogeometric approach. Applied Mathematical Modelling 37 (2013) 9174–9190.

[26] Jinhee Lee. In-Plane Free Vibration Analysis of Curved Timoshenko Beams by the Pseudospectral Method.Korean Society of Mechanical Engineers (KSME) International Journal, Vol. 17 No. 8, pp. 1156-1163, 2003.

[27] Michele Dilena, AntoninoMorassi, Experimental and modal analysis of steel concrete composite beams with partially damaged connection. Journal of Vibration and Control 2004 10: 897.

[28] Michele Dilena, AntoninoMorassi, Vibrations of steel–concrete composite beams with partially degraded connection and applications to damage detection. Journal of Sound and Vibration 320 (2009) 101–124.

[29] Mehdi Hajianmaleki, Mohamad S. Qatu, Vibrations of straight and curved composite beams: A review. Composite Structures 100 (2013) 218–232.

[30] V. Yildirim, Investigation of parameters affecting free vibration frequencies of helical springs, International Journal for Numerical Methods in Engineering 39 (1996) 99–114.

[31] V. Yildirim, Free vibration analysis of non-cylindrical coil springs by combined used of the transfer matrix and the complementary functions method, Communications in Numerical Methods in Engineering 13 (1997) 487–494.

[32] J. Lee, D.J. Thompson, Dynamic stiffness formulation, free vibration and wave motion of helical springs, Journal of Sound and Vibration 239 (2001) 297–320.

[33] Jinhee Lee. Free vibration analysis of cylindrical helical springs by the pseudospectral method. Journal of Sound and Vibration 302 (2007) 185–196.

[34] S. CHRISTIDES and A. D. S. BARR, ONE-DIMENSIONAL THEORY OF CRACKED BERNOULLI-EULER BEAMS, Int. J. Mech. Sci.Vol. 26, No. 11/12, pp. 639-648, 1984.

[35] J. K. SINHA, M.I.FRISWELL AND S. EDWARDS, SIMPLIFIED MODELS FOR THE LOCATION OF CRACKSIN BEAM STRUCTURES USING MEASUREDVIBRATION DATA, Journal of Sound and Vibration (2002) 251(1), 13 38.

[36] D.B. Robert, Formulas for Natural Frequency and Mode Shape, Van NostrandReinhold Company, New York, 1979.

[37] S. Shojaee, E. Izadpanah, N. Valizadeh, J. Kiendl, Free vibration analysis of thin plates by using a NURBS-basedisogeometric approach, Finite Elements in Analysis and Design 61 (2012) 23–34.

[38] H. Belgaid and A. Bouazzouni, Eigenvalue Analysis of Concrete-Steel Composite Beamsbased on a Timoshenko Modelusing the Isogeometric Collocation Method, Proceedings of the Twelfth International Conferenceon Computational Structures Technology,Civil-Comp Press, Stirlingshire, Scotland.(2014).

Abstract

"If people do not believe that mathematics is simple, it is only because they do not realize how complicated life is." John Von Neumann. In mechanical engineering, and more precisely in the field of mechanical structures modelling, the nature of the problems dealt with initially imposes the following challenges: that of mathematically reproducing a particular aspect of the behaviour of an element (relationship between stress and deformation, behaviour of damaged zones, thermal deformation ...), that of assembling all the aspects of its behaviour in a same mathematical system, that of modelling the influence of external elements on the element in question (boundary condition, initial conditions, contact, friction ...) and finally, that of assembling this element with others to model an entire structure. The challenges mentioned above place us in front of two kinds of difficulties: the complication of the elementary physical phenomena to be modelled and the complexity of the obtained systems. Analytical models of mechanical structures are concretely presented as systems of partial differential equations PDEs. The nature and the complexity of these depend of course on the nature of the problems treated.

In a second time, the system of equation being built, the challenge that presents itself is the resolution of this one. Since the advent of the air of computers and the exponential development of calculator's power, numerical methods have occupied the first place in the field of scientific computing. In fact, numerical methods and computer technology are two almost inseparable domains. Various numerical methods were successively proposed for the resolution of such PDE problems, each one trying to remedy to the failures of the preceding ones.

In the main of remedy to the difficulties of integration between finite elements computers codes and geometrical modellers (CAD software), T.J.R Hughs et al. introduced the concept of isogeometric analysis in 2005. Following their work, other authors published many results whose main concern was primarily to validate and improve it.

The limits of the collocation methods come out to be those of the shape functions used for approximating the solutions. In 2010, progress on this matter has been achieved giving rise to the isogeometric collocation method; the latter is presented as a collocation method using NURBS as shape functions. Hugh's article was followed and complemented by other works.

In the light of this state of art, four main objectives are aimed in this work:

a. To provide an automatic method for imposing common and special (damaged) boundary conditions. The proposed method is simple to use without making resort to too much intuition, solves a lot of posed problems, and is very worthwhile for implementation of the isogeometric collocation method in CAD software.
b. Study the applicability of IGA-C, determine the optimal parameters for its use, construct isogeometric models for mechanical structures and evaluate the method over existing methods.
c. Development of comprehensive and detailed algorithms for the practical implementation of the IGA-C. Indeed, until today, the said method has been presented only in a very abstract mathematical formalism. Moreover, it is in this objective that all the applications have been fully detailed. We hope this will certainly help its implementation in CAD software.
d. Construction of new models of structures under study and the enrichment of the scientific database.
e. Development of methods for damage modelling in structures.

Résumé

"Si les gens ne croient pas que les mathématiques sont simples, c'est seulement parce qu'ils ne réalisent pas à quel point la vie est compliquée." John Von Neumann. En mécanique, et plus précisément dans le domaine de la modélisation des structures mécaniques, la nature des problèmes abordés pose d'abord les défis suivants: reproduire mathématiquement un aspect particulier du comportement d'un élément (relations entre contraintes et déformations, comportement des zones endommagées, déformation thermique ...), assembler tous les aspects de son comportement dans un même système mathématique, modéliser l'influence des éléments externes sur l'élément considéré (condition aux limites, conditions initiales, contactes, frottements ...) Enfin, assembler cet élément avec d'autres pour modéliser une structure entière. Les défis précédemment mentionnés nous placent devant deux types de difficultés: la complication des phénomènes physiques élémentaires à modéliser et la complexité des systèmes obtenus. Les modèles analytiques de structures mécaniques se présentent concrètement comme des systèmes d'équations aux dérivées partielles (EDP). La nature et la complexité de celles-ci dépendent bien entendu de la nature des problèmes traités.

Dans un deuxième temps, le système d'équations étant construit, le défi qui se présente est la résolution de celui-ci. Depuis l'avènement de l'air des ordinateurs et le développement exponentiel de la puissance des calculateurs, les méthodes numériques ont occupé la première place dans le domaine du calcul scientifique. Différentes méthodes de résolution numérique d'EDPs ont été successivement proposées, chacun essayant de remédier aux manquements des précédentes.

Dans le but de remédier aux difficultés d'interaction entre les codes éléments finis et les logiciels de DAO, T.J.R Hughs et al Introduisent En 2005 le concept d'analyse isogéométrique. Suite à leurs travaux, d'autres auteurs ont publié de nombreux articles dont la principale préoccupation était de valider et d'améliorer la dite méthode.

Les limites des méthodes de collocation sont celles des fonctions de forme utilisées pour l'approximation des solutions. En 2010, des progrès ont été réalisés dans ce domaine, donnant lieu à la méthode de collocationisogéométrique ; cette dernière est présentée comme une méthode de collocation utilisant les B-Splines non uniformes rationnelles (NURBS) comme fonctions de forme. L'article de Hugh a été suivi et complété par d'autres travaux.

Dans ce projet de thèse, quatre objectifs principaux sont visés:

a. Fournir une méthode automatique pour imposer des conditions aux limites communes et non idéales (endommagées). La méthode proposée est simple à utiliser sans trop recourir à l'intuition, résout beaucoup de problèmes posés, et est très intéressante pour l'implémentation de la méthode de collocation isogéométrique dans les logiciels de CAO.

b. Étudier l'applicabilité de l'IGA-C, déterminer les paramètres optimaux pour son utilisation, construire des modèles isogéométriques pour les structures mécaniques et évaluer la méthode par rapport aux méthodes existantes.

c. Développement d'algorithmes complets et détaillés pour la mise en œuvre pratique de l'IGA-C. En effet, jusqu'à aujourd'hui, cette méthode n'a été présentée que dans un formalisme mathématique abstrait. C'est dans cet objectif que nous avons détaillé chacune des applications développées dans ce travail. Nous espérons que cela aidera certainement sa mise en œuvre dans les logiciels de CAO.

d. Construction de nouveaux modèles de structures et enrichissement de la base de données scientifiques.

e. Développement de méthodes de modélisation des endommagements dans les structures.

ملخّص

"إذا كان الناس لا يصدّقون بأن الرياضيّات بسيطة، فهذا فقط لأنهم لا يدركون مدى كون الحياة معقّدة." جون فون نيومان. في الميكانيكا ، وبصورة أدق في مجال نمذجة الهياكل الميكانيكية ، تطرح طبيعة المشاكل المعالجة التّحديات التالية: أوّلا، النّمذجة الرياضية لكل ظاهرة فيزيائية تؤثر على سلوك كل عنصر من الهيكل الميكانيكي المدروس (مثلا: العلاقات بين الإجهادات والتشوهات وسلوك المناطق التّلفة و التمدّد الحراري ...). ثانيا، تجميع كل الظواهر المؤثّرة على العنصر المدروس ضمن جملة رياضية موحّدة (مثلا: معادلات الحركة للعارضات و الصّفائح). من ثمّ تأتي نمذجة تأثير العناصر الخارجية على العنصر المدروس (الشروط على الحدود ، الشروط الأولية، الاحتكاك ...) . و أخيرا، تجميع هذا العنصر مع باقي عناصر الهيكل المدروس لتكوين نموذج رياضي كامل.

تضعنا التحديات المذكورة سابقاً أمام نوعين من الصعوبات: أوّلا، صعوبة نمذجة الظواهر الفيزيائية الأوّلية وتعقيد الأنظمة التي تمّ الحصول عليها. بشكل ملموس، تُعرَض النّماذج التحليلية للهياكل الميكانيكية على شكل جمل من المعادلات التفاضلية ذات المشتقّات الجزئيّة (Partial Differential Equations). بطبيعة الحال ، تتعلّق طبيعة وتعقيد هذه المعادلات بطبيعة المشاكل التي يتم تناولها.

في الخطوة الثانية يأتي تحدي حل المعادلات التّي تمّ بناؤها . منذ ظهور أجهزة الكمبيوتر والتطور المتعاظم لقوة الآلات الحاسبة، احتلت الطرائق العددية المرتبة الأولى في مجال الحساب العلمي. وقد تم على التوالي اقتراح طرق مختلفة للحل العددي للمعادلات التّفاضلية، حيث حاولت كل منها معالجة أوجه القصور في الأساليب السابقة.

من أجل تجاوز صعوبات التفاعل بين برامج العناصر المحدودة (Finite Elements Codes) وبرمجيات التّصميم بمساعدة الكمبيوتر (CAD) ، قدّم البروفيسور توماس هيوز (Thomas Hughes) وآخرون في عام 2005 مفهوم التّحليل الإيزوجيومتري (Isogeometric Analysis). منذ ذلك الحين، نشر مؤلفون آخرون العديد من المقالات و التي كان اهتمامهم الرئيسي فيها التحقق من الطريقة وتحسينها.

تعتبر أساليب الأطياف المزيّفة (Pseudo-Spectral Methods) أو المعروفة باسم أساليب الإرتصاف (Collocation methods) من أدق أساليب الحلّ العددي للمعادلات التفاضليّة إلا أنّ لهذه الأخيرة نقاط ضعف جعلتها قليلة الاستخدام. تكمن حدود أساليب الإرتصاف في دقّة الدّوال المستخدمة لمقاربة أشكال الحلول و قدرتها على مقاربة مجالات تغيّر واسعة. في عام 2010 ، حقّق البروفيسور توماس هيوز و آخرون تقدما في هذه المسألة باقتراح طريقة الإرتصاف الإيزوجيومتريّة (Isogeometric Collocation Method) و اللّتي قُدّمت على شكل طريقة أطياف مزيّفة باستخدام دوال ب-سبلين تآلفيّة غير منتظمة NURBS لمقاربة أشكال الحلول. تمّت متابعة مقالة هيوز واستكمالها بأعمال كثيرة أخرى.

في هذه الأطروحة ، تم معالجة أربعة أهداف رئيسية:

أ. اقتراح طريقة تلقائية لفرض شروط الحدود العامة وغير المثالية (مثلا حالة تواجد تلف أو احتكاك). تبدو الطريقة المقترحة سهلة الاستخدام دون الكثير من الحدس وتحل العديد من المشاكل ، كما تبدو ملائمة و سهلة للبرمجة مع طريقة الإرتصاف الإيزوجيومتري في برامج التّصميم بمساعدة الكمبيوتر.

ب. دراسة قابلية تطبيق طريقة الإرتصاف الإيزوجيومتري في مجال ديناميك الهياكل الميكانيكيّة وتحديد المعالم المثلى لاستخدامها وكذلك بناء نماذج إيزوجيومتريّة للهياكل الميكانيكية وتقييم الطريقة المدروسة بمقارنتها بالطرق القائمة.

ج. تطوير خوارزميات كاملة ومفصلة للتنفيذ العملي لطريقة الإرتصاف الإيزوجيومتريّة. في الواقع ، حتى اليوم ، تم تقديم هذه الطريقة فقط في الشكلية الرياضية التجريدية. ولهذا الغرض قمنا بتفصيل كل التطبيقات التي تمّ تطويرها في هذا العمل. نأمل أن يساعد هذا على تنفيذها في برامج التصميم بمساعدة الكمبيوتر.

د. بناء نماذج جديدة وإثراء قاعدة البيانات العلمية.

ه. تطوير طرق نمذجة الأضرار في الهياكل الميكانيكية.